

THE INFLUENCE OF MAGNETIC FIELDS ON THE
CONVECTION OF OXYGEN: THE GLENDA EFFECT

A Thesis

Presented to

the Faculty of the Department of Chemical Engineering
University of Houston

In Partial Fulfillment

of the Requirements for the Degree

Master of Science in Chemical Engineering

by

Donald Charles Clark

December, 1975

TO MY MOTHER AND MY FATHER,
AND TO MY BELOVED GLENDA SUE

ACKNOWLEDGEMENTS

This effort, as in every human endeavor, is not the manifestation of an individualistic accomplishment. Rather, a synthesis of a myriad of creative inspirations has occurred in this work, only a fraction claiming their origins in the author; indeed, the countless individuals contributing to this effort are too numerous to count, and to this nameless group, the author owes a deep debt of thanks. However, several names and institutions are prominent contributors to this endeavor and this thesis would be incomplete without acknowledging their contributions to it: to members of the faculty and staff of the Chemical Engineering Department and, particularly, to Dr. Wallace I. Honeywell, for their guidance and encouragement during the course of this investigation; to Roy Priest for his craftsmanship in the fabrication of the experimental apparatus; to Akhil Bidani and John Steimke for their contributions to various stages of the work; to Herb Kent for his assistance in the procurement of experimental supplies and equipment; to my dear friends, Kerry and Kathy Rock and Michael Harris for their undying friendship, which I forever will treasure; to Dr. J.M. Harris for instilling in me scientific boldness and confidence in my technical abilities; to the Department of Chemical Engineering and the National Science Foundation for their financial support of this work; and to NATO for the opportunity and support to study in Europe.

Without the philosophical and financial boosts of the author's brother, D. Walter Clark, this effort would have indeed been a painful experience. Additionally, the author wishes to express deep gratitude for the continuous and undying love and moral support of his parents,

not only throughout this work, but throughout his life. Finally, the author wishes to thank Glenda Sue Nielsen for her encouragement, love and understanding given to him throughout the duration of this project.

THE INFLUENCE OF MAGNETIC FIELDS ON THE
CONVECTION OF OXYGEN: THE GLENDA EFFECT

An Abstract of a Thesis
Presented to
the Faculty of the Department of Chemical Engineering
University of Houston

In Partial Fulfillment
of the Requirements for the Degree
Master of Science in Chemical Engineering

by
Donald Charles Clark

December, 1975

ABSTRACT

A theoretical model is derived, ab initio, to quantitatively describe the natural convective heat transfer of a nonionized paramagnetic gas between parallel vertical plates of differing temperature subjected to a steady magnetic field having a small non-vanishing gradient. Owing to the sensitivity of the magnetic permeability with temperature, normal convective flow can be radically altered, even reversed by application of the proper magnetic field configuration. The result may be expressed quantitatively by a dimensionless group, the Glenda number, which characterizes the magneto-thermal contribution to the total heat transfer analogous to the gravity controlled Grashof number. This study differs from earlier work in that the presence of a magnetic field gradient is included. A parametric dependence proportional to $\Delta T^2 p^2 H T^{-5} (\partial H_x / \partial z)$ is predicted theoretically for this magneto-convective heat transfer contribution, where p is the pressure, H is the magnetic field strength, ΔT is the temperature gradient between the plates, and T is the absolute temperature. With an approximate constant field gradient of 2 Oe/cm in an otherwise uniform field of 15000 Oe, the magnitude of the theoretically predicted heat transfer of oxygen agrees with the data of Vevai within experimental error. With the exception of the linear field dependence theoretically expected, the parametric dependencies of T , p , and ΔT are additionally in complete agreement with the experimental evidence; the deviation of the field dependence from the reported cubic dependence, however, remains inconclusive.

TABLE OF CONTENTS

CHAPTER	PAGE
PART I: THEORY	
I INTRODUCTION.....	1
Magnetohydrodynamics.....	4
Paramagnetism and Diamagnetism.....	6
Previous Investigations.....	13
Applications of the Glenda Effect.....	27
II DERIVATION OF THE FUNDAMENTAL EQUATIONS OF MAGNETOHYDRODYNAMICS.....	30
Magnetic Pressure and the Pondermotive Force.....	31
Magnetogasdynamic Momentum Balance.....	37
Application of Equation II-29 to the Glenda Effect Problem.....	40
III DERIVATION OF THE GLEND A EFFECT MODEL: A NEW MAGNETOCONVECTIVE HEAT TRANSFER MODEL.....	48
Introduction.....	48
Modelling of the Velocity Distribution of the Glenda Effect.....	51
A Heat Transfer Model of the Glenda Effect.....	66
Treatment of a Non-Constant Magnetic Field Gradient.....	74

PART II: EXPERIMENTAL

IV	THE DESIGN AND CONSTRUCTION OF A RECTANGULAR CELL AND MODIFICATION OF SUPPORT SYSTEMS.....	79
	Introduction.....	79
	The Rectangular Cell.....	81
	Experimental Support Equipment.....	87
	Vacuum System and Loading Manifold.....	87
	Heater Power Supply and Measurement Circuit.....	89
	Differential Temperature Measuring Circuit.....	89
	The Electromagnet System.....	92
V	MEASUREMENT OF THE FIELD GRADIENT	93
	Introduction.....	93
	Gaussmeter with DVM Measurements.....	96
VI	EXPERIMENTAL RESULTS OF EARLIER WORK AND COMPARISON WITH THE THEORETICAL MODEL USING MEASURED GRADIENT.....	101
	Introduction.....	101
	Experimental Results of J.E. Vevai (1973,18).....	102
	Simulation Study of the New Theoretical model Under Analogous Conditions of J.E. Vevai (18) at the Measured Field Gradient.....	109
VII	DISCUSSION OF THE RESULTS, RECOMMENDATIONS FOR THE FUTURE, AND CONCLUSIONS.....	112
	Comparison of Results.....	112

CHAPTER

PAGE

VII CONTINUES

Future Studies..... 117
Conclusions on the Project..... 121

APPENDIX

A Molecular Orbital of Oxygen..... 123
B Kinetic Theory Derivation of the Curie Law..... 124
C FORTRAN Program for the Glenda Effect Model
Simulation Study..... 127

References..... 132
General Reading Bibliography..... 134
Nomenclature..... 135

LIST OF TABLES

TABLE	PAGE
I EFFECTIVE FIELD GRADIENT.....	99a
II EXPERIMENTAL RESULTS OF MAGNETOCONVECTION IN MILLIWATTS AS A FUNCTION OF ABSOLUTE TEMPERATURE.....	108a
III EXPERIMENTAL RESULTS OF MAGNETOCONVECTION IN MILLIWATTS AS A FUNCTION OF FIELD STRENGTH.....	108b
IV EXPERIMENTAL RESULTS OF MAGNETOCONVECTION IN MILLIWATTS AS A FUNCTION OF THE ABSOLUTE PRESSURE.....	108c
V THEORETICALLY EXPECTED RESULTS OF MAGNETOCONVECTION AS A FUNCTION OF ABSOLUTE TEMPERATURE.....	111a
VI THEORETICALLY EXPECTED RESULTS OF MAGNETOCONVECTION AS A FUNCTION OF THE APPLIED FIELD STRENGTH.....	111b
VII THEORETICALLY EXPECTED RESULTS OF MAGNETOCONVECTION AS A FUNCTION OF THE ABSOLUTE PRESSURE.....	111c

LIST OF FIGURES

FIGURE	PAGE
I Insensitive Magnetic Field Homogeneity Plot.....	20a
II Flat Plate Geometry of the Model Showing Direction of Temperature Gradient and Applied Magnetic Field.....	48a
III Velocity Profiles for Paramagnetic Gases in Applied Magnetic Fields with the Field Gradient as Parameters....	63a
IV Heat Transfer Model for Laminarily Convecting Gases.....	66a
V The Glenda Effect Cell.....	82a
VI The Cell Fabrication Jig.....	85a
VII The High Vacuum System.....	87a
VIII Schematic of the Evacuating and Sample Gas Filling System.	88a
IX Cell Heater Circuit.....	89a
X Differential Temperature Measuring Circuit.....	90a
XI Electromagnetic System and Associated Cryostat System and Support.....	92a
XII Magnetic Field Strength as a Function of the Applied Current.....	92b
XIII Magnetic Field Gradient Mapping at 8.4 kOe.....	98a
XIV A Cylindrical Transport Cell.....	102a
XV Deviations in Average SBE Data at 80°K, $\Delta T=5.8^\circ K$ for Several Isobars.....	107a
XVI Variations of the Magnetoconvective Heat Flux for Both the Theory (Q_{G1}) and Experimental (Q_{MC}) in Oxygen with Average Gas Temperature, Magnetic Field Strength as Parameters.....	112a-d

LIST OF FIGURES CONTINUE

FIGURE	PAGE
XVII Variations of the Magnetoconvective Heat Flux for Both the theory (Q_{G1}) and Experimental (Q_{MC}) in Oxygen with Magnetic Field Strength, Various Values as Parameters.....	112e-f
XVIII Variations of the Magnetoconvective Heat Flux for Both the Theory (Q_{G1}) and the Experimental (Q_{MC}) in Oxygen with Pressure, Magnetic Field Strength as Parameter.....	112g-j
XIX Variation of the Experimental Magnetoconvective Heat Flux (Q_{MC}) in Oxygen with Temperature Gradient Across the Cell.....	115a

PREFACE

As can be readily observed in the Table of Contents of this thesis, this work involved both a theoretical derivation and an experimental verification of that theory. Despite this dual nature of the work, the project resembles little the initial proposal; indeed, the evolutionary path of this work follows a rather meandering and oftentimes seemingly dead-end road. It therefore may prove beneficial for the reader to have a brief tour of this same journey.

Originally, the project manifested itself in the design and construction of a rectangular cell to experimentally verify a viable, existant homogeneous field theory developed in these labs (W-H Park, 1972). Previous work (Vevai, 1973) by this group with cylindrical cells yielded results differing by five orders of magnitude from the theory. Attributing these differences to end effects and differing cell geometries, it was hoped a rectangular cell would provide better results. In this vein, a rectangular cell was designed and a prototype built and the support systems re-fabricated. During this time, a question arose which cast doubt on the existence of "magnetic pressure", the very crux of the Park model, and all experimental work was temporarily terminated to ascertain beyond any doubt whether to accept or refute this claim. After overcoming a high degree of magnetogasdynamic naivete through considerable reading of the general literature of the field, it was soon learned that "magnetic pressure" was indeed a viable consequence of the interaction of magnetic fields and fluids and thus the original Park theory retained its validity. However, by this time, it could be

seen that for common laboratory conditions, the magnetic pressure effect was negligibly small and therefore it was concluded that some other effect had to exist to explain the results.

Considering the possibility that the magnet system used might have indigenous inhomogeneities associated with the field, the single work of convective heat transfer of paramagnetic gases in a non-homogeneous field was consulted to perhaps fit the conditions, data and results of our labs to this nonhomogeneous theory. Upon analysis of this work, two conclusions could readily be made: i) that in the presence of large field gradients at room temperature, very large changes in the velocity of the convecting fluid occurred, and ii) no theoretical analysis was attempted to speak of, token at best; no velocity distribution or heat transfer model. Thus, owing to the well-known hyperbolic dependence of the paramagnetic permeability on temperature, it was reasoned that, provided some non-vanishing gradient did exist in the magnet system, the results could be based on an as yet undeveloped non-homogeneous field model derived from the first principles of magnetogasdynamics. Armed with the fact that every laboratory "homogeneous" magnet did indeed have characteristic inhomogeneities, albeit negligible, a new magnetoconvective heat transfer model incorporating any field gradient was developed ab initio, the results indicating that a gradient on the order of Oersteds/cm would give the proper experimental results; a number too small to be accurately measured (or so it was thought) with existing equipment over the 15000 Oersted field prevalent.

As a result, experimental efforts were re-instigated to measure the results of convective transport in a field with a superimposed, known linear field gradient of the proper magnitude. These measurements, however, were never made; a new technique was developed to measure small field gradients and the existing field was then mapped. When the measured gradients yielded results based on the new model which fell well within those obtained from the early experimental work, albeit a cylindrical geometry, further experimental work ceased.

Hopefully, this has served to rationalize, at least partly, the oscillation between the theoretical pursuits and the experimental efforts, and at the same time, serving as an introduction and purview of the entire investigation. It should be added at this time that this thesis was written in a format and at a level commensurate with the philosophy that the general reader will be a knowledgeable but by no means gifted chemical engineer, not a genius-cursed plasma physicist. Additionally, if the reader has no interest in the ab initio aspects of this work, no continuity will be lost by skipping chapter II in toto.

PART I :

THEORY

CHAPTER I

INTRODUCTION

Since the introduction of the kinetic theory in the 19th Century by Clausius, investigators have relied primarily upon available experimental measurements of macroscopic quantities to test refined mathematical models of their corresponding microscopic analogues, their ultimate objective being a kinetic theory relating molecular interaction parameters to accessible macroscopic quantities, such as density, pressure, and temperature. In this same manner, experimental measurement of the transport coefficients can be used to test the models of transport phenomena in gases, here the goal being a transport theory based on molecular interaction principles. Indeed, in the case of spherically symmetric atoms, such as the closed-shell Noble gases, the transport theories have been well developed and almost all phenomena fairly well understood. For the polyatomic cases, however, owing to their non-sphericity and greater internal degrees of freedom, the problem is considerably more acute. Fortunately, however, due largely to the pioneering work of Senftleben (1) and later, Beenakker (2), an experimental technique is now available which enables one to test the kinetic theory of polyatomic molecules with a greater sensitivity and subtlety than has been previously possible with more ordinary transport experiments. The basis for the measurement is the perturbing effect of external magnetic and electric fields upon the transport properties of dilute polyatomic gases,

called the Senftleben-Beenakker effect (S-B effect). The normal effect of these uniform external fields is a small decrease in the transport properties of low density gases; the decreases in transport coefficients being less than 1% at saturation and for the case of applied magnetic fields are unique functions of H/p , where H is the magnetic field strength and p is the gas pressure. The kinetic theory explanation is that the usual coupling between the molecular angular momenta and the velocity gradients present in the momentum or energy transport are partially destroyed when an external field is applied. This theory has proven highly successful in predicting field effects on the viscosity and thermal conductivity of simple polyatomics such as N_2 , CO , CH_4 , O_2 , and NO .

In the particular case of oxygen, small deviations from the expected S-B effect behavior are known to occur at the low pressure end of the H/p isotherm. Beenakker (3) has rationalized this behavior by an extension of the kinetic theory to include complicated field effects on the transport coefficients. Recently, however, while investigating the S-B effect of oxygen gas at $77^\circ K$ and at moderate pressures (20-35 torr), Honeywell (4) anomalously reported a significantly large increase in the apparent conductivity, an increase which could not be explained in terms of field effects on the transport properties alone. Realizing that at the pressures involved, the fluid is well into the continuum regime, which nonetheless does not preclude the application of the normal S-B effect theory, it was thought that the magnetic fields present might radically alter the normal convective processes present

normally not involved at lower pressures. Finding the literature rich in additional experimental evidence of similarly striking effects in oxygen, but devoid of any theoretical analysis to explain these observations from First Principles, Honeywell et al. (5) attempted to rationalize the results based on a homogeneous field model using the magnetic pressure influences on density (to be reviewed in this thesis), but failed to agree in magnitude with the observation of the effect by five orders of magnitude. It is now felt that this in large measure was due to neglect of the inherent field gradient associated with the magnet systems used, the effect of which, it turns out, can profoundly alter the normal convective flow. The basis for this new effect is the coupling of the highly temperature sensitive magnetic body force, a function of the field gradient, via the paramagnetic susceptibility, with the gasdynamic system of equations, giving rise to the large changes in flow characteristics, called the Glenda effect; it is the modelling of the Glenda effect which is described herein.

Magnetohydrodynamics

Magnetohydrodynamics (or as it is sometimes referred, magneto-gasdynamics, magnetofluid dynamics, or simply plasma dynamics) is singularly concerned with the interaction of fluids in flow and applied electromagnetic fields. In particular, the vast majority of the work in this area primarily deals with the effect of magnetic (electric) fields on the velocity of a fluid and the concomitant perturbation of the fields by the fluid's movement. The manifestation on a measurable macroscopic level of this quite obviously molecular-field interaction are the dielectric constant, ϵ , in the electric field case, and magnetic permeability, μ , (to be discussed in depth later) in the magnetic analogue. To characterize the relative influence the velocity and fields have on each other, the magnetic Reynolds number is frequently used, defined by equation [I-1]

$$Re_m = \mu \sigma u D \quad [I-1]$$

where σ is the electrical conductivity, u is the fluid velocity, and D is the characteristic distance involved. For large (>1) magnetic Reynolds numbers, the velocity of the fluid not only alters the applied fields, but initiates the creation of induced fields; for small Re_m (<1), no such induced fields exist. It turns out, however, that $Re_m > 1$ exists only on the cosmic level (e.g. centers of the planets, stellar bodies, galactic flow) and it is currently impossible, by laminar flows in the laboratory, to induce fields comparable to the applied field. It is quite obvious that a common fluid in flow such as

water or nitrogen does not fall within the realm of magnetohydrodynamics since no such interaction can occur. Equally obvious is the case of flowing plasmas: these non-fluid fluids cannot be considered by normal fluid dynamics owing to the intense electromagnetic coupling prevalent whereas their behavior is characterized nicely by magnetogasdynamics. The situation is not quite so obvious for the intermediate cases of paramagnetically permeable fluids, such as nitric oxide, oxygen (the case considered in this work), aqueous ferric perchlorate or dilute hexaphenylethane in benzene, at ordinary laboratory conditions of temperature and pressure. They are most assuredly not plasmas in the normal sense of the word, yet, of course, they interact strongly with applied magnetic fields and thus their behavior is largely amenable to magnetogasdynamic analysis. These paramagnetic substances are characterized by the existence of one or more unpaired electrons in the orbital configuration of the atom, ion or molecule, which gives rise to the observable mild attraction toward a magnetic field. This effect contrasts ferromagnetism, in which the attraction of certain elements (notably iron and cobalt) is extremely pronounced due to their characteristic crystal structure, and diamagnetism, a property of all matter, in which there is a slight repulsion from a field due to the field interaction with filled orbitals.

Paramagnetism and Diamagnetism

The exact molecular origins, nature, and motivation of magnetism, like gravity, is hardly understood, and any discussion in these areas quickly leads to philosophy, religion, the cosmos, and a headache. However, its effects, particularly paramagnetism and diamagnetism, can easily be visualized in terms of simple molecular theories. An electron, spinning on its own axis, independent of its motion in its orbital, behaves like a tiny magnet and thus produces a constant field whose sign is contingent on its spin quantum number, s ($=\pm 1/2$). This same single, unpaired electron placed in an orbital thus produces a net magnetic moment, λ , whose magnitude ideally is directly proportional to the angular momentum of the electron, $\sqrt{s(s+1)}$ and is commonly measured in units of the Bohr magneton:

$$1 \text{ Bohr magneton} \equiv \lambda_0 = \frac{eh}{4\pi m_e c} = 0.927 \times 10^{-20} \text{ ergs/Oe}$$

Thus,

$$\lambda = g_\ell \sqrt{s(s+1)} \lambda_0 \quad [I-2]$$

where g_ℓ is the Lande g -factor, having the value of 2.0 for a free electron. It is interesting to parenthetically note that for gases, this relation is fairly well-behaved, and is valid over a wide range of conditions, but for liquids, complex ligand-field interactions (spin-spin coupling) can occur which give rise to quite anomalous

behavior. For systems having more than one unpaired electron in different orbitals, the total spin quantum number, \tilde{S} , replaces its single electron counterpart in the moment equation [I-2] above. This value, of course, is a constant for any given atom, ion, or molecule and is independent of all external influences, such as temperature, pressure, magnetic field strength and thus becomes a property of that substance.

When a substance possessing an intrinsic magnetic moment is placed in an applied field, each molecule tends to align itself within the field such that its own field adds to the applied field thereby increasing the magnitude of the field flux within the substance which in turn causes an attraction toward the field. At the same time, however, thermal agitation of the molecules tends to be a randomizing influence on the optimal alignment of all molecules in the substance and thus temperature strongly influences the contribution of the individual, characteristic magnetic moments made to the total magnetic flux within the matter, although having no influence whatsoever on the indigenous moment itself. Quantitatively, this total magnetic flux can be expressed as

$$\vec{B} = \vec{H} + 4\pi\vec{I} \quad [I-3]$$

where \vec{B} is the magnetic flux vector within the substance, \vec{H} is the externally applied field, and \vec{I} is the intensity of magnetization vector which couples the total flux with the contribution of the

magnetic moment, λ . Dividing this expression by \vec{H} ,

$$\mu \equiv \frac{\vec{B}}{\vec{H}} = 1 + \chi_V \quad [I-4]$$

is obtained, where μ is the magnetic permeability of the substance, and χ_V is the volumetric susceptibility of the material under consideration. In the absence of mass, χ_V vanishes and thus the permeability of free space is unity; for the case of paramagnetic substances wherein the moment adds to the applied field, the permeability is greater than unity. Expressing the dependence of permeability in terms of the more common molar susceptibility, χ_M , (i.e. per unit mole), equation [I-4] becomes

$$\mu = 1 + \chi_M \quad . \quad [I-5]$$

In his classic studies, Pierre Curie showed that paramagnetic susceptibilities depend inversely on the absolute temperature and often follows or closely follows the behavior required by the relation, known as the Curie Law*,

$$\chi_M = \frac{C}{T} \quad [I-6]$$

where C is the Curie constant. In light of the randomizing influence of temperature discussed earlier, this result is not unexpected, and in fact, can easily be derived from the kinetic theory as described in

Appendix B which shows the value of C to be

$$C = \frac{N_o \lambda^2}{3k} \quad [I-7]$$

where N_o is Avagadro's number, and k is the Boltzmann constant. Combining equations I-7, 6, 5 and 2 (and using the total spin quantum number, \tilde{S}), the molar permeability of any material having one or more unpaired electrons can now be expressed in terms of molecular parameters, or

$$\mu = 1 + \frac{4N_o \lambda_o^2}{3kT} \left(\tilde{S}(\tilde{S}+1) \right) \quad [I-8]$$

in CGS units. For the application of this work, it is found in Appendix A that molecular orbital restrictions require that oxygen

* The Curie Law predicts that at $T = 0$, $\chi_M = \infty$ which is absurd. At absolute zero, all moments align themselves perfectly in the field and thus have maximum contribution to the flux. Thus, the Curie-Wiess Law,

$$\chi_M = \frac{C}{T-\theta}$$

where θ is a constant for a particular material, accounts for this behavior by providing a non-zero intercept. It is added that this in no way affects the sensitivity of χ_M to changes in T .

have two such unpaired electrons ($\tilde{S} = 1$). Thus, despite the fact that each oxygen molecule has an indigenous and constant magnetic moment of $2\sqrt{2} \lambda_0$, a large collection of such molecules shows the temperature dependent molar magnetic permeability of

$$\mu = \left(1 + \frac{1.02}{T} \right) \text{ ergs mol}^{-1} \text{Oe}^{-2} \quad [\text{I-9}]$$

and a corresponding Curie constant of $1.02 \text{ ergs}^\circ \text{Kmol}^{-1} \text{Oe}^{-2}$. Since on a laboratory scale, it is only with a large number of such molecules that any experiment can be performed, it is precisely in this paramagnetic permeability, or more commonly, in the prerequisite paramagnetic susceptibility where all experimental interest and evidence lays, and again, it is this permeability (or really, susceptibility) which manifests the molecular magnetic phenomena of matter on a macroscopic level.

Although not specifically treated in this thesis, it is of considerable academic interest to briefly consider the counterpart to paramagnetism, diamagnetism. If an electron is added to an orbital of a previously half-filled orbital, by the Pauli exclusion principle, the electron possesses a spin opposite to that of the first. Since the magnitudes of the two fields are identical but their signs opposite, there is no net intrinsic magnetic moment for the newly filled orbitals. Likewise, all internal, filled orbitals similarly have no magnetic moment. However*, since these matched electrons in their molecular orbital, in a crude sense, behave like a circulating current, when

placed in a magnetic field, by Lenz's law, the induced magnetic field produced by the current and the applied field is such that it opposes the existing field. Thus, in diamagnetic substances, not only is the magnetic flux vector within the substance slightly less than free space, but the material is repulsed by the field somewhat. It is evident, then, that diamagnetism is dependent only on the strength of the applied field and the size and shape of the filled orbitals involved, none of which, of course, are temperature dependent. Since diamagnetic contributions to the permeability are functions of the field strength, diamagnetism, like paramagnetism (paramagnetism recall is dependent on the temperature; paramagnetic moments are not), cannot be considered a property of matter. However, paramagnetism and diamagnetism can be differentiated in that the former has its origins in an intrinsic property of a particular substance (the moment), the latter does not, and it is only because a large number of molecules can be studied that the "property-ness" of paramagnetic moments is lost. It is noted, however, that since even paramagnetic substances possess at least one closed shell (except, of course, $H\cdot$, H_2^+ , He^+), all matter is thus diamagnetic. Equations I-3, 4, 5 still apply to diamagnetic substances, except that, owing to the induced field's opposition to the applied field, diamagnetic susceptibilities are negative implying diamagnetic permeabilities of less than unity. The magnitude of the diamagnetic effect is generally quite small even for large applied fields, usually two to three orders of magnitude less than paramagnetic effects. Thus, it is customary procedure, when dealing with paramagnetic substances, especially

isolated components such as this investigation with pure oxygen, to neglect the diamagnetic contributions to the total permeability of the sample; this investigation will be no exception to that tradition. This section is concluded by reiterating that the total magnetic permeability of matter, μ , depends on the magnetic susceptibility, χ_M , of that material,

$$\mu = 1 + \chi_M \quad [I-10]$$

which in turn depends on the sum of the paramagnetic (temperature dependent only) effect and the diamagnetic (field strength dependent only) contribution (which usually can be ignored for paramagnetic substances), neither of which can be considered properties of matter owing to their sensitivities to the external influences of temperature and field respectively. The paramagnetic effect depends, finally, on the indigenous moment, λ , a property of that material, and the ambient temperature,

$$\chi_M = 4 \frac{N_0 \lambda_0^2}{3kT} \left[\tilde{S}(\tilde{S}+1) \right] \quad [I-8]$$

Previous Investigations

Before delving into the rigors of the derivation of this new model, it might prove beneficial at this time to briefly but critically review the earlier work in this field of magnetoconvective heat transfer; after analyzing these efforts, the new model to explain the Glenda effect will briefly be introduced along with a presentation of its applications, potentials, and its limitations.

Perhaps the most classic work in this area is the case of Benard convection frequently discussed in the magnetogasdynamic literature. It will, however, only be mentioned in passing here, since it has little application to this investigation, in large measure owing to its treatment of field effects on a fluid in a vertical temperature gradient wherein the thermal buoyant forces exactly match the pressure gradient thus producing no flow whatever. This study in equilibrium differs considerably of course, from the current investigation since in any horizontal non-vanishing temperature gradient, velocities exist for all viscosities. It is interesting to note additionally, however, as with most other prior work in the field, the magnetic permeability of the fluid in this work is treated as a constant towards all parameters and it is only the density which is quantitatively coupled to temperature, which for paramagnetic fluids, is an obvious shortcoming.

Another somewhat classical investigation in this area was conducted by Gershuni and Zhukhovitskii in the Soviet Union in 1958 (6).

This theoretical study involved the convection of an electrically conducting fluid between two vertical parallel plates of differing temperature, in the presence of a magnetic field. Selecting an imaginary fluid whose electrical conductivity was sufficient to render the magnetic Reynolds number non-negligible, the moving fluid thus generated induced fields, in this case, in the same direction as the flow. Obviously, this induced field is a function of the velocity (and vice-versa) and can be characterized by the dimensionless parameter, Ha , the Hartmann number. Thus, the perturbed velocity distribution of the convecting fluid was obtained merely incorporating this Hartmann number. Additionally, the induced magnetic field distribution was similarly obtained. For negligibly small electrical conductivities, e.g. oxygen, the Hartmann number is vanishingly small, and as expected, this velocity distribution resolves to the ordinary Grashof convective distribution. To obtain this Hartmann distribution, the authors tacitly assumed that the permeability was constant, the field was gradient-free (a poor assumption for any real magnet system), and that the influence of temperature solely manifested itself in density changes. Once again, it is seen that the coupling between permeability and temperature is silently ignored as are the indigenous field gradients.

W-H Park, a colleague in these laboratories (5), in 1973 rigorously extended this same rectangular analysis by specific application to oxygen in a homogeneous field, incorporated the effect of magnetic pressure on the fluid density to rationalize the anomalously

large increase in heat transfer reported earlier (4) by workers in these same laboratories. Magnetic pressure is the admittedly rather generic term which is frequently used in magnetogasdynamic analysis to describe the lumped effects of an added magnetic (electric) stress tensor and electromagnetic striction pressures generated by the sensitivity of the magnetic permeability (dielectric constant) with density. This pressure is indeed a real pressure and superposes on the conventional hydrodynamic pressure. The classic example of this phenomenon in which the effect is quite pronounced, of course, lies in the so-called "pinch effect" of flowing plasmas, finding great application in the possible containment of thermonuclear fluxes. Realizing the very real existence of this magnetic contribution to the total pressure and its subsequent effect on density as the magnetic field is changed but at the same time not being aware of the magnitude of the changes involved, Park extended the normal Grashof-type temperature expansion of the density used in the Russian study to additionally include the effects of magnetic pressure via the magnetic permeability of oxygen by expanding the density in total pressure as well. Park characterized this added term to the expansion by a new dimensionless parameter, Mc , the magnetoconvection number, defined as

$$Mc \equiv \frac{GrCH_o^2}{RT_o^2} \quad [I-11]$$

where Gr is the Grashof number, R is the universal gas constant, T_o is the average absolute temperature, which was ascribed to characterize

the magneto-thermal contribution to the total heat transfer just as the Grashof number characterizes the natural thermal contribution. This new number manifested itself in the velocity as a linearly added term in the Hartmann distribution of the Russian work. However, in light of the negligibly low electrical conductivity of oxygen at those temperatures, this new magnetoconvective velocity profile simplified to merely a linearly additive contribution characterized by the magnetoconvection number to the normal dimensionless Grashof convective velocity distribution:

$$u_z^* = \frac{1}{12} (Gr + Mc) (x^{*3} - x^*) \quad [I-12]$$

and its concomitant addition to the heat transfer,

$$Q = \frac{\tilde{\rho} \tilde{C}_v \nu_o \Delta T}{90} (Gr + Mc) \quad [I-13]$$

where C_v is the heat capacity at constant volume and ν_o is the average kinematic viscosity over the temperature gradient. Thus, the ratio of the heat transferred in a magnetic field to that out of a field can be expressed simply as

$$\frac{Mc}{Gr} = \frac{CH_o^2}{RT_o^2} \quad [I-14]$$

In a cylindrical cell experiment, this ratio was found to be on the order of 10-20%, whereas equation [I-14] yielded an expected value of 10^{-5} .

This large discrepancy was indeed baffling and could not be rationalized from end effects and differing cell geometries alone. At the same time, however, adding to the enigma was the conclusion that there appeared to be no principles, either fundamental or calculational, which were violated in the analysis and thus the model appeared to be viable and seemed to demand error in the experimental endeavors. The analysis even incorporated the sensitivity of the permeability with temperature (although ignoring the complete contribution of the dependence, a small error), quite unlike past models. Its validity is even further strengthened upon further investigation of the magnitude of this magnetic pressure effect for those prevalent conditions.

Magnetic pressure, recall, is at the very heart of the model; any changes in velocity and/or heat transfer over Grashof convection can only be brought about by the effects of this term via its expansion in density. It has recently been found that Lehrer (7) quantified this very magnetic pressure contribution to the total pressure for paramagnetic gases by the expression

$$P_{\text{tot}} = p + \frac{pH_0^2 C}{2RT_0^2} \quad [\text{I-15}]$$

or

$$\Delta p_{\text{tot}} = \frac{pH_0^2 C}{2RT_0^2} \quad [\text{I-16}]$$

where p_{tot} is the total pressure of the system and p is the normal hydrostatic contribution to p_{tot} . For the conditions under which the experiments of Vevai were conducted, the magnetic pressure is found to result in a net pressure change due to magnetic field effects at 10 torr, 77°K, and subjected to 10^4 Oersteds, of only 10^{-3} torr! This indeed is a small change*, but it turns out its ultimate effect on velocity and heat transfer is even smaller when the sensitivity of density toward pressure and temperature changes is considered. Characterizing the sensitivity of density toward each by the respective partial differentiation with respect to each parameter, and using the ideal equation of state, i.e. $p=\rho RT$, the sensitivities

$$\frac{\partial \rho}{\partial T} = - \frac{p}{RT^2} \quad [\text{I-17}]$$

$$\frac{\partial \rho}{\partial p} = \frac{1}{RT} \quad [\text{I-18}]$$

are found. Thus, the sensitivity of density to even large pressure changes is mild, quite unlike its highly sensitive temperature

*It is parenthetically added that the change in pressure brought about by the temperature gradient alone, independent of the field, results in a far greater pressure change than the magnetic pressure indicated here. Even with this change however, the dependence of density on pressure is traditionally neglected on convection analysis owing to its low sensitivity, as is shown.

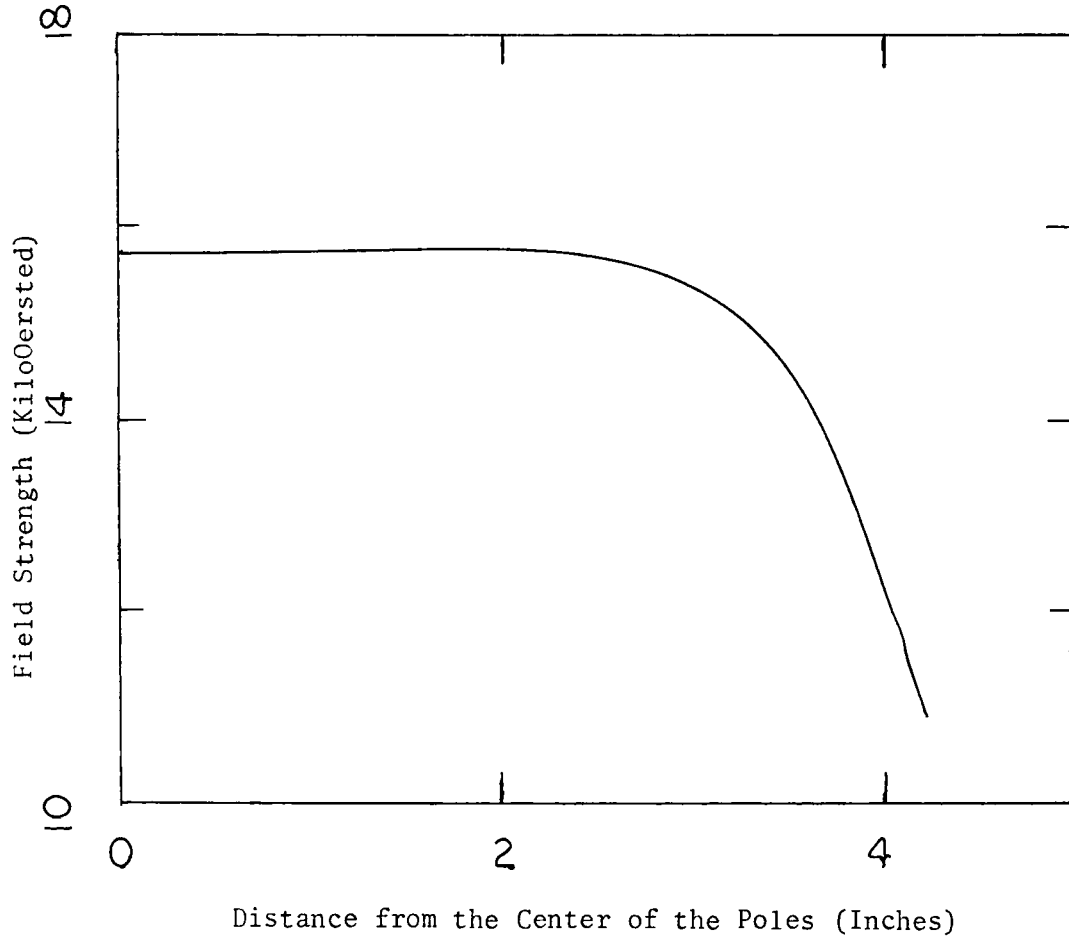
dependence. This of course, is a confirmation of scientific intuition: hyperbolic functions are always more sensitive to the domain than are linear functions. In light of this small magnitude and low sensitivity then, it can readily be seen that the ultimate effect of magnetic pressure on velocity distributions and heat transfer via density changes will indeed be quite vanishingly small. Thus, provided no other effects prevail which have their origins in an error in the original assumptions, an additive contribution to heat transfer on the order of 10^{-5} is not beyond reason, in agreement with that predicted by the Park model. Thus, it is concluded that since the model, along with its restrictions, is valid, to account for the large anomalous results, either the experiment is in error, or some other effect, stemming from faulty assumptions, prevails.

The possibility of the former is indeed remote in light of the incredible precision and accuracy by which the experiments were conducted; a change of one part in 10^5 capable of being detected. The latter possibility is given further credence by the recent evidence that a similar magnitude (i.e. ≈ 0.20) for magnetoconvective heat transfer has been reported (10), but that it was a decrease in heat transfer. Of course, upon inspection of equation I-11, for paramagnetic gases, the magnetoconvection number, Mc , is positive for all possible values. Thus, the Park model can only predict increases in heat transfer, not surprising in light of the positive nature of magnetic pressure for all possible values of paramagnetic gases (see equation I-16) and thus in no way can account for decreases in heat transfer. Therefore, some other

effect must be responsible for the anomalous behavior, an effect which must be explicable in terms of a viable shortcoming of the assumptions of the Park model. This shortcoming, of course, like that of the similar Russian work, lies in the tacit assumption of a perfectly homogeneous magnetic field, the assumption of which, although simplifying the analysis, results in the annihilation of several profoundly powerful gradient-based terms in the magnetogasdynamic equations.

It should be pointed out that Park's original assumption of a "homogeneous" magnet is not that far from reality, as can be seen in Figure I; over the length of the cell (1.5 inches from the center) the field is seen to be quite uniform. However, these measurements were made with insensitive instrumentation allowing only gross changes to be detected. Indeed, considerable expense, effort, and time has been spent to procure one of the most uniform, and stable magnets available. Nevertheless, non-vanishing gradients always exist in real magnet systems; with respect to the total field, these indigenous gradients are indeed negligible, but when considered alone, or moreover, when considered in the field-field gradient product, a small gradient becomes strikingly significant and indeed quite powerful. It is precisely this field-field gradient product in which lies the crux of the Glenda effect model.

With the new possibility that gradients, albeit vanishingly small, indeed may exist, the literature of magnetoconvection of fluids in non-uniform fields was consulted in hopes of fitting the available



FIELD HOMOGENEITY PLOT

FIGURE I

data, conditions, and results to existing, well-established models and thus provide an explanation of the anomalous behavior.

The first investigation considered was the work of Kibler and Wiley (8) of Convair Aerospace. This highly qualitative work (not a single equation was used in the entire paper) described a 10-fold increase in the convective cooling capacity of warm air subjected to an electric field. Although not specifically mentioning the existence of field gradients, their presence was obvious in light of their technique for field generation: an array of ten X-acto blades at 10 kilovolts, the resulting field gradients obviously rather intense. In light of the electrical nature of the work (electrical and magnetic effects are, however, related) and the complete lack of any theoretical treatment, its review is parenthetically ended by commenting that the effect was attributed in the analysis to some mysterious "electrical wind" and referenced an 1899 account of its observation.

In this same vein, Lykoudis and Yu at Purdue in 1962 (9) elegantly quantified this type of field interaction based on the sound principles of magnetogasdynamics. In this work, the free convection of an electrostrictive fluid enclosed between a horizontally heated wire and a coaxial, cooled cylinder, under an applied non-uniform radial electric field was examined. Again, however, the study involved electric field effects and thus had no coupling of the permeability with temperature. However, the increases in convective heat transfer in non-uniform electric fields was explicable in terms of electrostriction (differs from magnetostriction used by Park) induced by the

intense electric fields used. Thus, this analysis resembled very much the Park model in that stricture arguments were used to rationalize the behavior. The difference being, however, that the electrostrictive electric field effect has a much greater magnitude (owing to higher possible laboratory fields), than the magnetic analogue and thus describes the behavior quite well since there is no analogous electric coupling with temperature. Thus, just as in the Park model, a dimensionless electrostrictive number becomes added to the normal Grashof velocity distribution and heat transfer.

Whetted by the striking effect non-uniform electric fields have on convective flow at room temperature, the literature was searched to find an analogous description of convective heat transfer in non-uniform magnetic fields. The first reported experimental observation of the Glenda effect in oxygen, was the work of F. Klauer et al. in Germany in 1941 (14). Although the experimental efforts were rather commendable under the adverse conditions in which they were performed, no theoretical motivation was offered to explain the then quite unusual events. Between then and 1968, several other such experimental investigations appeared sporadically throughout the literature and reported similarly striking behavior of oxygen in non-homogeneous magnetic fields, again, no theoretical explanation. Since 1968, several sources referred the principle "theoretical" analysis in this area to a J.R. Carruthers and R. Wolfe at the Bell laboratories, their work appearing in the Journal of Applied Physics in 1968 (10). Despite the "theoretical" nature of the work, it was, in reality, almost exclusively an experimental

investigation. An extremely crude convection cell was constructed (from such traditionally forbidden materials in precision work as 1/4 inch thick copper, 1/4 inch copper tubing, plexiglass, and (shudder!) thermocouples), filled with oxygen at various concentrations (ranging from air to pure component) at one atmosphere, and subjected to magnetic fields with large field gradients. Not surprisingly, the convective transport was indeed a marked function of the field-field gradient product, although no such correlation was made. This effect was so pronounced even with air (21% oxygen) at room temperature, that depending on the magnitude and sign of the field-field gradient product, normal convective flow was not only observed to change direction (cigarette smoke was placed in the cell) but that its magnitude in that direction could be greater than normal free convection! At the same time, the cell in another part of the field convected in the same direction as free convection, but it was observed that the fluid was now well into the turbulent region vis. a vis. normal convection's quite laminar behavior.

The theory utilized to rationalize these observations was admittedly, token at best; no velocity distribution was obtained, no heat transfer model derived, no resolve made to even the classic magnetogasdynamic equations, not even a reference to their existence. Utilizing what appears to be the equation describing the force exerted by a non-uniform field on a paramagnetic sample in a simple Gouy balance experiment found in any freshman chemistry text,

$$F_m = 1/2(\rho\chi_w \nabla H^2) \quad [I-19]$$

these workers perturbed this force by a small change in temperature thus giving rise to a corresponding changes in the magnetic body force,

$$\delta F_m = 1/2(\chi_w \delta\rho + \rho \delta\chi) \nabla H^2 \quad . \quad [I-20]$$

Equating this to a corresponding change in the gravitational body force,

$$\delta F_g = \delta\rho g \quad [I-21]$$

where $\delta\rho$ is given by

$$\delta\rho = -\beta\rho_0\delta T \quad , \quad [I-22]$$

the equation describing the expected value of the field-field gradient product needed to achieve equality of forces is obtained:

$$H_x \left(\frac{\partial H_x}{\partial z} \right) = \frac{g}{[\chi_w + \rho(\partial\chi/\partial T)/(\partial\rho/\partial T)]} \quad [I-23]$$

Over and above the fact that one is immediately struck, upon inspection of equations I-20,21, and 22, by the high ambiguity of the exact nature of the delta symbol and their subsequent transformation to differentials in I-23, it is quite clear, just from the standpoint

that only equal forces were considered while the infinitely more common and worthwhile condition of non-equal forces giving rise to motion was ignored, that this "theoretical" analysis was seriously lacking in elegance and scope and begged extension and refinement.

Freshly armed with this striking experimental evidence of such powerful effects even under such adverse conditions as high temperature and low concentrations, and the concomitant lack of a viable model ab initio , coupled to the fact that "homogeneous" magnet systems could indeed have a non-vanishing field gradient, it was thought that the anomalous results reported earlier might be explicable based on field gradient effects at the low temperatures involved in the study. In this light, the Glenda effect model was initiated.

As will be seen shortly, this new model is entirely based upon the First Principles of magnetohydrodynamics which in turn are deriveable from the fundamental laws of thermodynamics, and, as far as these laboratories can ascertain, it is the first such quantitative model to be so derived. Just as Carruthers and Wolfe suggested, the crux of the analysis lies in the coupling of the temperature effects on the magnetic body force which, of course, incorporates the field-field gradient product. In the derivation, both the induced fields and the magnetic pressure effects are tacitly ignored; in light of the foregoing discussion, it can be seen that no generality is lost. Thus, the magnetic effects are concentrated in this gradient based body force, which is characterized by a new dimensionless parameter, G_1 , the Glenda number (to be defined later). Once again, this new

number merely adds linearly to the normal Grashof velocity profile and heat transfer in much the same manner as the magnetoconvection number, Mc , did, except that the magnitude of the contribution (i.e. G_1/Gr) now precisely fits these "anomalous" experimental results. Moreover, since the Glenda number incorporates the field gradient which can be of any sign, the additive contribution of the Glenda number can either lead to an increase or a decrease in velocity and heat transfer in accordance with the experimental observations (10), quite unlike the Park model.

Applications of the Glenda Effect

Thus having what appears to be a viable model to quantitatively describe the flow characteristics of paramagnetic fluids in a horizontal temperature gradient subjected to non-uniform fields, a question now naturally arises concerning the application of such a model and the effect it quantitatively describes to real-world problems and the limitations of both. Obviously, as can be readily perceived, since the effect (with which the applications are singularly concerned) is limited to paramagnetic substances (recall that diamagnetic materials have no temperature dependence), the number of fluids that can be thus affected is admittedly, rather small. Among the gases, only oxygen and nitric oxide (and NO behaves very anomalously itself) are susceptible; among the liquids* only solutions of certain transition metal salts (a few hundred exist) and a few stable free radicals are paramagnetic. Nevertheless, some very unique and striking applications exist, all based on the fact that the Glenda effect can be utilized to greatly increase, reduce, totally prevent, or even completely reverse

*It is noted that the model as proposed cannot similarly be used to quantitatively describe paramagnetic liquids in magneto-convective flows since the analysis is based on volumetric instead of mass susceptibilities and the ideal equation of state used throughout. Qualitatively, however, the results will be analogous and no striking deviations are anticipated.

convective flow and thus provide a "control valve" on the effect of gravity in free convection, a previously unobtainable event on earth.

One obvious resort of this effect is the application to space systems, wherein convective heat transfer, conventionally impossible in the zero gravity environment of space, may be a desired transport regime vis. a vis. forced mixing or conduction. In particular, oxygen tanks, omnipresent on all space craft for both life support systems and fuel oxidation, must be heated to prevent solidification from the unavoidable radiative heat transfer to the cryogenic temperatures of space. The source of the heat presents little problems (the sun, heaters, etc.); transferring this heat throughout the oxygen is an acute problem and resolve is traditionally made to reliance on molecular conduction. This heat transfer can obviously be increased greatly by inducing magnetoconvective transport flow through the application of a magnet of the proper field strength and gradient across the tank. Owing to the cryogenic temperatures prevalent in space, a small, lightweight properly designed superconducting magnet could be easily implemented to achieve this end.

In an exactly opposite, but nonetheless down-to-earth application of the effect, the principle problem in high temperature exotic crystal growth is considered. Many of the exotic crystals grown today, e.g. ruby for lasers, semiconductors for electronics, etc., are all grown as single crystals from solution melts. It turns out that the limitation on the growth of a large "perfect" single crystal (the goal

of all crystallographers) can ultimately be traced to the adverse effects of gravity on the growth, i.e. convection. Indeed, the first growth of a "perfect" crystal occurred on one of the skylab missions, in which heating and cooling was totally by molecular conduction and radiation. On earth, the convective currents within the melt, which cannot be prevented in crystal growing furnaces, leads to crystalline imperfections and limitations on the size of single crystals. If, on the other hand, a paramagnetic salt could safely be added to the solution melt without itself causing crystalline abnormalities, or if the crystal itself is paramagnetic (many of the semiconductors, by their very nature have unpaired electrons in their structure), the Glenda effect could then be advantageously used (provided the proper field is used) to counter or buck the natural convection processes occurring in the melt, thus negating the influence of gravity and thereby allowing the growth of "perfect" single crystals. Quite obviously, the feed-back controls on the field-field gradient system would have to be fairly sophisticated since viscous dissipation could damp only small deviations from the proper value.

CHAPTER II

DERIVATION OF THE FUNDAMENTAL EQUATIONS OF MAGNETOHYDRODYNAMICS

In almost every classic text in the field of magnetogasdynamics (see "General Reading Bibliography"), the basic system of dynamic equations is derived. However, these classic approaches often neglect many possible exigencies (e.g. a non-constant permeability) in field-effects on fluids and their applications are usually limited to quite simple systems. This lack of generality is often complicated by an unwieldy and non-consistent nomenclature coupled to questionable origins of the fundamental relations needed for the complete analysis. Fortunately, however, this confusion, by in large, was overcome in 1959 by the monumental work of B-T Chu at Brown University appearing in the Physics of Fluids (11). Assuming the existence of a continuum, utilizing only the fundamental laws of thermodynamics, the Maxwell equations, and the generalized Ohm's law, Chu in a very elegant and consistent fashion, derives what is considered to be the complete generalized, non-electromagnetically-classical system of fundamental equations of magnetohydrodynamics which stands today as the authoritative source of magnetogasdynamic principles, the Glenda effect model claiming its origins exclusively in this work. Although the most significant aspects of the work will be covered here insofar as its application to magnetoconvection is concerned, for an in-depth analysis, the interested reader should consult this reference.

Magnetic Pressure and the Ponderomotive Force

Although magnetic pressure per se will not specifically be treated or utilized in the modeling of the Glenda effect as has been discussed, its importance in the derivation of the generalized fundamental equations of magnetogasdynamics is of more than academic importance. Its derivation is begun by recalling that for a pure fluid in the absence of fields, the Gibb's Phase rule requires that the behavior of the system can thermodynamically be completely defined by a single function when only two of its state variables (e.g. p,T) are specified, traditionally written as

$$A = A(p,T) \quad [\text{II-1}]$$

where A is the Helmholtz free energy. Likewise, for a system undergoing a volume change, the work, w, may be expressed as

$$dw = -pd\left(\frac{1}{\rho}\right) \quad [\text{II-2}]$$

In the presence of magnetic fields, however, two other state variables must additionally be considered, these being manifested in constitutive-type equations defined as in equation I-4,

$$\vec{B} = \mu\vec{H} \quad [\text{II-3}]$$

$$\vec{D}_e = \epsilon\vec{E} \quad [\text{II-4}]$$

where \vec{E} is the applied electric field and \vec{D}_e is the electric excitation vector (analogous to the magnetic flux vector), thus rendering equation [II-1] to

$$A = A(p, T, \vec{B}, \vec{D}_e) \quad [\text{II-5}]$$

and the total work as

$$dw = -pd\left(\frac{1}{\rho}\right) + \vec{H} \cdot d\left(\frac{\vec{B}}{\rho}\right) + \vec{E} \cdot d\left(\frac{\vec{D}_e}{\rho}\right) \quad [\text{II-6}]$$

Thus,

$$dA = \frac{\partial A}{\partial p} dp + \frac{\partial A}{\partial T} dT + \frac{\partial A}{\partial \vec{D}_e} d\vec{D}_e + \frac{\partial A}{\partial \vec{B}} d\vec{B} \quad [\text{II-7}]$$

But since it is known that

$$A = \hat{U} - TS \quad [\text{II-8}]$$

and that the first and second laws of thermodynamics require

$$d\hat{U} = dw + TdS \quad , \quad [\text{II-9}]$$

where S is the entropy of the system, and \hat{U} is thermodynamic internal energy of the system, then

$$dA = -SdT - pd\left(\frac{1}{\rho}\right) + \vec{H} \cdot d\left(\frac{\vec{B}}{\rho}\right) + \vec{E} \cdot d\left(\frac{\vec{D}}{\rho}\right) \quad . \quad [\text{II-10}]$$

Thus, comparing equations II-7 and II-10, the relations

$$S = - \frac{\partial A}{\partial T} ; \quad E_i = \rho \frac{\partial A}{\partial D_{ei}} \quad [\text{II-11 a\&b}]$$

$$H_i = \rho \frac{\partial A}{\partial B_i} ; \quad p = \vec{D} \cdot \vec{E} + \vec{B} \cdot \vec{H} + \rho^2 \left(\frac{\partial A}{\partial \rho} \right) \quad [\text{II-11 c\&d}]$$

are obtained. Utilizing the principle of superposition, the total Helmholtz free energy is split into its mechanical and electromagnetic contributions,

$$A^{\text{tot}} = A^{\text{em}} + A^{\text{m}} \quad , \quad [\text{III12}]$$

the constitutive equations II-3,4 placed into the electromagnetic component of the differential in equation II-10 and integrating,

$$A^{\text{tot}} = A^{\text{m}} + \frac{1}{2\rho} \left[\frac{D^2}{\epsilon(\rho, T)} + \frac{B^2}{\mu(\rho, T)} \right] \quad [\text{II-13}]$$

is obtained. Now for an ideal gas, A^{m} has been well established and thus the total Helmholtz free energy can be expressed as

$$A^{\text{tot}} = \frac{1}{2\rho} \left[\frac{D^2}{\epsilon(\rho, T)} + \frac{B^2}{\mu(\rho, T)} \right] + A_0 - \left(S_0 - \frac{R}{\gamma-1} \right) (T-T_0) + RT \ln \left[\left(\frac{\rho}{\rho_0} \right) \left(\frac{T_0}{T} \right)^{(\hat{\gamma}-1)^{-1}} \right] \quad [\text{II-14}]$$

where the zero subscripts refer to standard state conditions, and $\hat{\gamma}$ is the ratio of the heat capacities. Differentiating this total Helmholtz free energy with respect to density and substituting the constitutive equations II-3,4 where needed, equation II-11d becomes an expression of the total pressure, hydrostatic and electromagnetic

$$p = \rho RT + \frac{1}{2}(\vec{B} \cdot \vec{H} + \vec{D}_e \cdot \vec{E}) - \frac{\rho}{2} \left(E^2 \frac{\partial \epsilon}{\partial \rho} + H^2 \frac{\partial \mu}{\partial \rho} \right) \quad [\text{II-15}]$$

where it is evident that the electromagnetic contribution, p^e , is the sum of the Maxwellian stress tensor and the electromagnetostriuctive pressures (a result of a changing volume).

Retaining the generality of a non-constant dielectric constant, ϵ , and magnetic permeability, μ , (e.g. $\mu = \mu(\rho, T)$ and $\epsilon = \epsilon(\rho, T)$), at the same time simplifying the analysis by stipulating a vanishing applied electric field but not neglecting the possible creation of induced electric fields, relativistic invariant theory is called upon to characterize the total electromagnetic stress tensor, $\underline{\underline{T}}_{ij}^e$, as

$$\underline{\underline{T}}_{ij}^e = -p^e \delta_{ij} + D_{ei} E_j + B_i H_j \quad [\text{II-16}]$$

where δ_{ij} is the Kronecker delta. Now Chu contends that if the induced electric field, \vec{D}_e , is crossed into the magnetization vector \vec{B} , an "electromagnetic momentum" vector, \vec{G} , per unit volume, is created, defined by

$$\vec{G} = \vec{D}_e \times \vec{B} \quad . \quad [\text{II-17}]$$

This momentum is attached only to the space volume of the moving fluid and is not convected with the media as is momentum in the classical Navier-Stokes sense. Chu stipulates that the change in \vec{G} with time, t , is the gradient of the electromagnetic stress tensor, $\underline{\underline{T}}_{ij}^e$, diminished by the "ponderomotive" force, \vec{F} , (the additive body forces per unit volume due only to electromagnetic origins in toto), or rewritten,

$$f_j = \frac{\partial T_{ij}^e}{\partial x_i} - \frac{\partial G_j}{\partial t} \quad . \quad [\text{II-18}]$$

If \vec{j} and ρ^e denote, respectively, the current and charge density, then the Maxwell relations,

$$\vec{\nabla} \times \vec{E} = -\frac{\partial \vec{B}}{\partial t} \quad [\text{II-19a}]$$

$$\vec{\nabla} \times \vec{H} = \frac{\partial \vec{D}}{\partial t} + \vec{j} \quad [\text{II-19b}]$$

$$\vec{\nabla} \cdot \vec{B} = 0 \quad [\text{II-19c}]$$

$$\vec{\nabla} \cdot \vec{D}_e = \rho^e \quad [\text{II-19d}]$$

can be utilized, in conjunction with equations II-16,17,18, to

obtain the total pondermotive force

$$\vec{f} = \rho \vec{e}\vec{E} + \vec{j} \times \vec{B} - \vec{\nabla} p^e + B_k \vec{\nabla} H_k + D_{ek} \vec{\nabla} E_k \quad . \quad [\text{II-20}]$$

Recalling that

$$p^{\text{tot}} = p^m + p^e \quad [\text{II-21}]$$

where

$$p^e = \frac{1}{2}(\vec{B} \cdot \vec{H} + \vec{D} \cdot \vec{E}) - \frac{1}{2\rho} \left(H^2 \frac{\partial \mu}{\partial \rho} + E^2 \frac{\partial \epsilon}{\partial \rho} \right) \quad [\text{II-22}]$$

was previously defined, the pondermotive force resolves to be

$$\vec{f} = \rho \vec{e}\vec{E} + \vec{j} \times \vec{B} + \frac{1}{2} [D_{ek} \vec{\nabla} E_k - E_k \vec{\nabla} D_{ek}] + \frac{1}{2} [B_k \vec{\nabla} H_k - H_k \vec{\nabla} B_k] + \vec{\nabla} \frac{1}{2\rho} [E^2 \frac{\partial \epsilon}{\partial \rho} + H^2 \frac{\partial \mu}{\partial \rho}] \quad [\text{II-23}]$$

which differs from the classical result of

$$\vec{f} = \rho \vec{e}\vec{E} + \vec{j} \times \vec{B} - \frac{1}{2} E^2 \vec{\nabla} \epsilon - \frac{1}{2} H^2 \vec{\nabla} \mu + \vec{\nabla} \frac{1}{2\rho} [E^2 \frac{\partial \epsilon}{\partial \rho} + H^2 \frac{\partial \mu}{\partial \rho}] \quad [\text{II-24}]$$

which in turn is obtained from its more general counterpart above by allowing $\vec{u} \rightarrow 0$.

Magnetogasdynamic Momentum Balance

Chu flatly assumes that the pondermotive force by which the electromagnetic fields interact with the fluid dynamics is an "internal force" and does not enter explicitly into the momentum balance.

Allowing F_j to be the external force per unit volume that acts on a fluid element, and $\underline{\tau}_{ij}$ to be the total stress tensor in the fluid due to the joint action of the mechanical and electromagnetic effects, the total force acting at the surface, Ψ , can be characterized as

$$\int_{\Psi} \underline{\tau}_{ij} d\Psi_i + \int_V \rho F_j dV$$

Just as in the normal Navier-Stokes derivation, this must precisely equal the net rate of change of the electromagnetic and mechanical momentum inside the control surface, Ψ , plus the mechanical momentum convected away, i.e.

$$\frac{\partial}{\partial t} \int_V [G_j + \rho u_j] dV + \int_{\Psi} \rho u_i u_j d\Psi_i = \int_{\Psi} \underline{\tau}_{ij} d\Psi_i + \int_V \rho F_j dV . \quad [\text{II-25}]$$

Using Leibniz's rule and Gauss' theorem,

$$\frac{\partial G_i}{\partial t} + \frac{\partial \rho u_j}{\partial t} + \frac{\partial \rho u_i u_j}{\partial x_i} = \frac{\partial \tau_{ij}}{\partial x_i} + \rho F_j \quad [\text{II-26}]$$

is obtained.

Now the internal shear stress tensor, $\underline{\tau}_{ij}$, given above, can be

broken into its two contributions as

$$\underline{\underline{\tau}}_{ij} = \underline{\underline{\tau}}_{ij}^e + \underline{\underline{\tau}}_{ij}^m \quad [\text{II-27}]$$

Of course, the mechanical shear stress tensor is readily obtained (12) from classical hydrodynamics,

$$\underline{\underline{\tau}}_{ij}^m = \eta_0 \left(\frac{\partial u_i}{\partial x_j} + \frac{\partial u_j}{\partial x_i} \right) - \frac{2}{3} \eta_0 \frac{\partial u_k}{\partial x_k} \delta_{ij} - p^m \delta_{ij} \quad [\text{II-28}]$$

where η_0 is the coefficient of bulk viscosity. Recalling that

$$\underline{\underline{\tau}}_{ij}^e = -p^e \delta_{ij} + D_{ei} E_j + B_i H_j \quad [\text{II-16}]$$

and that the electromagnetic momentum can be expressed as

$$\frac{\partial G_j}{\partial t} = \frac{\partial \underline{\underline{\tau}}_{ij}^e}{\partial x_i} - f_i \quad , \quad [\text{II-18}]$$

equation [II-26] is transformed into the fundamental momentum equation for magnetohydrodynamic systems

$$\rho \frac{D\vec{u}}{Dt} = \vec{\nabla} \cdot (\underline{\underline{\tau}}_{ij}^m) + \vec{f} + \rho \vec{F} \quad [\text{II-29}]$$

where the left hand side is the substantial derivative, $\underline{\underline{\tau}}_{ij}^m$, given by equation II-28, being the ordinary (mechanical) Reynolds shear tensor, \vec{f} , given by equation II-23, being the total pondermotive

force, and \vec{F} being the conventional, non-electromagnetically based external body forces. Therefore, all electromagnetic effects are concentrated in the pondermotive force term, \vec{f} ; in the absence of all field effects (except gravity, of course), \vec{f} vanishes leaving the conventional Navier-Stokes momentum balance. Thus, it could be argued that conventional fluid dynamic analysis is a highly specific implementation of the more general magnetogasdynamic analysis.

This section is closed by parenthetically adding that the work of a plasma in a field, and the magnetohydrodynamic energy, both equally as rigorously derived in Chu's analysis, will not be considered in this work owing to their complete lack of application to the specific problem considered.

Application of Equation II-29 to the Glenda Effect Problem

Before any investigation of the Glenda effect may be undertaken utilizing the foregoing analysis, it is obvious that equation II-29 must be simplified and adjusted to accommodate the conditions of the investigation as well as be broken into its componential parts. It is reiterated that all analyses will be performed in the Cartesian Space, with x in the direction of the applied field, and z vertical, and this endeavor begins by considering the pondermotive force given above,

$$\vec{f} = \rho \vec{E} + \vec{j} \times \vec{B} + \frac{1}{2} [D_{ek} \vec{\nabla} E_k - E_k \vec{\nabla} D_{ek}] + \frac{1}{2} [B_k \vec{\nabla} H_k - H_k \vec{\nabla} B_k] + \vec{\nabla} \frac{1}{2\rho} [E^2 \frac{\partial \epsilon}{\partial \rho} + H^2 \frac{\partial \mu}{\partial \rho}] \quad .$$

[II-23]

With the stipulation that there are no externally applied electric fields, despite the disappearance of the first term and the electrostrictive term, the subsequent demise of the electric excitation vector, D_{ek} , cannot as equally be assumed, since induced fields may exist. However, owing to oxygen's negligibly small electrical conductivity and its subsequent low magnetic Reynold's number in such low velocity fields, its disappearance will little effect the analysis and \vec{f} can now be written as

$$\vec{f} = \vec{j} \times \vec{B} + \frac{1}{2} [B_k \vec{\nabla} H_k - H_k \vec{\nabla} B_k] + \vec{\nabla} \frac{1}{2\rho} H^2 \frac{\partial \mu}{\partial \rho} \quad . \quad [II-30]$$

Recalling that the negligibly small magnetic pressure effects are manifested in the magnetostrictive term, generality will not be lost by considering the overall contribution of this last term to be negligibly small, especially in light of the magnitude of the other two terms. Moreover, implementation of the quite valid Boussinesq approximation of Rayleigh, used quite frequently throughout the heat transfer magnetogasdynamic literature, which neglects the variations of density except insofar as they modify the action of the gravity body force term, lends further credence to the elimination of this density dependent strictive term. Thus, the pondermotive force becomes

$$\vec{f} = \vec{j} \times \vec{B} + \frac{1}{2} [B_k \vec{\nabla}_k H_k - H_k \vec{\nabla}_k B_k] \quad [\text{II-31}]$$

In most classical systems (i.e. μ is a constant, implying $\nabla\mu=0$), the second term disappears upon implementation of the constitutive equations, II-3,4, and the very familiar Lorentz force remains, which is the traditional definition of the pondermotive force. However, in the system considered in this investigation,

$$\mu = f(T) = g(x) \quad [\text{II-32}]$$

and therefore

$$\nabla\mu \neq 0 \quad . \quad [\text{II-33}]$$

Parenthetically, it is added that both Park and the Soviet workers, incorrectly allowing this gradient to vanish under the Boussinesq approximation, were fortunate in this action, since, as will be seen, under the conditions considered, this gradient makes no contribution whatever to the velocity profile and overall heat transfer. Thus, this second term is found to be

$$\frac{1}{2}[\vec{B}\nabla\vec{H}-\vec{H}\nabla\vec{B}] = -\frac{1}{2}H^2\vec{\nabla}\mu \quad . \quad [\text{II-34}]$$

Therefore,

$$\vec{f} = \vec{j}\times\vec{B} - \frac{1}{2}I^2\vec{\nabla}\mu \quad . \quad [\text{II-35}]$$

Thus, the magnetogasdynamic momentum equation can be written as

$$\rho\frac{D\vec{u}}{Dt} = -\vec{\nabla}p_{\text{hyd}} + n_0\nabla^2\vec{u} + \vec{j}\times\vec{B} - \frac{1}{2}H^2\vec{\nabla}\mu + \rho F \quad [\text{II-36}]$$

Considering next the nature of the $\vec{j}\times\vec{B}$ term, a Maxwell equation II-19b is recalled

$$\vec{\nabla}\times\vec{H} = \frac{\partial\vec{D}}{\partial t} + \vec{j} \quad . \quad [\text{II-19b}]$$

Noting that, since the investigation is singularly concerned with steady state processes,

$$\frac{\partial \vec{D}}{\partial t} = 0 \quad , \quad [\text{II-37}]$$

$\vec{j} \times \vec{B}$ can be expressed as

$$\vec{j} \times \vec{B} = (\vec{\nabla} \times \vec{I}) \times \vec{B} \quad [\text{II-38}]$$

with a constitutive equation

$$\vec{B} = \mu \vec{H} \quad [\text{II-3}]$$

where

$$\nabla \mu \neq 0 \quad . \quad [\text{II-33}]$$

Using standard vector operator procedures, it can be shown that

$\vec{j} \times \vec{B}$ resolves in componential form, to

$$\begin{aligned} \vec{j} \times \vec{B} = & \left[\left(\frac{\partial H}{\partial z} x - \frac{\partial H}{\partial x} z \right) B_z - \left(\frac{\partial H}{\partial x} y - \frac{\partial H}{\partial y} x \right) B_y \right] \vec{i} \\ & + \left[\left(\frac{\partial H}{\partial x} y - \frac{\partial H}{\partial y} x \right) B_x - \left(\frac{\partial H}{\partial y} z - \frac{\partial H}{\partial z} y \right) B_z \right] \vec{j} \\ & + \left[\left(\frac{\partial H}{\partial y} z - \frac{\partial H}{\partial z} y \right) B_y - \left(\frac{\partial H}{\partial z} x - \frac{\partial H}{\partial x} z \right) B_x \right] \vec{k} \quad . \end{aligned} \quad [\text{II-39}]$$

Since in this investigation the externally applied field has only x character, owing to the relative magnitudes of B_x , B_y , and B_z ,

the only terms of significance become

$$\vec{j} \times \vec{B} = \left\{ \left(\frac{\partial H}{\partial x} y - \frac{\partial H}{\partial y} x \right) B_x \right\} \vec{j} - \left\{ \left(\frac{\partial H}{\partial z} x - \frac{\partial H}{\partial x} z \right) B_x \right\} \vec{k} . \quad [\text{II-40}]$$

Now the possibility of the existence of the terms $\partial H_x / \partial y$ and $\partial H_x / \partial z$ can readily be visualized as either intentional or indigenous magnetic field gradients, but the induced fields (H_y and H_z) are the result only of the bulk fluid in flow. These induced fields, however, are dependent on the induced current, \vec{j}_{ind} , via Maxwell

$$\vec{j}_{\text{ind}} = \vec{\nabla} \times \vec{H}_{\text{ind}} \quad [\text{II-41}]$$

which in turn is dependent on the velocity via the generalized Ohm's Law

$$\vec{j}_{\text{ind}} = \sigma (\vec{E} + \vec{u} \times \vec{B}) . \quad [\text{II-42}]$$

Since the applied electric field is zero, the convective velocity only vertical, and the applied field horizontal (i.e. $\vec{B} = B_x$ only), \vec{j}_{ind} can only be in the y^{th} direction. Thus, \vec{H}_{ind} can only be either in the z^{th} direction or x^{th} direction, it cannot be in the y^{th} direction. Thus, there cannot exist any H_y term or its gradient. Thus, $\vec{j} \times \vec{B}$ reduces to

$$\vec{j} \times \vec{B} = \left\{ - \left(\frac{\partial H}{\partial y} x \right) B_x \right\} \vec{j} - \left\{ \left(\frac{\partial H}{\partial z} x - \frac{\partial H}{\partial x} z \right) B_x \right\} \vec{k} \quad [\text{II-43}]$$

which, upon substitution of the constitutive equations, becomes

$$\vec{j} \times \vec{B} = \left(-\mu H \frac{\partial H}{\partial y} \right) \vec{j} + \left(\mu H \frac{\partial H}{\partial x} \frac{\partial}{\partial z} - \mu H \frac{\partial H}{\partial z} \frac{\partial}{\partial x} \right) \vec{k} \quad . \quad [\text{II-44}]$$

It is parenthetically added that when the assumption of perfect homogeneity is made, this term resolves precisely to the condition found earlier by Park and the Russian workers, i.e.,

$$\vec{j} \times \vec{B} = \mu H \frac{\partial H}{\partial x} \frac{\partial}{\partial z} \quad [\text{II-45}]$$

which is characterized solely by the additive Hartmann number as mentioned earlier, which for oxygen, of course, owing to its low electrical conductivity, is negligible. With reference to both the Russian work and Park's model, it is recalled that for fluids of negligible Hartmann number, identical velocity profiles and heat transfer rates are obtained whether this effect is incorporated or not. This conclusion is further substantiated by the fact that the negligible magnetic Reynold's number demands a vanishingly small induced field in any direction. Thus having eliminated the induced gradient, $\vec{j} \times \vec{B}$ can now be written as

$$\vec{j} \times \vec{B} = \left[-\mu H \frac{\partial H}{\partial x} \frac{\partial}{\partial y} \right] \vec{j} + \left[-\mu H \frac{\partial H}{\partial z} \frac{\partial}{\partial x} \right] \vec{k} \quad . \quad [\text{II-46}]$$

Having a refined description of the $\vec{j} \times \vec{B}$ term in the magnetogas-dynamic momentum equation applicable to the system currently under

investigation, equation II-36 can now be written as

$$\rho \frac{D\vec{u}}{Dt} = -\nabla p_{\text{hyd}} + \eta_0 \nabla^2 \vec{u} + \left(0\vec{i} - (\mu H \frac{\partial H}{x \partial y}) \vec{j} - (\mu H \frac{\partial H}{x \partial z}) \vec{k} \right) - \frac{1}{2} H^2 \nabla \mu + \rho \vec{F}. \quad [\text{II-47}]$$

Considering the gradient of the scalar permeability term,

$$-\frac{1}{2} H^2 \nabla \mu = -\frac{1}{2} H^2 \frac{\partial \mu}{\partial x} \vec{i} \quad [\text{II-48}]$$

is found since $\mu = \mu(T(x))$ only. Visualizing the external body force to be only that associated with gravity, i.e.

$$F_z = g, \quad [\text{II-49}]$$

and assuming that steady, laminar flow exists only in the z^{th} direction, the magnetogasdynamic momentum equations applicable to this investigation, in their componential form, become

(i) x component:

$$-\frac{\partial p_{\text{hyd}}}{\partial x} = \frac{1}{2} H^2 \frac{\partial \mu}{\partial x} \quad [\text{II-50a}]$$

(ii) y component:

$$-\frac{\partial p_{\text{hyd}}}{\partial y} = \mu H \frac{\partial H}{x \partial y} \quad [\text{II-50b}]$$

(iii) z component (with which we are singularly interested):

$$\frac{\partial p}{\partial z} \text{hyd} + \mu H_x \frac{\partial H}{\partial z} = \eta_0 \frac{\partial^2 u}{\partial x^2} + \rho g \quad . \quad [\text{II-50c}]$$

The momentum analysis is concluded by observing that for "perfectly" homogeneous fields, this system reduces to the ordinary Navier-Stokes analysis, which for convective transfer, leads to normal Grashof characterization. Thus, it is easy to see the rationale that Park must have used to focus the only seemingly possible magnetic effect into the changes in density initiated by magnetic pressure - an apparently perfectly valid conclusion for absolutely gradient-free conditions, despite its gross violation of the Boussinesq approximation itself, a condition Park seems to have overlooked. However, upon close inspection of the field-field gradient product in equation II-50c, owing to the traditionally large magnitude of the absolute applied field strength at which values most laboratory "homogeneous" magnets are operated (1-100 thousands Oersteds), almost any non-zero field gradient can lead to a substantial field-field gradient product and subsequently profoundly influence the velocity distribution. Of course, all laboratory magnets, even exotic homogeneous ones, are indeed, quite real, and have, by their very nature, minute, but most assuredly non-vanishing, characteristic, inherent field inhomogeneities. It is precisely to such an indigenous field gradient of the magnetic system used that the anomalous results found in these laboratories are attributed.

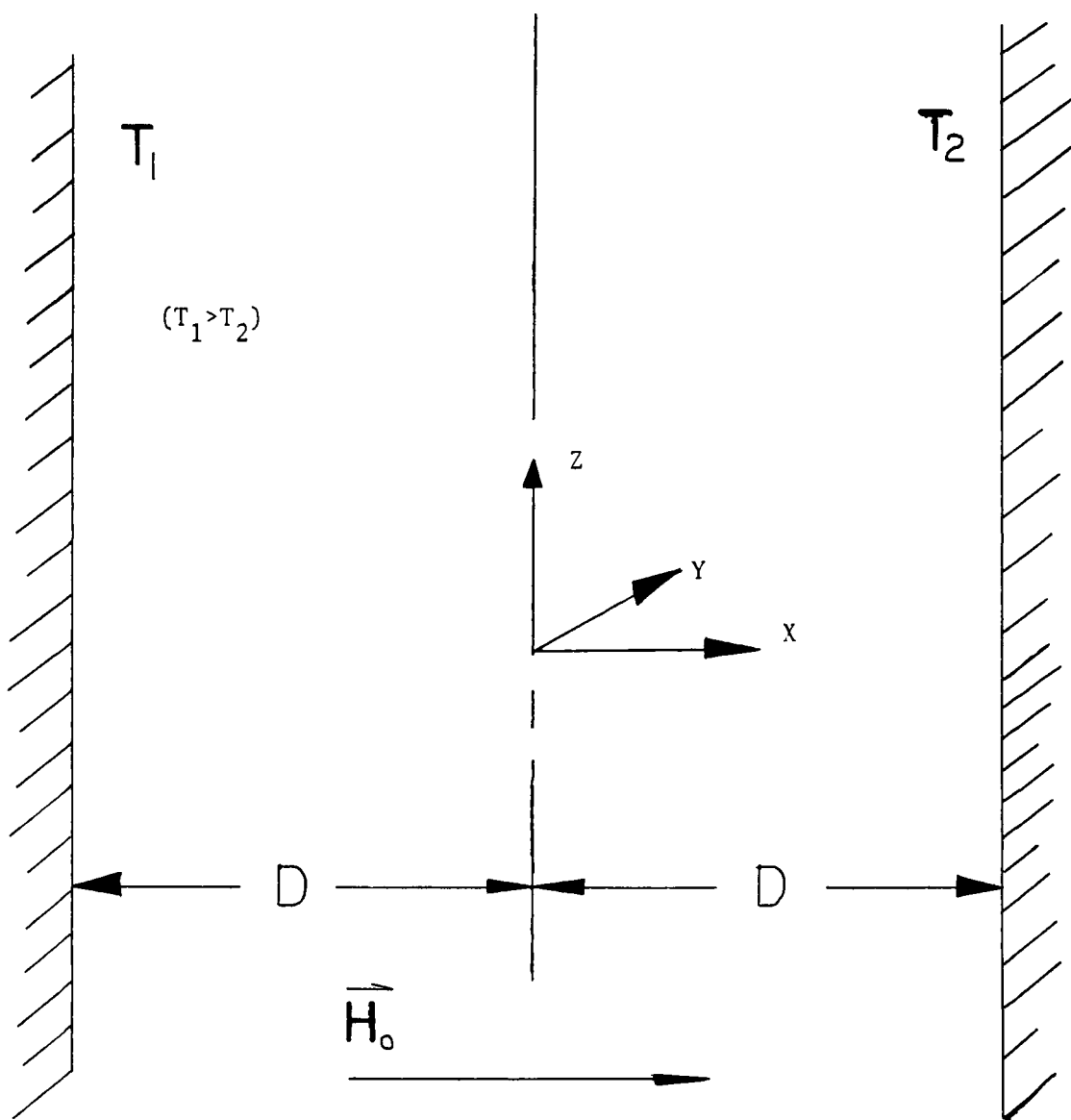
CHAPTER III

DERIVATION OF THE GLENDA EFFECT MODEL: A NEW MAGNETOCONVECTIVE HEAT TRANSFER MODEL

Introduction

Before considering the direct application of the set of momentum equations derived in the previous chapter to describe the dynamic aspects of the Glenda effect, the specific boundary conditions of the system analyzed in this thesis are considered in the simplified geometry of Figure II. The fluid (oxygen in this particular application), is confined between two rigid, semi-infinite, vertical, parallel plates separated by a distance of $2D$, held at the steady uniform temperatures T_1 and T_2 , respectively, with $T_1 - T_2 \equiv \Delta T > 0$. The origin of the Cartesian space is placed midway between the plates with the positive x axis directed normal to the lower temperature plate and the positive z axis oriented vertically, anti-symmetric with gravity (requiring then, the value of gravity to be g , i.e. -980cm/sec^2). A steady, very nearly uniform, "homogeneous" external magnetic field, \vec{H}_0 , having a small but nonetheless a non-vanishing, characteristic field gradient, is applied perpendicularly to the plates so that $H_0 = H_x$.

The complete treatment of thermal convection in an external electromagnetic field, of course, must additionally satisfy the equations



FLAT PLATE GEOMETRY

FIGURE II

for conservation of mass and energy as well as the momentum balance. As Chu points out, provided the induced fields are negligible (true for low magnetic Reynolds and Hartmann numbers as in the case of oxygen considered here), the continuity equation remains unchanged as the normal hydrodynamic conservation relations (12), or

$$\vec{\nabla} \cdot (\rho \vec{u}) = - \frac{\partial \rho}{\partial t} \quad , \quad [\text{III-1}]$$

for steady state processes resolving to

$$\vec{\nabla} \cdot \vec{u} = 0 \quad . \quad [\text{III-2}]$$

Ignoring the electromagnetically induced contributions to the energy of the convecting system (traditionally valid for fluids of even moderate Hartmann and magnetic Reynolds number, such as mercury), the conventional Prandtl energy balance of normal hydrodynamics (12) is implemented to obtain the temperature distribution across the gradient,

$$\vec{u} \cdot \vec{\nabla} T = \text{Pr}^{-1} \vec{\nabla}^2 T \quad [\text{III-3}]$$

where Pr is the Prandtl number. In this application of semi-infinite plates, we again assume only vertical laminar flows, i.e. $u_x = u_y = 0$ (valid for relatively low temperature gradients in the direction indicated, independent of the x and y body forces), and experimentally strive for this condition by designing a cell with as large an L/D as

possible, where L is the overall length of the actual cell. This constraint, of course, requires the z -directed velocity to be steady and concomitantly requires a linear, molecular, temperature distribution, i.e. $T=T(x)$ only, or

$$\nabla^2 T = 0 \quad \text{[III-4]}$$

as is considered in normal Grashof convective analysis. With the boundary conditions on the temperature distribution of

$$T = T_1 \quad \text{at} \quad x = -D \quad \text{[III-5]}$$

$$T = T_2 \quad \text{at} \quad x = D \quad , \quad \text{[III-6]}$$

the expected linear dimensionalized temperature distribution, a function only of x , becomes

$$T = - \frac{\Delta T}{2D} x + T_0 \quad \text{[III-7]}$$

Thus having a viable continuity relation, a valid temperature distribution, and a workable system of momentum equations, the actual modelling of the Glenda effect can now be undertaken.

Modelling of the Velocity Distribution of the Glenda Effect

This section is begun by re-writing the final products of this resolution effort for energy, mass and momentum balance for the investigation considered in their componential forms:

(i) mass:

$$u_y = u_x = 0 \quad \text{[III-8a]}$$

$$u_z \neq 0, \quad \frac{\partial u}{\partial z} = 0 \quad \text{[III-8b]}$$

(ii) energy (T=f(x)):

$$T = -\frac{\Delta T}{2D} x + T_0 \quad \text{[III-7]}$$

(iii) momentum (where interest singularly lies):

(a) xth component:

$$-\frac{\partial p}{\partial x} \text{hyd} = \frac{1}{2} H^2 \frac{\partial \mu}{\partial x} \quad \text{[III-9]}$$

(b) yth component:

$$-\frac{\partial p}{\partial y} \text{hyd} = \mu H \frac{\partial H}{x \partial y} \quad \text{[III-10]}$$

(c) zth component:

$$\frac{\partial p}{\partial z} \text{hyd} + \mu H \frac{\partial H}{x \partial z} = \eta_0 \frac{\partial^2 u}{\partial x^2} z + \rho g \quad \text{[III-11]}$$

As was done in Chapter II, it has been tacitly assumed that flow exists only in the z direction, a fact that appears to disagree with the spirit of the x and y components of the momentum equation stipulating the existence of non-zero body forces in each direction when subjected to a field. When in fact motion cannot be completely assumed uniquely z-directed, as can be shown, for modelling purposes, the majority of the flow can indeed be considered z-directed for low magnetic body forces owing to the overriding presence of the gravity body force. Visualizing for the moment the case of a vanishing temperature gradient, the x-directed pressure gradient vanishes ($\nabla\mu=0$ now), the y component pressure gradient becomes identical to the field-field gradient (y direction) product magnetic body force, and the z component reflects the sum of the gravity body force and the z-directed field-field gradient product magnetic body force and no motion results whatever. Upon implementation of a gradient in the temperature, the resulting analogous changes in both the density and the paramagnetic permeability cause the initiation of a z velocity; the permeability changes also initiate a slight heat transfer increase in the x and y directions from the vertical hot plate not unlike a conventional horizontal hot plate convecting into a quiescent fluid of cooler temperature, which for small ΔT 's, can occur independent of motion, quite unlike the vertical analogue where motion is always associated with any ΔT . Additionally, the regions over which both the x and y magnetic body forces act are very much smaller than the corresponding z forces. Thus, in light of the differing magnetic forces

and a z acting gravity force, for the gradients anticipated throughout the entire "homogeneous" magnet, it is felt that the velocity will largely be z-directed, thereby simplifying enormously the analysis through the elimination of the inertial terms in the momentum equation. It is parenthetically added that this is by no means a universally applicable assumption for all magnet systems; indeed, as will be seen shortly, in the case of the superconducting magnet, possessing a large z-directed field with large gradients in all directions, it is considered that its associated increased heat transfer contribution arises solely from just such an x and y directed motion, not from any increased z directed velocity. As a final confirmation of the validity of this assumption of z velocity preponderance, the Carruthers and Wolfe work is cited wherein only vertical velocities were observed in smoke tracer studies in the presence of large gradients. Thus, for the particular case of the x-directed magnetic field, attention is focused solely on the zth component momentum equation as written and the linear temperature distribution.

Allowing, for the moment, the magnetic body force, $H_x \frac{\partial H}{\partial z}$, to take on only non-vanishing constant values, h, defined as

$$h \equiv H_x \left(\frac{\partial H}{\partial z} \right) \quad , \quad \text{[III-12]}$$

tacitly implies that the indigenous field gradient is i) uniformly linear over the applicable region, and ii) its magnitude, with respect to H_x itself, is quite small, thus allowing the absolute magnitude of

the applied magnetic field strength to additionally be considered a constant. Indeed, in the investigation conducted by Carruthers and Wolfe (10) wherein highly linear but nonetheless huge field gradients existed, the field-field gradient product over the distance of the field of concern was highly non-linear as expected thus precluding this constant assumption to that particular work. However, in the case of high-quality, "homogeneous" laboratory magnets, such as used in this study, any inherent gradient will indeed be small when compared to the value of the applied field itself. Thus, equation III-11 can now be written

$$\frac{\partial p}{\partial z} \text{hyd} + \mu h = n_0 \frac{\partial^2 u}{\partial x^2} z + \rho g \quad . \quad [\text{III-13}]$$

Before proceeding further, a short discussion on the striking similarity of the two body forces per unit volume, μh and ρg , is considered.

First, both of the agents responsible for the forces (h and g) are z -directed constants - one always acts in a negative direction (g) and the other (h) can adopt any sense contingent on the sign of the field-field gradient product. Second, the coefficients (μ and ρ), both of whose magnitude solely determines the net effect of the body force on the velocity distribution, are not only both functions of x i.e.

$$\mu = f_1(T) = g_1(x) \quad [\text{III-14a}]$$

$$\rho = f_2(T) = g_2(x) \quad [\text{III-14b}]$$

but both have analogous temperature dependence as can be seen upon inspection of equations I-5 and 6 and the ideal equation of state, i.e.

$$\mu \propto \frac{1}{T} \quad \text{[III-15a]}$$

$$\rho \propto \frac{1}{T} \quad \text{[III-15b]}$$

Thus, it is not surprising then, to expect that both μh and ρg will behave most analogously under these conditions. Under this assumption then, what follows is merely a simple extension of the normal Grashof-type convection analysis to include the effects of this new and wholly analogous term.

Reiterating that it was assumed that magnetic pressure has negligible influence on the density leading to changes in velocity (recall that the magnetoconvection number, Mc , which manifests this effect, was negligibly small, and that the Boussinesq approximation requires its elimination), density is expanded in a Taylor's series only in temperature about the average temperature of the system, T_o , i.e.,

$$\rho = \rho_o \left(1 - \beta(T - T_o) \right) \quad \text{[III-16]}$$

where

$$T_o \equiv \frac{1}{2}(T_1 + T_2) \quad \text{[III-17]}$$

and β defines the coefficient of thermal expansion,

$$\beta \equiv - \frac{1}{\rho_o} \left(\frac{\partial \rho}{\partial T} \right) p \Big|_{T_o} . \quad [\text{III-18}]$$

A similar expansion is performed on the magnetic permeability, μ , about this same temperature T_o and its associated permeability, μ_o ,

$$\mu = \mu_o \left(1 - \gamma(T - T_o) \right) \quad [\text{III-19}]$$

where the previously unreported term, γ , defined by

$$\gamma \equiv - \frac{1}{\mu_o} \left(\frac{\partial \mu}{\partial T} \right) p \Big|_{T_o} , \quad [\text{III-20}]$$

has been aptly named in this work the coefficient of thermomagnetic permeability. It has been tacitly assumed in both expansions that, over the small temperature gradients utilized, the second - and higher - ordered terms in the expansion are negligible and therefore deleted.

Placing these expansions in the momentum equation III-13,

$$\frac{\partial p}{\partial z} \text{hyd} + \mu_o h \left(1 - \gamma(T - T_o) \right) = \eta_o \frac{\partial^2 u}{\partial x^2} z + \rho_o g \left(1 - \beta(T - T_o) \right) \quad [\text{III-21}]$$

is obtained. Again using the reasoning similar to that employed in conventional free convection analysis and keeping in mind that $\mu_o h$ is just as viable a body force as is $\rho_o g$, the pressure gradient in the system must be a result of both the weight of the fluid and its

completely analogous magnetic partner; if this were not exactly true, a net bulk flow in one direction would result - a direct violation of the mass balance over any Δz required owing to the existence of closed ends, which, although far removed at infinity, are nonetheless quite solid and impermeable. Thus the total pressure gradient can be written as

$$\frac{\partial p}{\partial z} \text{hyd} = - \mu_0 h + \rho_0 g \quad [\text{III-22}]$$

rendering the force balance equation III-21 to be

$$- \mu_0 h \gamma (T - T_0) = \eta_0 \frac{\partial^2 u}{\partial x^2} z - \rho_0 g \beta (T - T_0) \quad . \quad [\text{III-23}]$$

Rearranging the temperature distribution equation III-7 in terms of T_0 and T , and substituting this linear expression of the temperature into equation III-23 and rearranging, the equation

$$\eta_0 \frac{\partial^2 u}{\partial x^2} z = \mu_0 h \gamma \frac{\Delta T}{2D} x - \rho_0 g \beta \frac{\Delta T}{2D} x \quad [\text{III-24}]$$

is obtained, the physical meaning of which is that the viscous forces (i.e. the left hand side) are just balanced by the sum of the buoyant forces and the magnetic forces (the right hand side). Combining,

$$\eta_0 \frac{\partial^2 u}{\partial x^2} z = \frac{\Delta T}{2D} x (\mu_0 h \gamma - \rho_0 g \beta) \quad [\text{III-25}]'$$

is obtained, clearly indicating again, the analogous behavior of the two forces involved.

Safely passing to the total derivative in velocity owing to its singular dependence on x , and dividing by the absolute viscosity,

$$\frac{d^2u}{dx^2} = \frac{\Delta T x}{2D\eta_0} (\mu_0 h \gamma - \rho_0 g \beta) \quad [\text{III-26}]$$

is obtained. Since all the terms inside the parenthesis are constant, adding that even if h is no longer considered a constant but some function of z as is the case considered later, this same quantity still remains constant with respect to x making the integration trivial.

Defining this constant to be Γ ,

$$\Gamma \equiv \frac{\Delta T}{2D\eta_0} (\mu_0 h \gamma - \rho_0 g \beta) \quad , \quad [\text{III-27}]$$

and integrating to find the velocity profile,

$$u_z = \frac{\Gamma x^3}{6} + C_1 x + C_2 \quad [\text{III-28}]$$

is obtained. Implementing the strong boundary conditions of zero slip at the wall and mass balance over any thickness Δz , analogously employed in free-convection analysis, i.e.

$$1. \quad u_z = 0 \quad \text{at} \quad x = \pm D \quad [\text{III-29a}]$$

and

$$2. \int_{-D}^D u_z(x) dx = 0 \quad , \quad [\text{III-29b}]$$

provides the dimensionalized velocity profile of a vertically convecting fluid across a temperature gradient subjected to an applied magnetic field with a non-vanishing gradient:

$$u_z = \frac{\Gamma}{6} (x^3 - xD^2) \quad . \quad [\text{III-30}]$$

As is customary engineering procedure, this equation is rendered non-dimensional through implementation of the following relations, in conjunction with the well-known viscosity relation,

$$\nu_o = \frac{\eta_o}{\rho_o} \quad [\text{III-31}]$$

$$(a) \quad x = x^*D \quad [\text{III-32a}]$$

$$(b) \quad u_z = \frac{\nu_o u_z^*}{D} \quad [\text{III-32b}]$$

$$(c) \quad T = T^*\Delta T \quad [\text{III-32c}]$$

where the * refers to the corresponding dimensionless variables, and the non-dimensional expression of the velocity distribution becomes

$$u_z^* = \frac{1}{12} \left[\frac{\mu_o h \gamma \Delta T D^3}{\rho_o \nu_o^2} - \frac{g \beta \Delta T D^3}{\nu_o^2} \right] (x^{*3} - x^*) \quad . \quad [\text{III-33}]$$

This second term, of course, is the well-known dimensionless Grashof number, Gr. The Grashof number can then be defined as

$$\text{Gr} \equiv -g\beta \frac{\Delta T D^3}{\nu_o^2} \quad [\text{II-34}]$$

where, for the ideal gas approximation, β , the thermal expansion coefficient can simply be expressed as

$$\beta = \frac{1}{T_o} \quad . \quad [\text{III-35}]$$

The nature of this first term, which concentrates all magnetic effects, however, is not as recognizable. Using previously defined relations, this term can be expressed as

$$\frac{\mu_o h \gamma \Delta T D^3}{\rho_o \nu_o^2} = -h \frac{\Delta T D^3}{\rho_o \nu_o^2} \left. \frac{\partial \mu}{\partial T} \right|_{P, T_o} \quad [\text{III-36}]$$

where all terms are readily definable or measureable except the thermo-magnetic permeability, the sensitivity of the magnetic permeability with temperature.

The treatment of this term, however, presents no special problems since the permeability can be related to temperature via its own defining equation and the Curie Law (see equations I-5,6). These relations, notwithstanding, cannot be immediately implemented since the traditional Curie Law, as stated in equation I-6, is in terms of the molar susceptibility (i.e. susceptibility, or really, permeability per unit mole), all available literature expressing the molar paramagnetic susceptibility

Curie constant, C , in these terms. Dividing these molar values by the molecular weight, M , of the species involved (for this application, $M=32 \text{ gmol}^{-1}$) and multiplying by the density, ρ_0 , valid in the Boussinesq approximation, returns the susceptibility to the units demanded by the momentum equation, force per unit volume. Using the ideal equation of state to define ρ_0 ,

$$\rho_0 = \frac{pM}{RT_0} \quad [\text{III-37}]$$

and the extension of equation I-5, the volumetric permeability can be expressed as

$$\mu \Big|_{\text{vol}} = 1 + \frac{Cp}{RT_0^2} \quad [\text{II-38}]$$

where C is the molar Curie constant. Differentiating this with temperature, and evaluating at T_0 as required by equation III-36, the thermomagnetic permeativity

$$\left. \frac{\partial \mu}{\partial T} \right|_p \Big|_{T_0} = -2 \frac{Cp}{RT_0^3} \quad [\text{III-39}]$$

is obtained. Thus, the first term in the velocity distribution (i.e. equation III-36) can now be written as

$$\left(\frac{\Delta T D^3}{\rho_0 \nu_0^2} \cdot \frac{2hCp}{RT_0^3} \right) \cdot$$

But

$$p = \frac{\rho_o RT_o}{M} \quad , \quad [\text{III-40}]$$

valid again under the Boussinesq approximation, in conjunction with the definition of h , implies this term to resolve to a new, previously unreported dimensionless group, defined by

$$Gl \equiv 2 \frac{D^3 \Delta T}{\nu_o^2} \left(\frac{C}{MT_o} \right) H_x \left(\frac{\partial H}{\partial z} x \right) \quad , \quad [\text{III-41}]$$

henceforth referred to as the Glenda number, which characterizes the magneto thermal contribution to the total heat transfer just as the Grashof number characterizes the natural thermal contribution. This new number, of course, merely adds to the normal dimensionless convective velocity profile as did the magnetoconvection number, Mc

$$u_z^* = \frac{1}{12} (Gr + Gl) (x^{*3} - x^*) \quad . \quad [\text{III-42}]$$

Quite obviously, when $H=0$ (no field case), the Glenda number vanishes and the profile resolves to normal Grashof convection as expected. Moreover, the sign of the Glenda number can be of any value contingent on the sense of the field-field gradient product, thus accounting for increases and decreases in magnetoconvective heat transfer as observed (5,10).

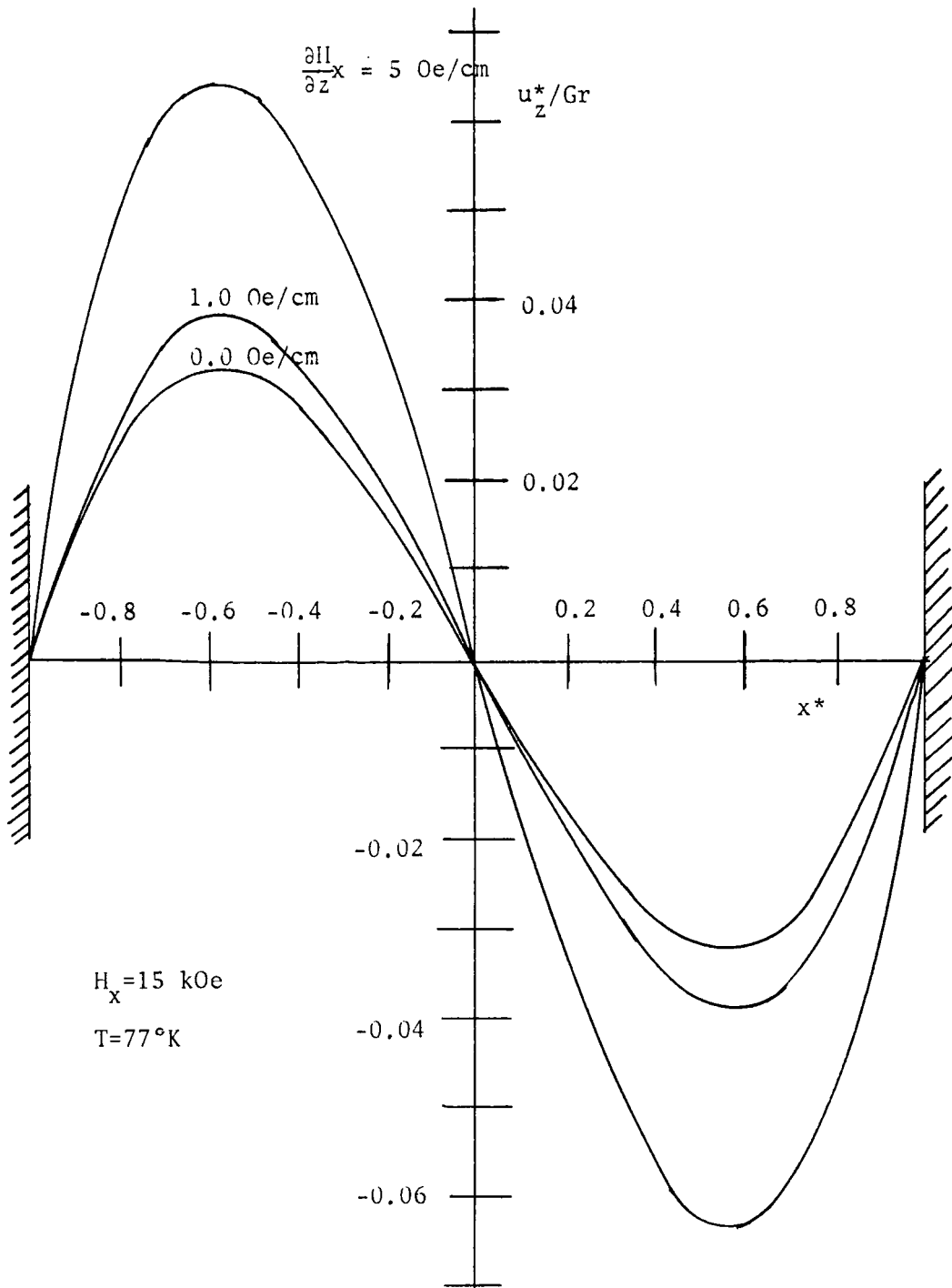
Just as in Park's analysis of magnetic pressure, the ratio of the velocity over the entire range of values of the fluid in a field to that over the same range out of a field, gives an indication of the increase in convective heat transfer from magnetic effects. This ratio, defined by ϕ , which experimentally was found to be on the order

$$\phi \equiv \frac{G1}{Gr} = -2 \frac{CH}{MT_0 g} \left(\frac{\partial H}{\partial z} x \right) \quad [\text{III-43}]$$

of 20%, however, cannot a priori be computed as could the analogous magnetoconvective ratio, Mc/Gr owing to the unknown nature of the field gradient associated with the magnet system used. Indeed, the particular magnet utilized was prized for having no gradient whatsoever. Nonetheless, theoretical velocity profiles were obtained by dividing the velocity distribution, equation III-42, by the Grashof number,

$$\frac{u^*}{Gr^z} = \frac{1}{12} (1 + \phi) (x^{*3} - x^*) \quad , \quad [\text{III-44}]$$

thus allowing ϕ to be a parameter wherein all terms remain fixed except the field gradient which was allowed to take on half decade values from 10^{-4} to 10^2 Oecm⁻¹. Three such profiles with gradient values zero, one and five Oecm⁻¹, respectively, allowing $C=1.02$ ergs^oKmol⁻¹Oe⁻², $H_x=15k$ Oe, $T_0=77^\circ K$, to be fixed, are shown in Figure III. From these distributions, it can be estimated that, provided the Glenda effect model is indeed correct, an increase in convective heat transfer on the



VELOCITY PROFILES FOR OXYGEN GAS IN APPLIED MAGNETIC FIELDS
WITH FIELD GRADIENTS AS PARAMETERS

FIGURE III

order of 20% (a direct consequence of an increased velocity distribution) would require a field gradient on the order of one to five Oersteds per centimeter, probably closer to one than five. Additionally, this same simulation study showed that under these conditions, the larger field gradients (e.g. 100 Oe/cm) render the Grashof contribution insignificant to the overall heat transfer velocity profiles, now completely magnetically controlled and obviously no longer laminar and indeed probably quite turbulent, explaining at least in part not only the marked effects observed earlier by Carruthers and Wolfe at even higher field gradients and at higher temperatures, but their apparent difficulty in modelling the Glenda Effect, giving only the token analysis.

That characteristic gradients on the order of Oersteds/cm can exist in traditionally "homogeneous" magnet systems is reflected not only in scientific intuition regarding real laboratory instrumentation in general coupled to the huge absolute magnitudes of the applied fields (≈ 15 k Oe), but also in a technical data sheet of a high quality homogeneous magnet system supplied by a well known competitor of the system used in this work in which the indigenous field inhomogeneity was indeed on the order of Oersteds/cm. Unfortunately, no such analogous material was available for the particular magnet system used in the studies conducted in these laboratories and the prospects of measuring such a change over 15k looked indeed rather dim. This section is closed with the observation in retrospect that, provided the measured effect was indeed the Glenda effect and its associated model as given above is correct, it is of almost unbelievable good fortune that the study was indeed

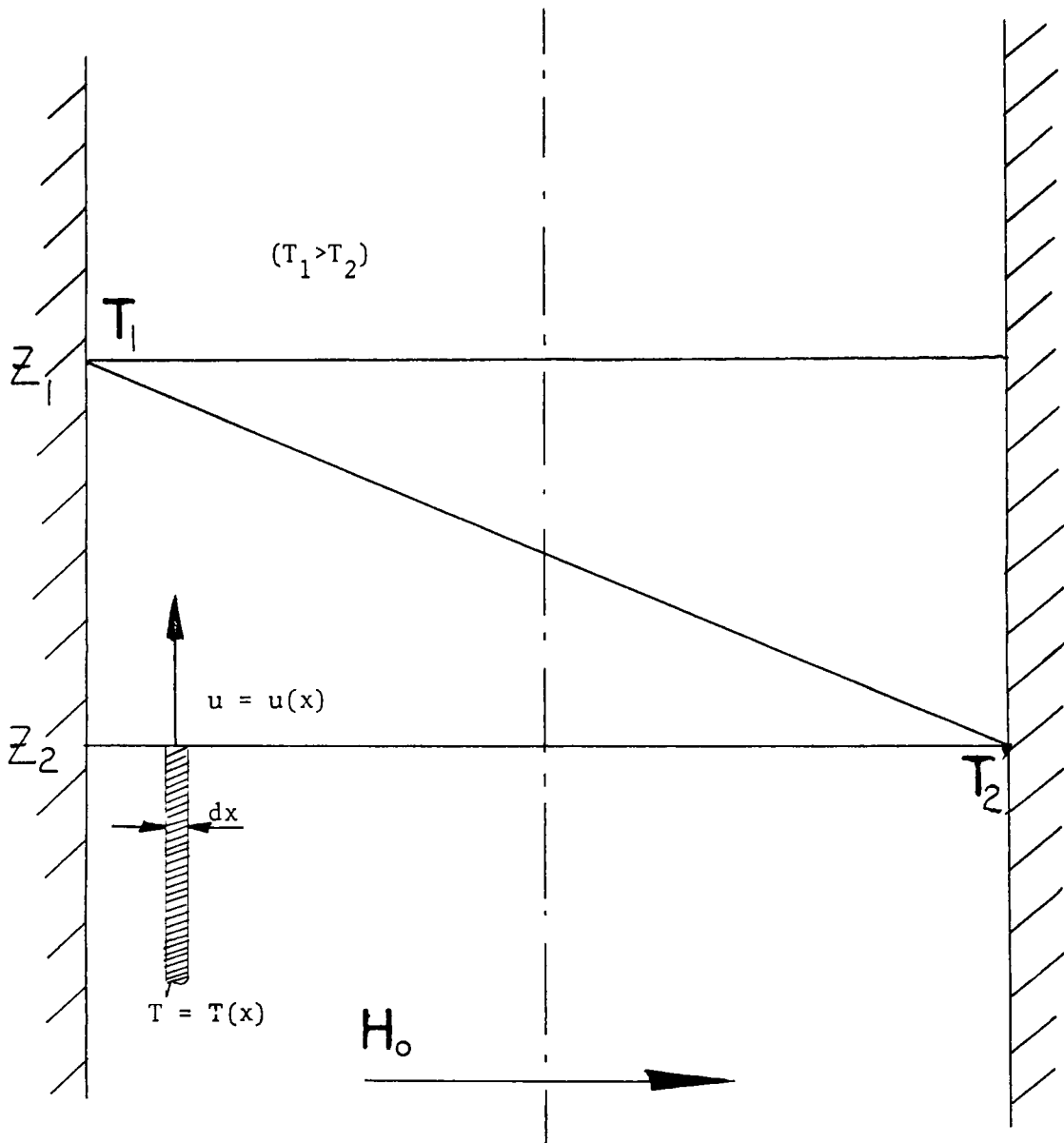
performed on a "homogeneous" magnet system - since the Glenda effect is so markedly sensitive to the field gradient, any system other than a "homogeneous" one would most assuredly have caused extreme modeling difficulties insofar as eventual agreement with available experimental results.

A Heat Transfer Model of the Glenda Effect

For all practical purposes, elucidation of the correct velocity profile for the Glenda effect represented the greatest hurdle in this theoretical venture to describe the behavior of paramagnetically susceptible fluids in a magnetic field. Since the Glenda number, which singularly concentrates all magnetic effects in convection processes, merely adds to the conventional Grashof number of free convection, the heat transfer model of which has been thoroughly investigated (13), the magnetic extension of this self-same model will be presented here for completeness and academic interests only.

This heat transfer is visualized to occur in a control volume defined in Figure IV, where $|z_1 - z_2| \equiv \Delta z > 0$ and the volume extends a distance ℓ in the y axis. For all z , the media has a linear temperature gradient as shown across the control volume from T_1 to T_2 as discussed earlier. For heat transfer purposes (which of course has no explicit x dependence), this control volume is considered to be perfectly mixed and thus have a uniform temperature of $T_o = 1/2(T_1 + T_2)$. An arbitrary fluid element of thickness dx and depth ℓ is convected into (or for that matter, out of) the control volume at a velocity $u_z = u_z(x)$ at a temperature $T = T(x)$. Assuming a constant value for the heat capacity at constant volume, C_v , over the small temperature gradient considered, the heat transferred by that element of fluid can be represented as

$$q = \dot{m} C_v \Delta T_o \quad [III-45]$$



HEAT TRANSFER MODEL FOR LAMINARLY CONVECTING GASES

FIGURE IV

where \dot{m} is the time rate of change of the mass into (or out of) the control volume, and ΔT_0 is the temperature difference between that particular fluid element and the control volume. Now in light of

$$\dot{m} = \rho_0 u_z(x) A \quad \text{[III-46]}$$

and

$$A = \ell dx \quad , \quad \text{[III-47]}$$

the heat transferred into (or away from) the control volume by that fluid element can now be represented in more amenable terms

$$q = \rho_0 C_V u_z(x) \ell (T - T_0) dx \quad , \quad \text{[III-48]}$$

where the Boussinesq approximation has been utilized again in equation III-46 to consider only the reference density, ρ_0 . Visualizing the heat transferred to be that convected away from the hotter plate, T_1 , in the positive z direction, this expression is integrated over all z from $-D$ to 0 to obtain the total heat transferred, or,

$$Q = \rho_0 C_V \ell \int_{-D}^0 u_z(x) (T - T_0) dx \quad . \quad \text{[III-49]}$$

Of course, in the particular case of a real, close-ended cell, this heat eventually is dissipated into the cooler wall via the closed top

end, hopefully in a subtle manner. Additionally, owing to very real fabrication constraints on the construction of the cell (e.g. the hotter plate must have an extremely low thermal mass, i.e. thin, to respond rapidly to changes in temperature), the actual cells, in both the cylindrical and rectangular geometries, were symmetric about a thin hot plate of T_1 . Thus having two symmetrical cold plates at T_2 and concomitantly two vertical convecting zones in which heat is equally transferred, the total heat transferred from the hotter plate will, of course, be twice the value given in equation III-49. In light of this, re-dimensionalizing the velocity distribution and integrating, the total heat transferred

$$Q = (Gr + G1) \frac{\rho \cdot v \cdot \ell \Delta T C_v}{90} \quad \text{[III-50]}$$

is obtained. Of this total value, that arising solely from the Glenda effect, can be represented as the magnetothermal contribution to the overall heat transfer, or

$$Q_{G1} \equiv G1 \rho \cdot C_v \cdot v \cdot \ell \frac{\Delta T}{90} \quad \text{[III-51]}$$

Using the definition of the Glenda number given in equation III-41, and provided C_v is given in calories $^{\circ}\text{K}^{-1}\text{gm}^{-1}$ and the Curie constant in the traditional $\text{ergs}^{\circ}\text{Kmol}^{-1}\text{Oe}^{-2}$, this Glenda effect contribution, in milliwatts, can be given as

$$Q_{G1} = \frac{\rho_o \Delta T^2 C \& D^3 C}{45 \nu_o T_o^2 M} \nu \omega H_x \left(\frac{\partial H}{\partial z} x \right) \quad [\text{III-52}]$$

where ω is the conversion constant between milliwatts and calsec⁻¹ given by

$$\omega \equiv 4.18 \times 10^3 \text{ mWseccal}^{-1} \quad . \quad [\text{III-53}]$$

Lumping all terms in equation III-52 which remain constant with pressure, temperature and field changes, the sensitivity of this Glenda effect heat transfer term to the variable parameters can be expressed as

$$Q_{G1} \propto \frac{\rho_o \Delta T^2}{\nu_o T_o^2} H_x \left(\frac{\partial H}{\partial z} x \right) \quad . \quad [\text{III-54}]$$

To ascertain the functional dependence of this term to the experimentally measureable quantities pressure, temperature and field strength, the density, ρ_o , and kinematic viscosity, ν_o , must be broken into their substituent components. As has been done in the past, the ideal equation of state is utilized to characterize the density

$$\rho_o = \frac{pM}{RT} \quad [\text{III-55}]$$

or, if the temperature is in degrees Kelvin and pressure in torr, then

$$\rho_o = \left(\frac{p}{T}\right) (5.118 \times 10^{-4}) \quad [\text{III-56}]$$

is obtained in CGS units for oxygen. For similar reasons, the kinetic theory is utilized to characterize the kinematic viscosity via the absolute viscosity, η_o , through elementary kinetic theory (15), which requires that viscosity have the temperature dependence given by

$$\eta_o = \frac{\bar{c} m_a}{2\sqrt{2}\pi\sigma_o^2} \quad [\text{III-57}]$$

where m_a is the mass of an atom, σ_o is the collision cross sectional area and \bar{c} is the average molecular speed, given by

$$\bar{c} = \frac{\sqrt{8RT_o}}{\sqrt{\pi M}} \quad [\text{III-58}]$$

which, of course, is based on the simple Boltzmann distribution of molecular velocities. Thus,

$$\eta_o = \frac{m_a}{2\sqrt{2}\pi\sigma_o^2} \frac{\sqrt{8RT_o}}{\sqrt{\pi M}} \quad [\text{III-59}]$$

or, for the case of oxygen (15), for which the molecular collision cross sectional area is found to be 3.57 \AA^2 (15),

$$\eta_{o2}^0 = 1.21 \times 10^{-5} \sqrt{T} \quad [\text{III-60}]$$

in CGS units and T in degrees Kelvin. Not content, however, with the large discrepancy between these values and those from the literature (16), an empirical equation was found (16) and used in lieu of the kinetic theory

$$\eta_o = \hat{\eta}_o \left(\frac{\hat{T}_o + A}{T_o + A} \right) \left(\frac{T_o}{\hat{T}_o} \right)^{\frac{3}{2}} \quad [\text{III-61}]$$

which computes the absolute viscosity η_o at any temperature T_o in CGS units based on the viscosity $\hat{\eta}_o$ at some given temperature \hat{T}_o and constant A. For oxygen,

$$\hat{\eta}_o = 203.9 \times 10^{-6} \text{ poise} \quad [\text{III-62a}]$$

$$\hat{T}_o = 296 \text{ }^\circ\text{K} \quad [\text{III-62b}]$$

$$A = 127 \quad . \quad [\text{III-62c}]$$

In this same parameter estimation vein, the specific heat at constant volume is computed from the kinetic theory (15) which stipulates four contributions to the constant volume specific heat for linear molecules:

$$\text{i) Translational} \quad \frac{3}{2}R \quad [\text{III-63a}]$$

$$\text{ii) Rotational (linear)} \quad R \quad [\text{III-63b}]$$

$$\text{iii) Vibrational} \quad \frac{R\hat{x}^2 \exp(\hat{x})}{(\exp(\hat{x}) - 1)^2} \quad [\text{III-63c}]$$

$$\hat{x} = \frac{\tilde{\epsilon}}{kT_o} \quad [\text{III-64}]$$

iv) Electronic

-0-

[III-64]

where $\bar{\epsilon}$ is the vibrational energy level spacing, on the order of 10^{-13} ergs for most diatomics. At the low temperatures at which these investigations were conducted, the vibrational contribution to the total heat capacity is negligible and the term resolves simply to

$$C_v = \frac{3}{2}R + R = 0.15 \text{ cal } ^\circ\text{K}^{-1} \text{ gm}^{-1} \quad [\text{III-65}]$$

which, not surprisingly, is in excellent agreement with the available literature (16) at those temperatures.

Having these relations then, equation III-54, written

$$Q_{G1} \propto \frac{\rho_o \Delta T^2}{v_o T_o^2} H_x \left(\frac{\partial H}{\partial Z} x \right) \quad [\text{III-54}]$$

with

$$\rho_o \propto \frac{p}{T_o} \quad [\text{III-66}]$$

and

$$v_o \propto \frac{T_o^2}{p} \quad , \quad [\text{III-67}]$$

can be expressed in terms of functionally measureable variables as

$$Q_{G1} \propto p^2 \Delta T^2 T_0^{-5} H_x \left(\frac{\partial H}{\partial z} x \right) \quad [\text{III-68}]$$

and any experimental investigation would be expected to follow such a dependence. Quite obviously, the magnitude of this relation, equally if not more important than the parametric dependence, will require knowledge of the proportionality constant which in turn is determined from the geometry of the particular cell used and the nature of the fluid convected (see equation III-52) and will be considered in the experimental section.

Treatment of a Non-Uniform Magnetic Field Gradient

It is recalled that this foregoing analysis was based on a constant-valued magnetic body force term, h , defined in equation III-12

$$h \equiv H_x \left(\frac{\partial H}{\partial z} \right) \quad . \quad \text{[III-12]}$$

However, in light of the fact that it is highly unlikely that any "homogeneous" magnet, designed specifically to have no gradient whatever, have a conveniently linear "flaw", i.e. a linear characteristic gradient, a non-constant gradient is now considered to extend greater generality to the Glenda effect model just presented. Nonetheless, it is assumed that despite a potentially non-linear gradient in the field of a "homogeneous" magnet system, the absolute magnitude of the gradient, or better, the total change in the field over the region of interest, is negligibly small compared to the strength of the applied field thereby allowing the field itself to be treated as a constant. Even for the poorest of "homogeneous" magnets, this is quite a safe assumption over a surprisingly large region.

If the field gradient is no longer constant, then obviously

$$\frac{\partial^2 H}{\partial z^2} \neq 0 \quad \text{[III-69]}$$

and the gradient itself becomes a function of z . This then implies that this body force (not unlike gravity) may change at various

vertical positions; thus the analysis becomes no different than treating a non-constant gravity body force term. Obviously, then, this z-dependent body force is merely integrated over the region of interest mimicking the action of the cell itself in so doing to obtain the effective gradient, one that would cause identical results had it occurred linearly over this same region, i.e.

$$\left. \frac{\partial H}{\partial z} x \right|_{\text{eff}} = \frac{1}{|z_1 - z_2|} \int_{z_1}^{z_2} \left(\frac{\partial H}{\partial z} x \right) dz \quad [\text{III-70}]$$

where z_1 and z_2 correspond to the ends of the region of interest. This result, of course, dictates that uniformly symmetric gradients about the center of the region of interest (e.g. a parabolic profile) would have a net zero effective gradient and thus leads to no Glenda effect and no magnetoconvection whatever, as would be expected. Parenthetically, it is mentioned that the incipient thinking in this area initially doubted the possibility of the existence of the Glenda effect in this investigation based on the argument that any indigenous gradient would indeed possess just this centro-symmetry - when in fact, it turns out that there is nothing particularly magical about the origin at all, the indigenous gradient occurring anywhere. Additionally, this model indicates that short regions of high gradient can be as efficacious toward the overall Glenda effect as long regions of low gradient, equally as expected. Since no other terms in the velocity profile or heat transfer model have such a z dependence (the z dependence of gravity is traditionally ignored), this newly computed effective gradient, multiplied by the previously defined constant-valued absolute applied magnetic field

strength, merely replaces h in the entire analysis of Chapter III, i.e.,

$$h = H_x \left. \frac{\partial H}{\partial z} \right|_{\text{eff}} \quad \text{[III-71]}$$

In the actual fields measured, as will shortly be seen, the gradients were manifested in several regions of rather striking linearity, each region of reasonably small magnitude (2 - 3 Oe/cm) and each changing sign with its adjacent slope, indicating the short, non-linear sections between linear segments were of very low magnitude and thus could safely be ignored. Nonetheless, that one particular sign predominated over the whole cell was wholly obvious. Modelling the exact integral given in equation III-70 above to handle several regions of linearity, a linear combination of the field gradient - distance product is utilized to approximately compute this self-same effective gradient, or

$$\text{grad} \left|_{\text{eff}} = \frac{1}{|z_1 - z_2|} \sum_{i=1}^n a_i \text{grad}_i \quad \text{[III-72]}$$

where the a_i are the lengths over which the corresponding grad_i acts and n is the number of such linear slopes, or,

$$\text{grad} \left|_{\text{eff}} = \sum_{i=1}^n f_i \text{grad}_i \quad \text{[III-73]}$$

where the f_i are the corresponding fractional distances involved. Owing to the obvious difficulty in elucidating the exact effective gradient as given in equation III-70, and the negligible error resulting in the use of equation of equations III-71 or -72, these latter models will exclusively be used in the experimental investigations to determine the effective gradient.

This chapter is concluded by observing that, with the proper analytical technique, any field gradient, regardless of magnitude, can be treated by the logical extension of equation III-70 to encompass a now changing applied field strength, i.e.

$$\left(H_x \frac{\partial H}{\partial z} \right) \Big|_{\text{eff}} = \frac{1}{|z_1 - z_2|} \int_{z_1}^{z_2} H_x \left(\frac{\partial H}{\partial z} \right) dz \quad [\text{III-74}]$$

thus rendering even traditionally non-uniform magnetic fields, such as those used by Carruthers and Wolfe in their investigation, highly susceptible to analysis and introduces the quite real possibility of beginning to quantify very pronounced Glenda effects, even into the turbulent region, which, of course, is of greater value to heat transfer applications. Moreover, as can be readily seen, the magnitude of this term, which, of course, dictates to what degree the Glenda effect occurs, is independent of the actual magnitudes of the field and field gradient and depends only on the magnitude of their product. Therefore, it can be visualized that a magnet system having a huge applied field with a small indigenous gradient, as was the case in this investigation

(where the weight of the magnet and support equipment approached 5000 lbs, and its cost approached ten times this value), can be replaced by a properly designed system of much smaller absolute magnitude but whose associated gradient is quite large (then, perhaps a few hundred pounds, or even less, and no more than ten times this value in cost), thereby making the applications mentioned in Chapter I much more attractive.

PART II

EXPERIMENTAL

CHAPTER IV
THE DESIGN AND CONSTRUCTION OF A
RECTANGULAR GLENDA EFFECT CELL AND MODIFICATION
OF SUPPORT SYSTEMS

Introduction

Thus having what appears to be, at the very least, a reasonable model of the Glenda effect, the next quite obvious step in the investigation of magnetoconvection is to subject this analysis to the acid test of the experimental laboratory for ultimate approval or rejection. In light of the plethora of highly elegant and precise data, conditions and results available (4) giving the absolute magnitude of magnetoconvection heat transfer in milliwatts as functions of temperature, pressure, and field strength for oxygen in a homogeneous field, a simple application of these data and conditions to equations III-51 (magnitude) and III-68 (parametric dependence) and subsequent comparison of these results with those obtained in the experimental investigations would seem to be all that is required to test this new Glenda effect model. Of course, since in this early work, the magnet was assumed, a priori, to be gradient-free and therefore no gradient data whatever was available on the particular magnet system used in the investigation, the model demanded (see equation III-51) that the indigenous field be experimentally mapped to ascertain its characteristic gradient; the results of which thus rendering the comparison wholly doable. When in fact, this indeed was

what was eventually done, the results of which appearing in Chapter VI, the experimental efforts not directly associated with this particular determination of inherent field gradient are worthy of inclusion and discussion at this time. As was mentioned earlier, this in large measure was due to the highly experimental nature of the initial project and, subsequent to the Glenda effect model endeavors, the immediate (and, it turns out, incorrect) conclusion that any characteristic field gradient on such a reputedly "homogeneous" magnet would indeed be so small as to escape detection by ordinary methods, demanded that any Glenda effect experimental endeavour would require the establishment of a known-valued, superposed, small-magnitude linear field gradient and the acquisition, under now completely different conditions, of wholly new data and their subsequent results for comparison with the Glenda effect model. Since it wasn't until the later stages of this latter pursuit that a new technique was devised to map even small characteristic field gradients, the ultimate results of which causing the new model to agree exceptionally well with the earlier results and thereby no longer indicating the need for further work, in conjunction with the experimental nature with which the earlier project was wholly concerned, it should be quite obvious that these experimental endeavours not only represented a large fraction of the overall project, but will be of paramount importance to the colleagues extending the project, thereby rendering import to the incorporation of these experimental efforts in this thesis.

The Rectangular Cell

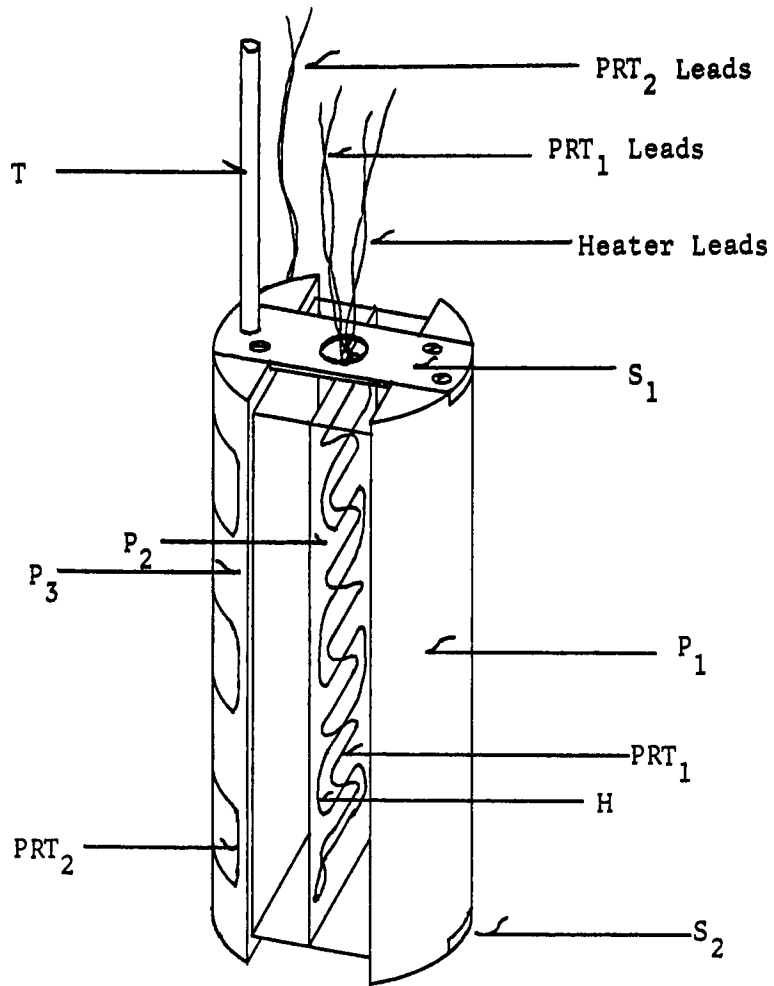
Since the original Park model, which this project was singularly designed initially to experimentally verify, was derived in rectangular Cartesian space, as was the new Glenda effect model, a rectangular magnetoconvection cell was designed and a prototype developed to accomplish this task modelled largely after previous cylindrical cells. The primary consideration in its design was its obvious need of as large an L/D as possible and still fit within the constraints of the entire experimental apparatus. Therefore, the following broad design criteria were applied to the apparatus:

- (a) rectangular, large L/D,
- (b) it should be operable over a wide temperature range, 20°K to 320°K,
- (c) its physical dimensions should be such as to make it compatible with existing cylindrical cell holders so that both the available magnet systems, viz: the 100000 Oersted superconducting solenoid magnet and the 16000 Oersted iron-core electromagnet, and finally,
- (d) since the magnetoconvective data is manifested in detectable temperature changes in one plate, the incorporation of previously proven (4) temperature detectors and heaters is desired.

In light of the constraint of a cylindrical cell holder and its associated circular cross-sectional attachments (e.g. radiation shields, lead holders,

tubing manifolds, etc.), a 3 inch vertical cell was chosen such that its outside geometry was cylindrical, diameter of 1.25 inches (thereby accomodating the cell holder nicely), while its inside geometry was rectangular, as shown in Figure V. The cell wall (not shown in the Figure), connecting P_1 to P_3 along the front and back and both ends in a continous fashion, is made from 5 mil mylar thereby isolating the cell from its vacuum environment. Finishing the cell is the third plate, P_2 , made from thin aluminum foil, and at a distance of 0.359 inches from each plate P_1 and P_3 , which acts both as a heater and as a thermometer. The mylar, having no structural strength whatever is bridged by the two support caps, S_1 and S_2 , which supports the plates P_1 and P_3 and maintains rigidity in the cell.

This particular design has many experimental advantages. First, the two plates, P_1 and P_3 which are at the same, cooler temperature, T_2 , are specifically designed to have as a large a thermal mass as possible thus allowing the treatment of that temperature as a constant, independent of (small) heat transfer changes in the large. Additionally, these self-same plates, being made of pure copper, and having circular cross section, are in excellent thermal contact with the cylindrical constant temperature cryostat, thereby improving their stability. Over and above its high L/D, the cell's depth, ℓ , is of such magnitude (0.800 inches) as to hopefully preclude any adverse wall effects. The mylar walls, bridging the plate gap not only act to isolate the convection region from the vacuum region, but also serve to support the "hot" third plate, P_2 . Five mil mylar was chosen in this applicaion



THE RECTANGULAR
MAGNETOCONVECTION CELL

FIGURE V

for its low gas diffusion rates, its high strength and flexibility even at cryogenic temperatures (any thinner would have caused structural and leak problems), and its exceedingly low thermal conductivity, approaching that of oxygen itself (any thicker causing too high a conductivity), thereby permitting gaseous thermal effects to prevail. Additionally, the heat shrinking ability of mylar was advantageously used to increase the rigidity of the cell and smoothness of the cell walls. Moreover, the polyester nature of mylar made its union to all three plates facile with the use of specialized cryogenic polyester epoxies (specifically designed to be quite flexible even at cryogenic temperatures). The hot third plate, P_2 , is composed of a symmetrical aluminum foil bi-layer with a platinum resistance thermometer (PRT_1) and a 845 Ω /ft 1 mil Evanohm heater between in a matrix of epoxy adhesive*. The thinness of this plate allows rapid thermal equilibrium to new temperatures to occur as a result of a changing driving force, ΔT , as the convection changes, provided, of course, that there is constant heat flux between plates and that the outer plates, P_1 and P_3 , remain at essentially a constant temperature. Thus, any change in the temperature of the thinner, rapidly responding inner plate, will be a reflection of any changes that arise from the Glenda effect (or other related magnetic phenomena, e.g. the Senftleben-

*For the details of the selection and operation of the PRT and Evanohm heaters, see reference (4).

Beenakker effect).

In the outer walls, there are no heaters and they thus adopt the temperature of the cryogen, variable over a relatively wide range. This, of course, eliminates the need for a feed-back control circuit to continuously monitor and heat the outer temperatures. One outer wall, however, (they both are assumed to behave identically), incorporates another platinum resistance thermometer, PRT_2 , and joins PRT_1 of the inner plate in opposite arms of a high precision Wheatstone bridge thus providing an excellent differential measuring technique of resistance (temperature) change. Electrical communication from the inner plate is achieved through the top end mylar via small wires sealed in epoxy adhesive and pass through the support cap, S_1 , to the cell holder; all wires are twisted to reduce noise and Lorentz force problems. Gaseous communication is provided by an 1/8 inch stainless steel tubing, T , connecting one cavity to the external gas sampling manifold; communication between cavities is achieved through small holes in plate P_2 .

The disadvantages of this particular cell design are wholly manifested in its rather difficult fabrication owing primarily to its small size. The actual attachment of the mylar to the small lips on the cell walls in such a fashion as to preclude gross leaks, of course, is a difficult enough step, but the most difficult problem facing the experimental work is the proper placing of the inner plate such that it is precisely centered and orthogonal to the coordinate system and at

the same time allowing for sealed communication to the outside environment; in fact, however, owing to the actual construction of a prototype cell only and that the theoretical pursuits began during this time, this step never was actually performed, although it appears to be quite doable at this time, in large measure owing to the existence of a unique cell-fabrication jig.

To facilitate the obviously tedious construction procedure of the cell after its machining, a combination holding and fabrication jig was constructed, shown in Figure VI. This particular configuration not only held the cell halves such that they could be freely rotated to any desired position, but at the same time always maintaining relative alignment between the two halves through a special shafting arrangement such that no undue stresses were placed on the mylar or adhesives during any time of the assembly. The sliding bearing support, SB, had complete lateral freedom on precision tracks so that one-half could easily be manipulated in the absence of the other; at every position, the cell halves still maintaining proper alignment. The foot, F, is provided to facilitate vertical assembly if desired. Owing to the relatively long curing time (2 days) of the special polyester cryogenic adhesive chosen (Crest Products, Santa Ana, California, #7450 A&B), and its highly non-thixotropic but nonetheless highly viscous character, it was considered best to fight the adverse effects of gravity towards this combination of properties by extending through a simple gear-train the same shafting network used to maintain constant proper alignment of the cell halves and incorporate a motor to slowly rotate (4rpm) the halves

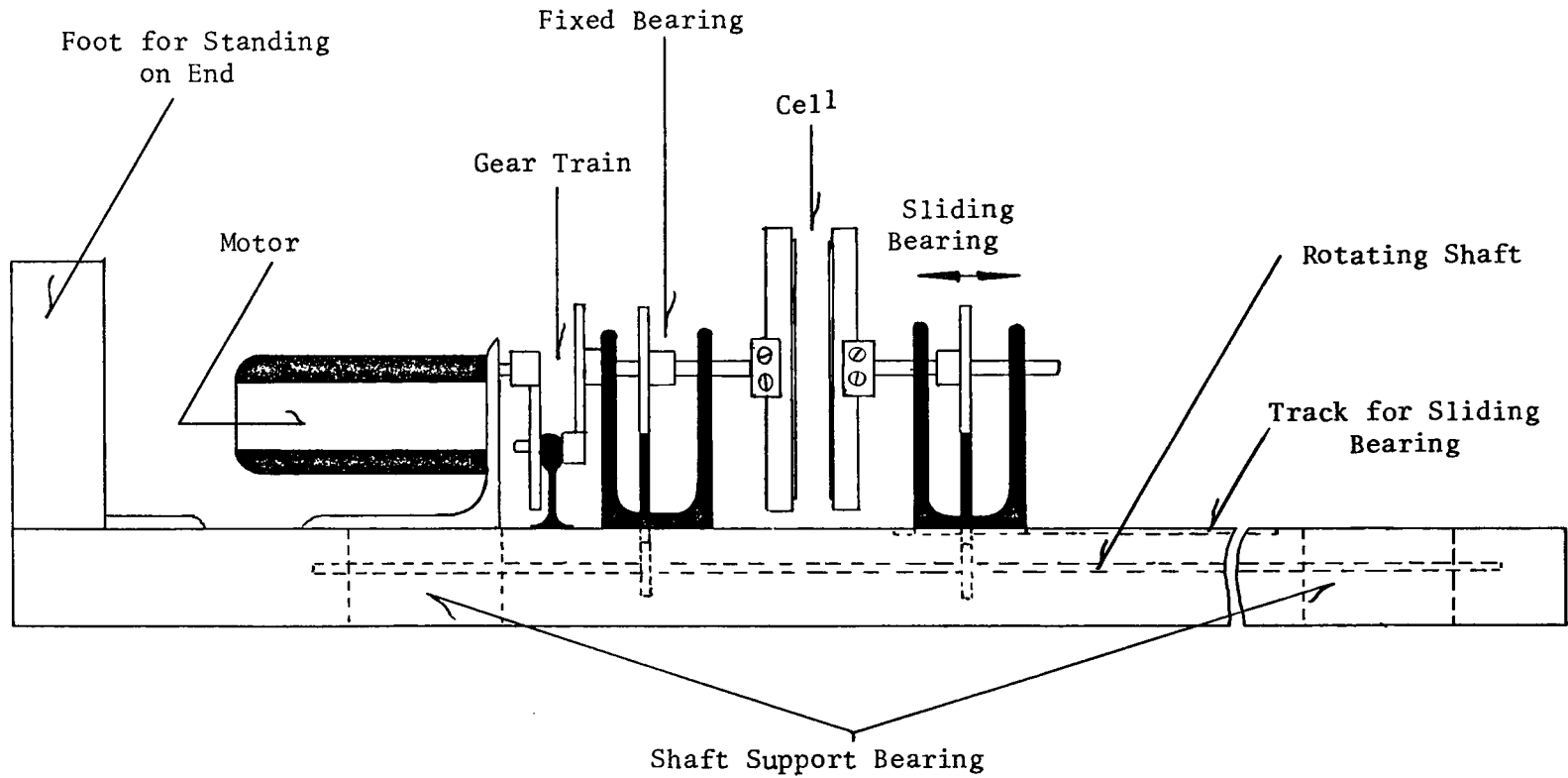


FIGURE VI: FABRICATION JIG

during curing thereby giving an even distribution of adhesives, hopefully alleviating leak associated problems.

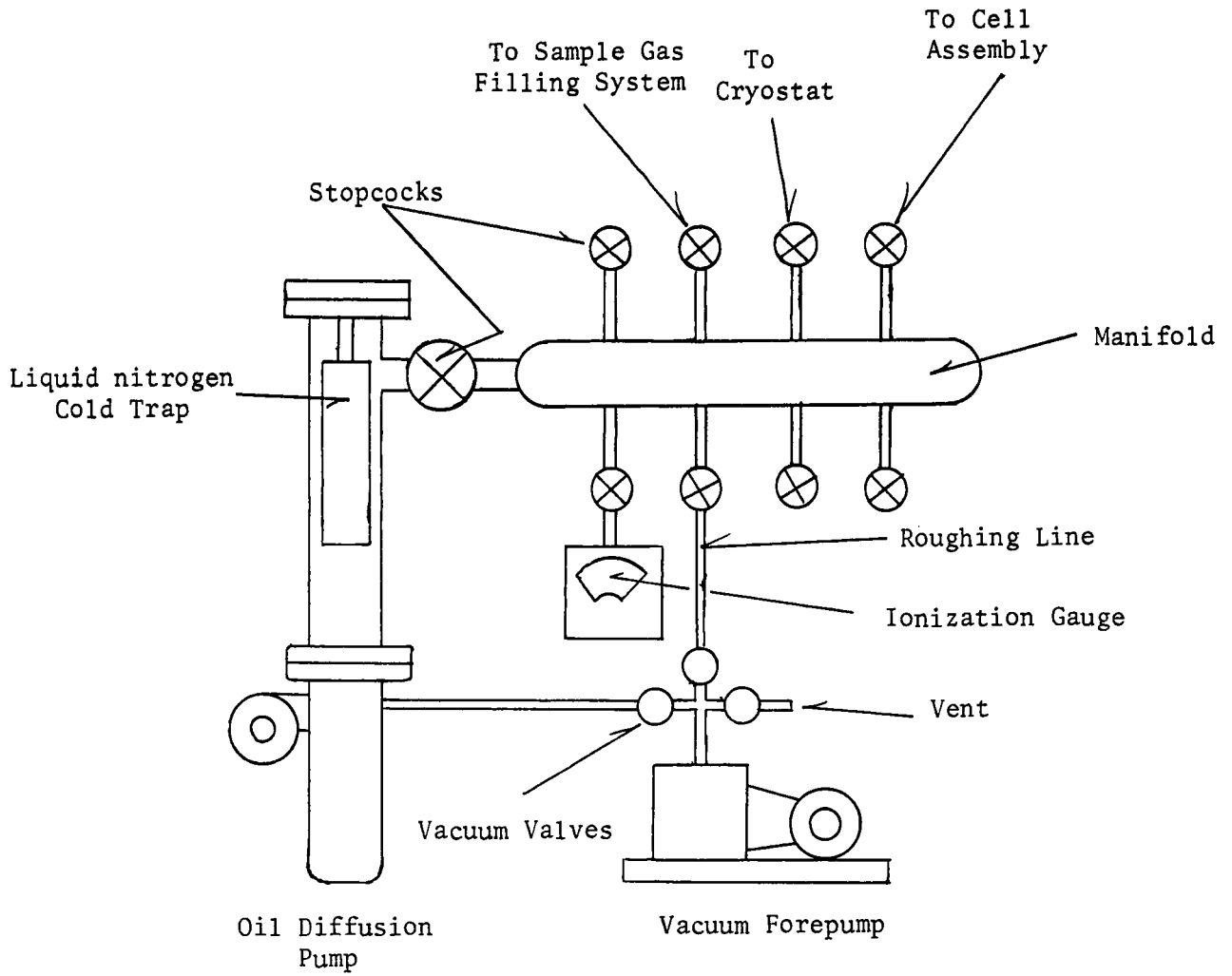
It is suggested that following manufacture of the hot plate, P₂, including the communication holes, heater and PRT, this assembly be bonded first inside a rectangular band of mylar (mylar creases very well) of the proper length (polyester epoxy used for the mylar-mylar seal) circumscribing an oil-coated brass block of the inside dimensions of the cell mounted on the fabrication jig. After curing, this rectangular band of mylar with the third plate attached inside, is slipped off the block, and bonded to one half of the cell body; the other half is then slid into position, never having lost its original alignment with the first, bonded, and cured under rotation. After curing, the end caps are re-attached to both halves and the cell removed from the jig. After silver soldering the tubing to the cell, it is attached to the cell holder, radiation shields inserted, and the holder assembly placed in the cryostats. For details of the cell holder and cryostat, the interested reader should consult reference (18).

Experimental Support Equipment

For various reasons, nearly all of the numerous support equipment (e.g. detectors, gas systems, etc.) associated with the actual data acquisition of magnetoconvective effects in oxygen, was either scrapped and totally replaced or at the very least, rebuilt to original specifications. Additionally, the vast majority of the prior work conducted in these laboratories (on the Senftleben-Beenakker effect), although of a similar nature, was by in large concerned with extremely small changes in heat transfer (on the order of 1 part in 10^5) and the concomitant precise measurement of cell pressures in the one torr region, the result, of course, being the existence of highly sensitive and accurate measuring instrumentation. Since the Glenda effect initiates changes on the order of 10-100% at 20-50 torr, this sensitivity was obviously no longer a requirement.

Vacuum System and Loading Manifold

The vacuum system used in this investigation, shown in Figure VII, was modelled after that used in earlier investigations (18). However, unlike that work, one large diffusion pump is utilized for all operations and all gas handling equipment is centralized in one location: the vacuum rack (cart). This diffusion pump-high vacuum system, consists of a continuously operating, air cooled National Research Corporation 3 inch silicone oil diffusion pump (model HSA-150) utilizing a Welch Scientific 1402 Duo-Seal forepump. The system is capable of attaining less than 10^{-8} torr in the normal operating range and has a maximum



SCHEMATIC OF THE HIGH VACUUM SYSTEM

FIGURE VII

pumping speed of 140 liters/sec. This provides the vacuum backbone to the dewars of the cryostat, the hopefully adiabatic volume surrounding the cell, the helium heat exchange chamber (a section of the cell holder used to communicate thermal energy to and from the cryogen), and the evacuation of the cell itself between loadings.

A Consolidated Vacuum Corporation, cold-cathode type Phillips Gauge (model #RHG-09) with a range of 10^{-7} torr to 0.5 torr monitors the pressure of any region outside the cell cavity itself. Since studies of the Glenda effect are largely concerned with the relatively high pressure region (20-50 torr) where the temperature changes are more pronounced, a precision Wallace and Tiernan bellows type absolute pressure gauge (model 61A-ID-0800) with a range of 0 to 800 torr is utilized for all cavity pressure measurements.

The sample filling system, shown in the dashed rectangle of Figure VIII is used both to evacuate and to fill the cell with either oxygen for the actual measurement of the Glenda effect, or argon for measurements of the heat transfer of a non-magnetically susceptible gas under identical conditions to test the detector sensitivity towards magnetic fields. The Wallace and Tiernan vacuum gauge monitors the pressure of this loading manifold during evacuation and purging operations as well as the cell pressure. Both the research grade lecture cylinders of argon and oxygen are attached to the system simultaneously through two high purity, vacuum duty Matheson pressure regulators. A 2.5 inch Curtin Scientific Bourdon-type Vacuum gauge (model 125) with

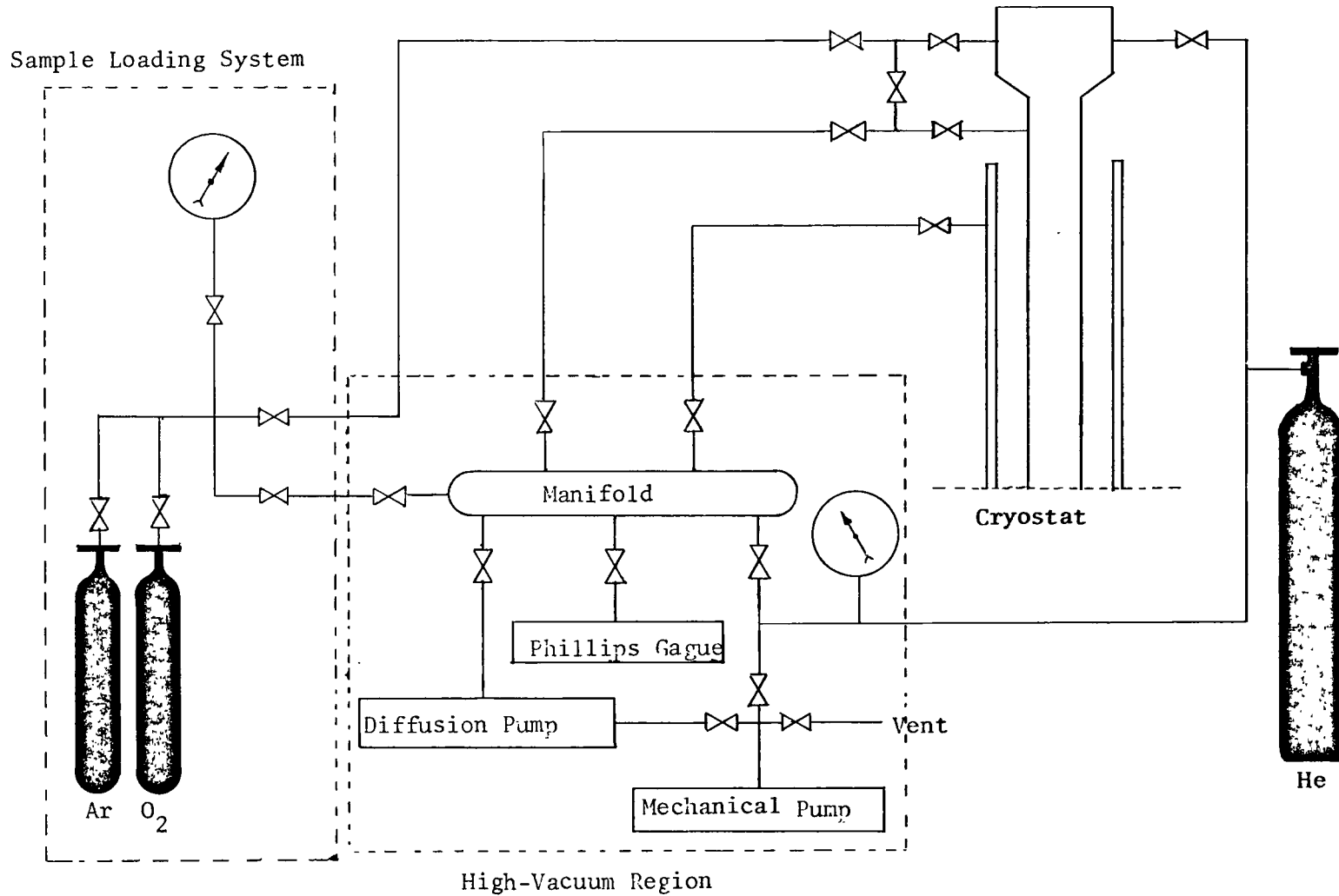


FIGURE VIII: SCHEMATIC OF VACUUM EQUIPMENT AND SAMPLE SYSTEM

a range of 0-30 inches of mercury is used in the helium heat exchanger loading system to monitor the evacuation and loading to its approximate half atmosphere ($\pm 25\%$) requirement.

Heater Power Supply and Measurement Circuit

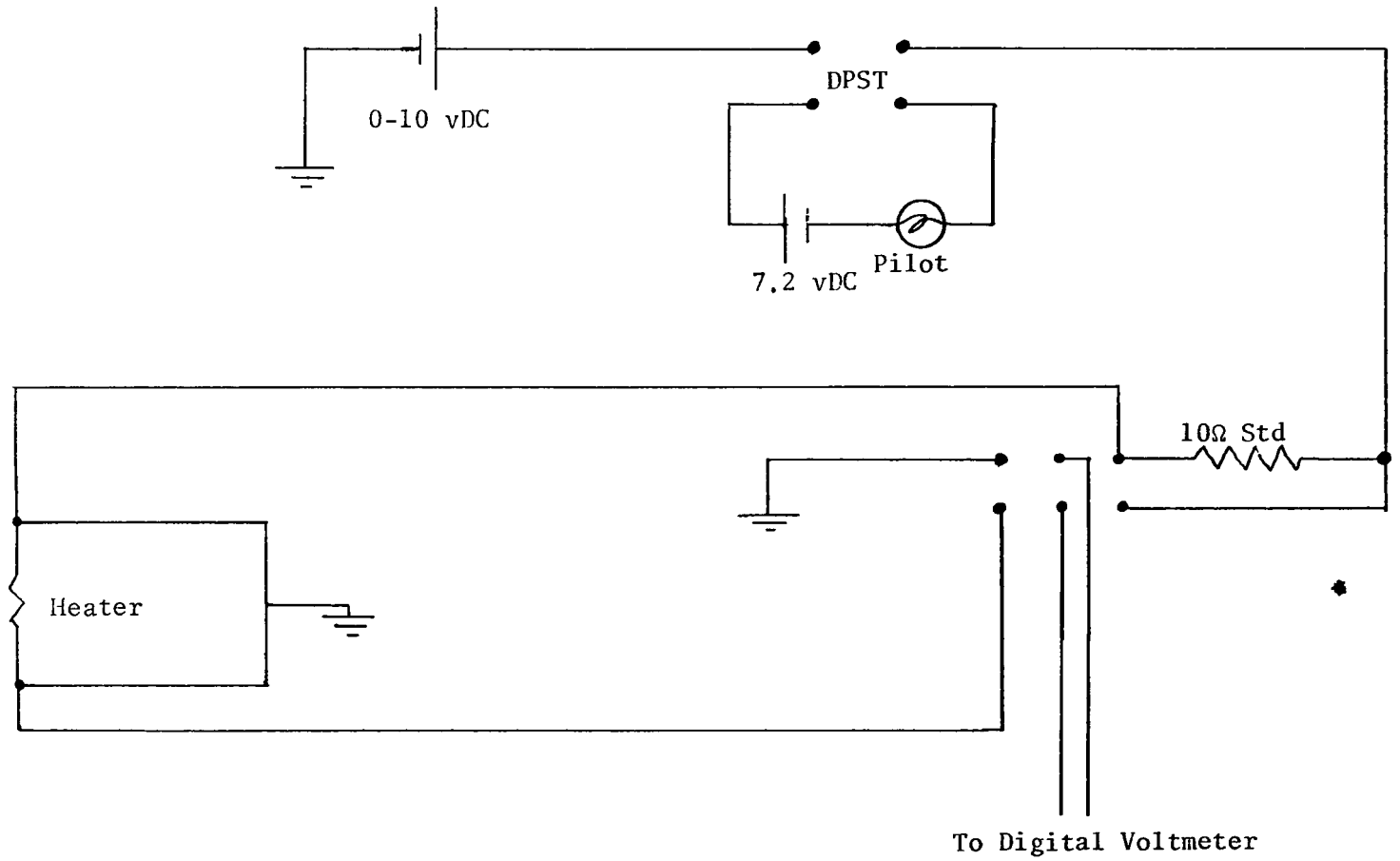
The electric current which is passed through the resistive heater of the inner plate is monitored by a special four-lead type potential detector. The quantity of heat energy supplied to this plate is determined by measuring the potential drop across the resistive heater, V_H , and that across a standard 10Ω resistor, V_{std} , in series with it. Then the milliwatts of heat supplied is given by $V_H \cdot V_{std} \cdot 100$. Figure IX shows the circuit diagram of the heater power supply and measuring circuit and shows the four-lead current-potential method of accurate voltage determination independent of lead losses standard in precision work. A Pacific Photometric Instruments regulated power supply (model 2000) 0-20 volt D.C. is used to energize the heater circuit. Voltage measurements are made using a Data Technology Corporation digital voltmeter (model 370).

Differential Temperature Measuring Circuit

It is recalled that each plate possesses a PRT which, of course, allows the temperature changes prevalent to be monitored differentially, i.e. the detection of the change of the temperature of the inner plate, T_1 , relative to the constant-temperature outer plate, T_2 . (For an in depth analysis on the relative merits of this type of analysis and the

FIGURE IX

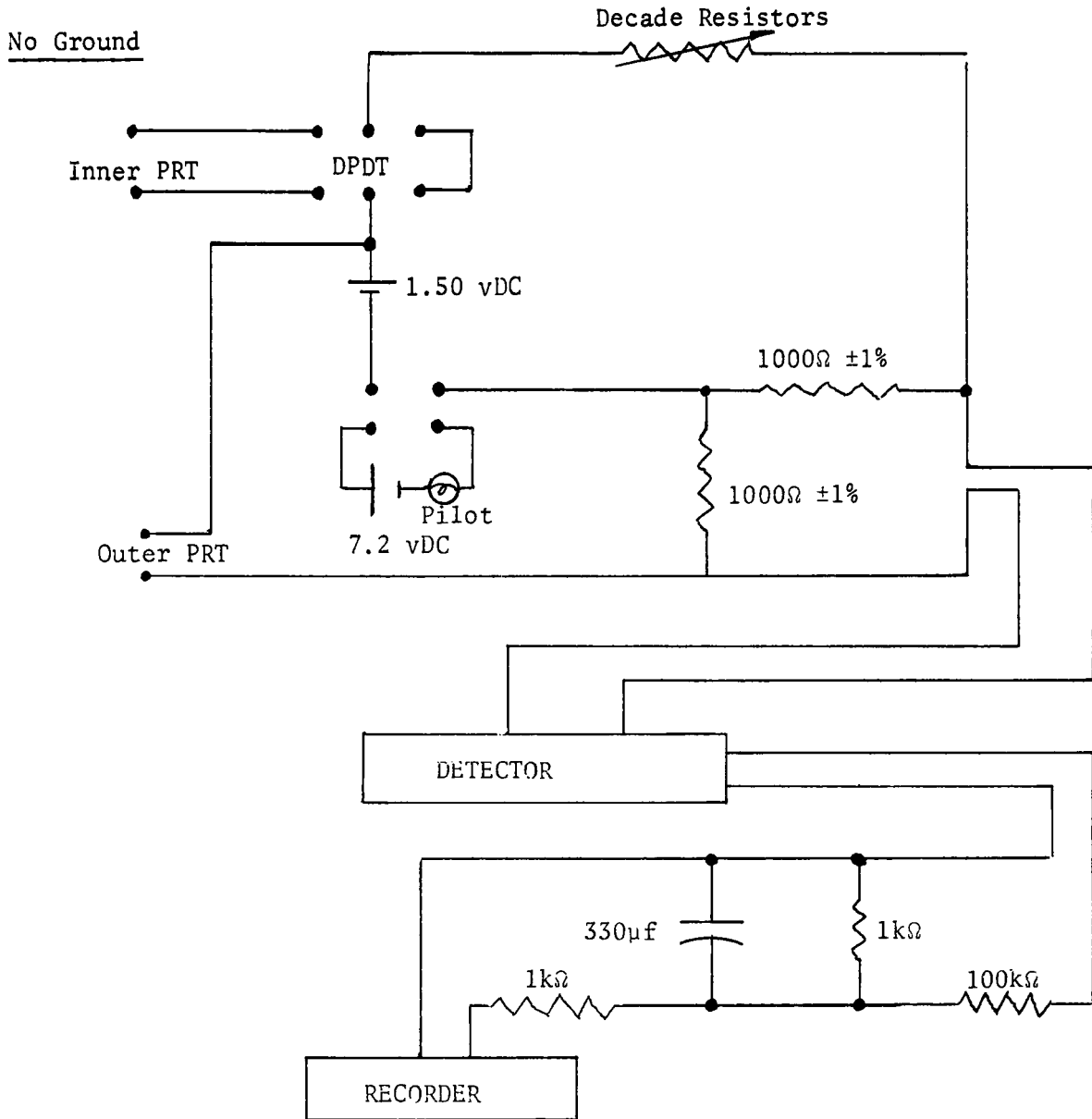
CELL HEATER CIRCUIT



use of platinum resistance thermometers in general, the interested reader should consult (18) and (19)). To accomplish this task, the PRT's are wired into opposite arms of a Wheatstone bridge as indicated in Figure X, so that, for the small resistive imbalance detected here, the deviation voltage is directly proportional to the change in ΔT , the temperature gradient across the cell. For optimum sensitivity, it was empirically determined that the values of the fixed arm resistances should be 1000Ω each as indicated.

All electrical connections in the Wheatstone bridge circuit were made with copper wire of as great a thickness as possible (24 AWG inside the probe, 10 AWG outside it, and 10 solid within the bridge). Soldered connections were made using low thermal EMF solder, each joint cooled slowly to keep their grain structure small. All cables were twisted and shielded to reduce electrical noise; between the probe and bridge thermally insulated to reduce thermal noise from the environment. The bridge itself was confined within a completely enclosed steel drawer of the central electronic cabinet and filled with insulation material thereby providing excellent thermal and electrical isolation and at the same time allowing excellent accessibility to its components.

The imbalance bridge voltage is amplified by a Keithley D.C. Electronic Nanovolt null detector (model 147), sending the output signal for display to a Houston Instrumentation's Omrigraphic Recorder (model 6520) via a twin-T filter as shown, which removes a cyclic 4.5 Hertz disturbance produced by the interaction of the detector chopper



DIFFERENTIAL TEMPERATURE MEASURING CIRCUIT

FIGURE X

frequency with the line frequency. The excellent sensitivity of such a detector coupled to the differential bridge allowed the ultimate sensitivity of one part in 10^5 . Parenthetically, this sensitivity, normally not needed for the pronounced Glenda effect studies, was specifically incorporated in the design not only because the technology existed from earlier work, but this system permits Senftleben-Beenakker effects to be studied as well, if need be. Having determined the temperature gradient across the cell, the absolute temperature (or really the average temperature) was, of course, calculated from the absolute temperature of one plate, notably the constant-valued outer one, determined by measuring the absolute resistance of the outer plate PRT in the bridge by shorting across the inner plate PRT as shown in Figure X and comparing the values to known calibration data (18).

The Electromagnet System

A Magnion L-96 laboratory iron-core electromagnet, energized by a model HS-1265B power supply was used in all the Glenda effect studies. A pair of foil wound, chilled water cooled copper coils form the pole cores, having a peak load of one ohm each and dissipating a continuously variable current from 0.1 amps to 65 amps at 130 volts with stability of 1 part in 10^4 at moderate fields over an 8 hour period. The pole caps are 9 inches in diameter, tapered to 7.5 inches with a 2 inch air gap. Each cap is equipped with special " μ -shims", micrometer controlled soft iron cores of both coils and caps allowing for extremely fine field homogeneity adjustments. A schematic of the magnet system, along with its associated cryostat appears in Figure XI. The field strength-current function is given in Figure XII.

92a

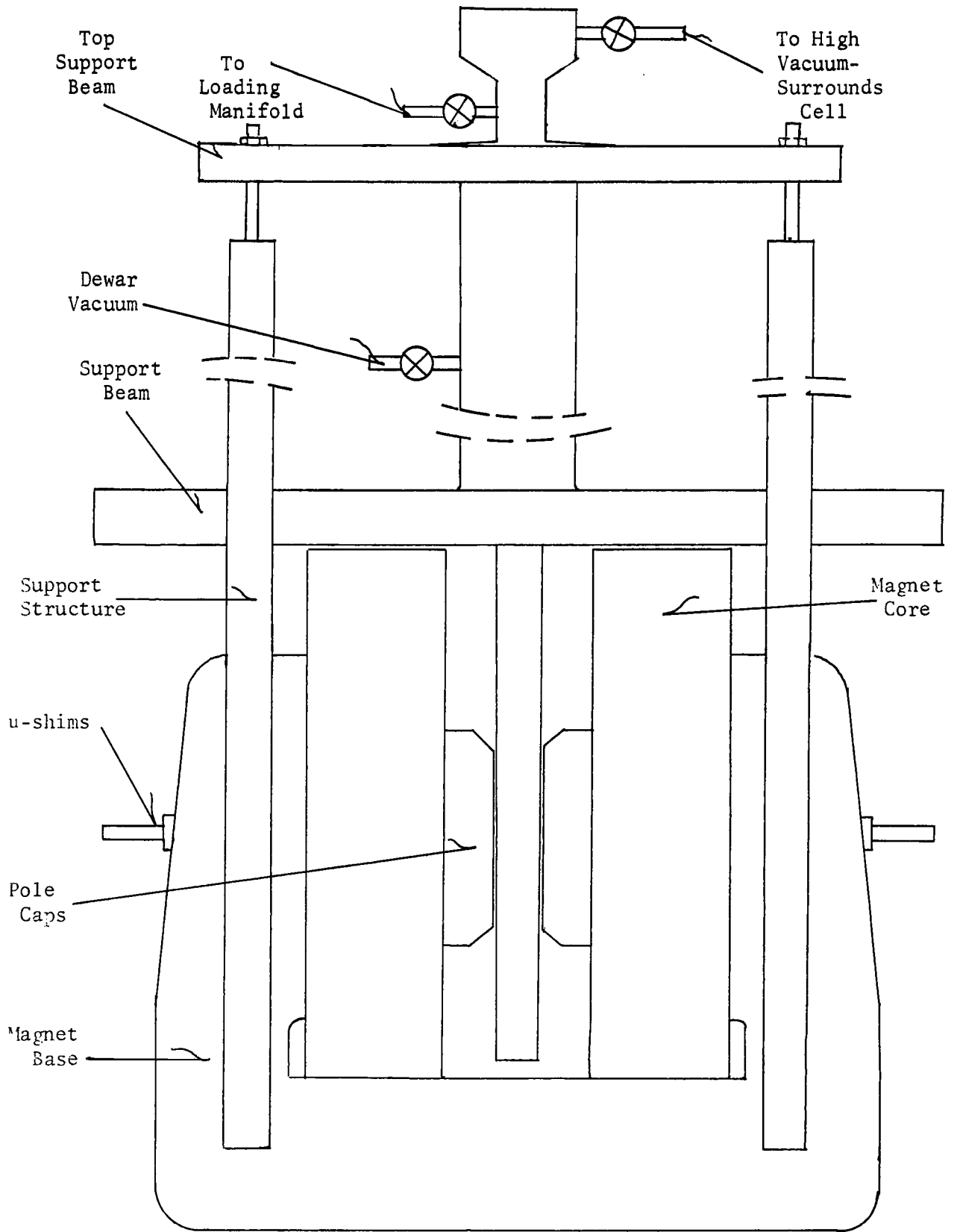


FIGURE XI: ELECTROMAGNET SYSTEM AND ASSOCIATED CRYOSTAT

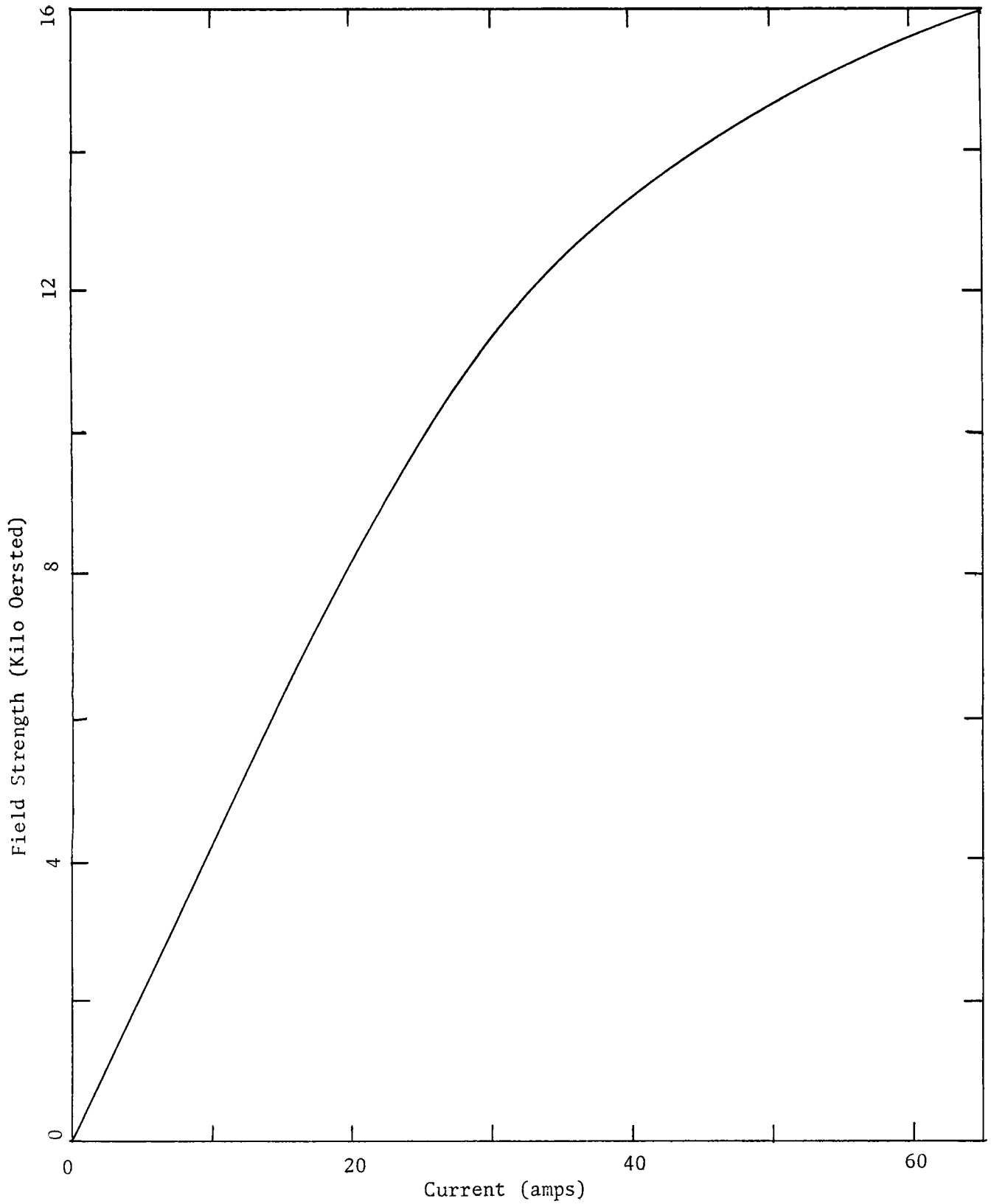


FIGURE XII: FIELD STRENGTH AS A FUNCTION OF APPLIED CURRENT

CHAPTER V

MAGNETIC FIELD GRADIENT STUDIES

Introduction

As can readily be concluded in the foregoing chapters, the sine qua non of the new Glenda effect model lies in any associated magnetic field gradient, whether indigenous or superposed, and even the most token experimental verification of the model must address itself to the determination of that gradient. In this vein, several questions naturally arise: first, if there does indeed exist an associated indigenous field gradient in the system studied, what is its magnitude? Is it within the detection range of existing instrumentation? Would the excessive applied field value "wash-out" any non-uniformity and render its detection impossible? Are there other techniques of measuring such small gradients in large fields?

The first endeavour in this area involved the attempted mapping of the characteristic field gradient of the magnet employed in the previous investigations with a F.W. Bell Incorporated model 620 Gaussmeter, with a T-6010 temperature compensated transverse field probe with analogue output. This instrument merely measures as a function of field strength the induced Hall voltage across a small semiconducting chip in the field passing a small A.C. current orthogonal to both the field and the Hall potential (the Hall effect). Unfortunately, due to

the analogue nature of the output (meter), and the high field strengths at which the studies prevailed (≈ 10 k Oe), only changes on the order of 100's Oe/cm were capable of being detected and unfruitful results such as that shown in Figure I were obtained, indicating that indeed, according to these measurements, the magnet was quite uniform, especially in the center three inches where the cell was confined. However, it is recalled that gradients on the order of 1 Oe/cm were expected to give the indicated results; the possibility of the existence of such a gradient was thus not removed, but its detection at the time seemed impossible. Undaunted, and under the assumption that any characteristic field gradient was very small, various attempts were made at superposing on the applied field (and its indigenous gradient - whatever its value) known linear field gradients, which, of course, would be quite easy to measure with the existing Gaussmeter in the absence of the applied field. This superposition, however, would obviously require the acquisition of completely new data for analysis, a problem that, by in large, caused little other than temporal concern owing to the experimental efforts to date with the support systems.

After eliminating the possibility of using small Helmholtz coils*

*Parenthetically, it is added that it may be possible to superpose a very complex Helmholtz coil system in a long fashion such that one end of this pattern possesses more turns than the other in a linear manner. The lack of adequate working space between the pole faces and the probe cryostat, in conjunction with no previous reports of success or failure of such an idea precluded its further investigation at this time.

in any geometry about the cell to produce the desired gradient, since the only possible gradient of such an arrangement is in the same direction as the field itself, i.e. $\partial H_n / \partial n$, whereas a $\partial H_x / \partial z$ was required, other techniques, not precisely superposing fields, but nonetheless seemingly valid, were considered, all of which unfortunately again required precision field measurements. In retrospect, however, this measurement problem appears to have been overlooked at that time and the other possible gradient inducing schemes were thoroughly investigated instead (such as purposeful μ -shim misalignment, iron pole face wedges, re-adjustment of the pole faces, or commercial gradient wedges), none of which, it turns out, were implemented since any technique would have permanently altered the already "homogeneous" character of the magnet and the preservation of its original integrity was a foremost consideration.

•

Gaussmeter With Digital Output Measurements

Having reached the unfortunate conclusion that no external linear field gradient whatsoever, could easily be induced across the cell in the existing magnet system, resolve was therefore made to develop new sensitive techniques with which to again attempt to map the existing characteristic field gradient of the system. After an early fruitless venture in the development of a differential Hall effect probe in which the two potentials from two identical Hall elements in differing field regions were added before signal amplification and display, it was discovered that the analogue output from the final amplification stage of the existing Hall effect Gaussmeter could be tapped for digital display on a 6 digit DVM. Moreover, it was learned that this configuration yielded a sensitivity of one part in 10^5 in relative field strength thus enabling determinations of the field strength on the order of 0.1 Oe relative. This revelation, needless to say, caused considerable excitement in these laboratories since the gradients anticipated to cause the results observed earlier were now well within this new measuring capability. This sensitive capability, of course, would be completely useless if the magnet itself possessed an inherent non-uniform field drift on the order of its characteristic gradients and the earlier measurements were therefore addressed to the elucidation of the temporal stability over the time period during which a field mapping could be made.

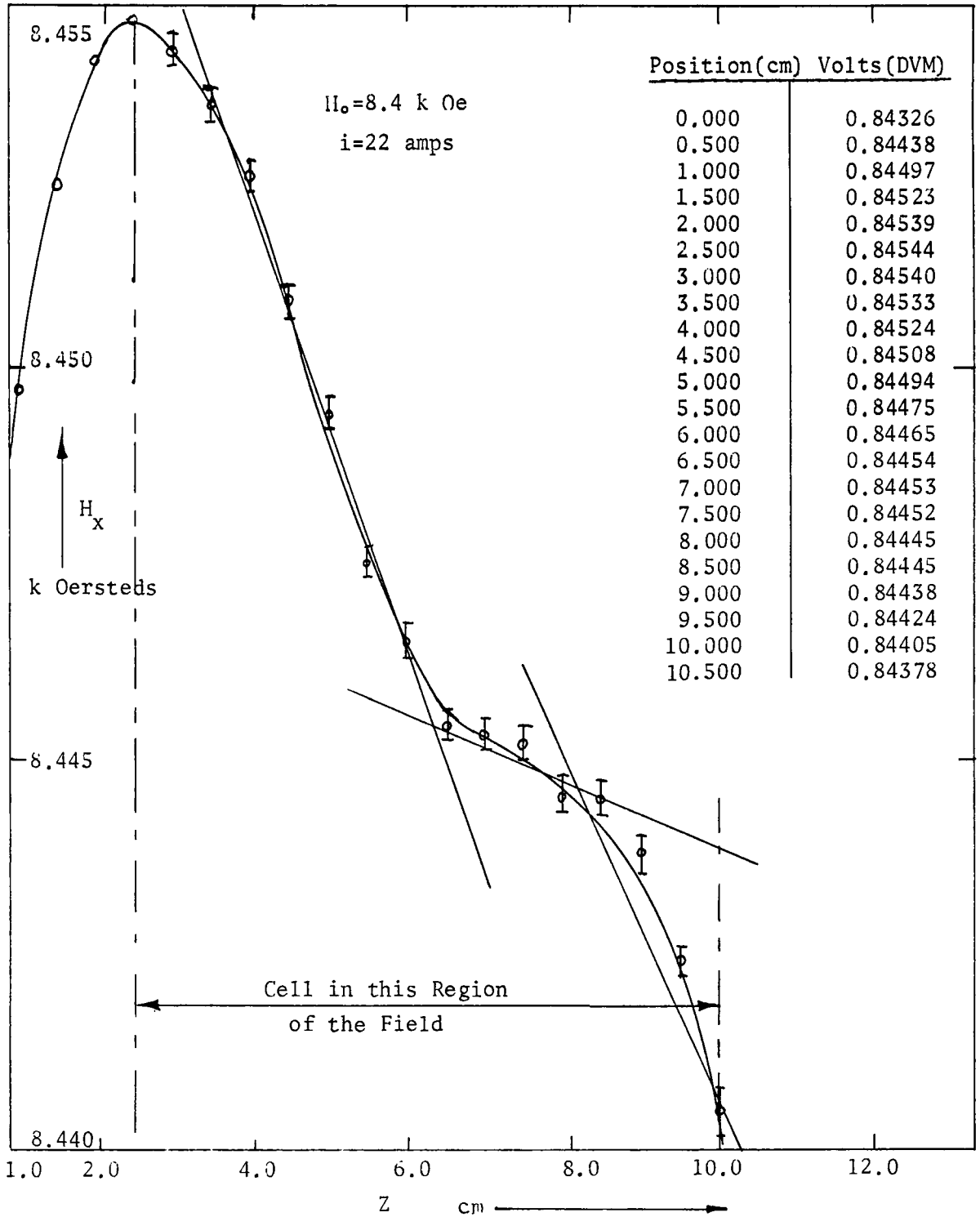
A probe holder was designed and fabricated to precisely position

the probe anywhere within the pole gap volume. A six-inch, orthogonal 3-dimensional Uni-Slide micrometer-positioner was mounted on the supporting beam of Figure XI and connected the probe in a notched cradle via an 18 inch 1/4 inch thick aluminum strap. This 3-dimensional freedom allowed precise centering of the probe on the z-axis and at the same time permitted rapid and accurate position measurements on that axis over the center six inches of the pole gap. All leads from the probe to the Gaussmeter and to the DVM were shielded to prevent electronic noise and both instruments incorporated ballast transformers to smooth line voltage fluctuations. The 0-1 volt full scale output voltage was directly proportional to the field strength, the proportionality constant being a function of the field decade range setting of the Gaussmeter. With this configuration, 22 voltage-distance readings every 1/2 centimeter (0.000 cm \rightarrow 10.500 cm) could be made in 5 minutes at each field setting, and thus this time period became the stability criterion.

With the probe fixed in the center of the gap, voltage versus time readings were determined at several field settings to characterize the drift over 10 minutes thereby giving a 100% safety margin. Surprisingly enough, these results indicated that the magnet was quite stable in the 7 kOe to 13 kOe region, drifting less than 0.2 Oe in 10 minutes, increasing to \approx 1.0 Oe/10 min at 14 kOe and above and \approx 5.0 Oe/10 min at 6 kOe and below. Fortunately, with the exception of 14.1 kOe, all available magnetoconvection data and results (18) were taken at the moderate fields where the field drift was smallest.

Under these favorable conditions, the fields at 8.4 kOe, 9.5 kOe, 11 kOe, 12 kOe, 13 kOe, and 14 kOe were mapped along the z axis, the range extending 2.5 cm in each direction beyond the 7.5 cm (3 inches) center region where the cell measurements were made. At each field strength, three different field mappings at least an hour apart were made; a 6 hour temperature-current equilibrium period for the magnet was allowed between field settings. These conditions were necessary to minimize field drift and confirm each gradient and the results indicated that although two different runs an hour apart may have disagreed everywhere by one or two Oersteds, the gradients were identical within the experimental error in every case, and it is, of course, the gradients in which singular concern lies in this investigation.

A representative plot and data appear in Figure XIII showing the magnetic field strength as a function of vertical position at 8.4 kOe. As expected, the field increases as the center is approached. But, at about 3 cm from the center (where the cell begins), the field almost uniformly decreases well past the center, slows its decrease for about 1.5 cm just past the center, then decreases rapidly again to the end of the cell and beyond as clearly shown in Figure XIII. It is quite evident that the maximum field does not occur at the center of the cavity and that the field is most assuredly decreasing everywhere in the cavity, each slope being on the order of -2 Oe/cm, well within the value anticipated from the theoretical considerations alone. Similar such mappings were obtained at all field strengths thereby generating a family



FIELD UNIFORMITY PLOT AT 3.4 KILO OERSTEDS

FIGURE XIII

of curves, each of differing absolute magnitude, but each of analogous non-uniformity. With the exception of 13 kOe and 14 kOe field strengths, individual datum yielded a relative error of only ± 0.2 Oe and a drift of ± 0.2 Oe/10 min. At 13 kOe and 14 kOe, however, the individual data showed a relative error of ± 0.3 Oe, and a drift of ≈ 1 Oe/10 min, casting high uncertainty at the higher field settings.

Fitting these results to the model discussed previously in Chapter III concerning non-linear field gradients and the handling of multiple linear slopes, the arithmetic averages at each field strength of the effective gradients over the cell region were calculated and with their errors displayed in Table I. These errors not only reflect the relative error in individual datum measurements and the overall associated drift, but include an estimate in the error of this method over the exact integral of the slope over the distance of the cell.

It is quite evident upon inspection of Table I, that with the exception of the gradient measured at 14 kOe, all gradients were quite constant with increasing field strength, within experimental error being -2 Oe/cm ± 0.5 over the wide range of field strengths. The value at 14 kOe, although slightly lower than the expected -2 Oe/cm, has a large associated error putting even this value within the constant value of -2 Oe/cm, although any conclusions based on this value alone were, quite obviously, highly suspect and therefore avoided.

This chapter is concluded by reiterating that since the magnet system used was "homogeneous", these gradients merely reflected the characteristic production flaws, misalignments, etc., of that particular

TABLE I

EFFECTIVE FIELD GRADIENT AVERAGES
AT VARIOUS FIELD SETTINGS

<u>FIELD STRENGTH (OERSTEDS)</u>	<u>EFFECTIVE GRADIENT (OE/CM)</u>
8.4 k	-2±0.5
9.5 k	-2±0.5
11.0 k	-2±0.5
12.0 k	-2±0.5
13.0 k	-0.9±0.8
14.0 k	-0.5±1.5

magnet alone and cannot be extended to any other analogous homogeneous magnet. If any adjustable parameter of this magnet system is altered, e.g. the μ -shims, pole face alignment, or even small scratches or dents on pole cap pieces, this gradient value would no longer be valid. Thus, each and every "homogeneous" magnet system engaged in the investigation of this behavior or analogous phenomena, must be similarly characterized and mapped. It is added that a simple but highly effective Lorentz-force experiment provided graphic evidence showing the applied field to indeed be in the negative x direction, as expected from the sign of the gradient and the additive nature of the results.

CHAPTER VI
EXPERIMENTAL RESULTS OF EARLIER WORK
AND COMPARISON WITH THE GLENDA EFFECT MODEL
USING MEASURED FIELD GRADIENTS

Introduction

It is recalled that the conclusion of the theoretical discussion was that the then available data and results could result from an indigenous field gradient of between one and five Oersteds/cm over the cell length. Having thus ascertained with reasonable certainty that just such a characteristic gradient did in fact exist on the magnet system used in these previous investigations (18), it was an obvious step to compare the theoretically predicted results (incorporating the now known gradient) using precisely the same experimental conditions, with those results actually obtained in the rigors of the experimental laboratory.

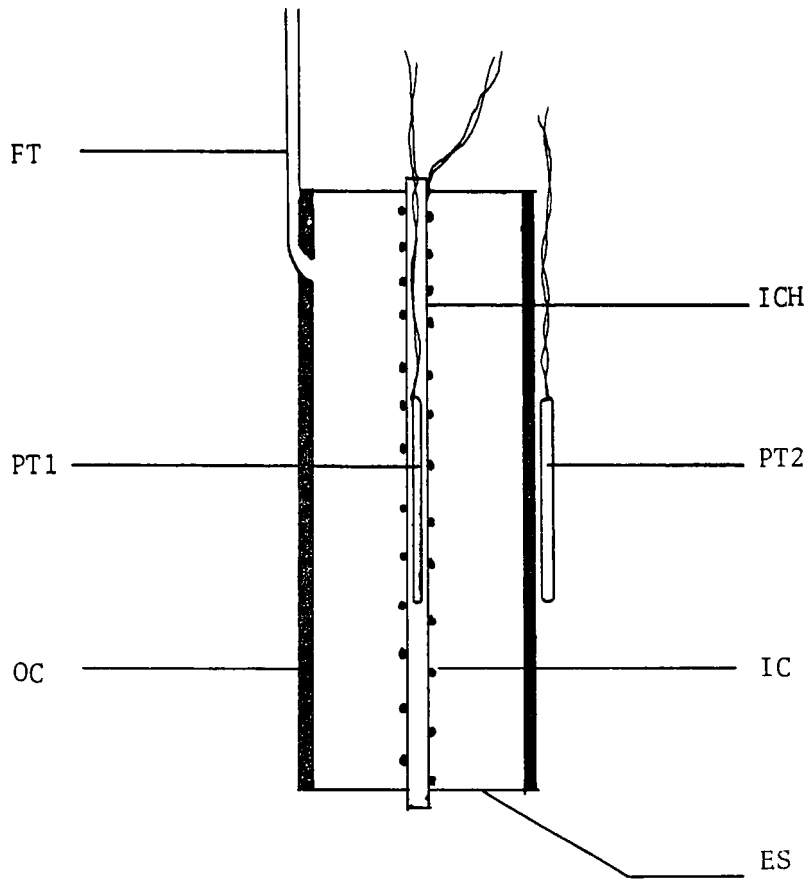
As the scarcity of previous work in the area of magnetoconvection clearly indicates, essentially only one investigation exists providing the elegant data needed for the comparisons, notably J.E. Vevai of these laboratories (18). In 1973, Vevai conducted an exhaustive experimental investigation using a similarly sized cell, discussed in Chapter IV, except of cylindrical design. The results of the magnetic contribution to the overall convective heat transfer was given in

milliwatts as functions of pressure, temperature, and field strength which therefore rendered this study readily comparable to the modelling undertaken in this thesis (see equations III-52 and III-68). All of these former experimental efforts applicable to the Glenda effect modelling will be thoroughly described in this section; however, for a greater in-depth study of these experimental results, the interested reader should consult reference (18).

Experimental Results of J.E. Vevai

All measurements were performed in a simplified thermal transport cell, not unlike the one shown in Figure V in function, utilizing a completely cylindrical geometry as shown in Figure XIV with a cell outside diameter of 1.25 inches and a length of 3.0 inches. The outer cylinder, OC, was made relatively massive from pure copper, its temperature constant with its intimate contact with the inside walls of the cryostat. The inner "hot" cylinder, IC, by contrast, was a thin walled aluminum tube (with an o.d. of 0.120 inches) made from crease-free foil in order to keep its thermal mass as small as possible for rapid temperature change response without compromising an essentially uniform temperature along its length. A D.C. voltage applied to a 14 inch length of 1 mil diameter Evanohm heater wire (ICH) wrapped uniformly and bifilarly around the inner cylinder served to supply heat energy to this inner cylinder. The sample gas was confined to the annular space between the two cylinders by a pair of vacuum tight end seals, ES, made from 1 mil, mylar film and bonded to both cylinders with cryogenic polyester adhesive.

102a



CYLINDRICAL THERMAL TRANSPORT CELL

FIGURE XIV

Gaseous communication to and from the cell was achieved through an 1/8 inch stainless steel feed-through tube, FT, silver soldered through the outer cylinder cell wall. The temperature sensors used for the measurements were platinum resistance thermometers, one, PT1, mounted inside the inner cylinder and the other, PT2, attached to the cell wall, and each attached to opposite arms of a sensitive Wheatstone bridge, thus giving a differential temperature sensing device as discussed earlier.

As in the rectangular cell, the electrical heat flux supplied to the inner cylinder remained constant as did the temperature of the outer cylinder. Therefore, whenever a magnetic field was applied across the cell, under these conditions, the increase in heat transfer through the Glenda effect within the gas caused a corresponding decrease in the temperature of the inner cylinder, T_1 , the change designated by δT_1 , after achieving steady state. Thus, all magnetoconvective contributions to the overall heat transfer must be expressible in terms of this one experimentally obtainable variable, in conjunction with known values of the field, pressure, average cell temperature and temperature gradient, and total heat flux from the inner cylinder.

This, however, is still an experimentally incomplete picture as yet. It is recalled in Chapter I that the Seftleben-Beenakker effect, ever-present in all poly-atomic gases subjected to magnetic fields across a temperature gradient, results in a decrease in the thermal conductivity of all such gases in heat transfer and is not considered

part of the convective Glenda effect; thus, this SBE contribution to the overall heat transfer must be considered in any experimental treatment of the data and leave the magneto-thermal contribution to the overall heat transfer as a pure reflection of only the Glenda effect.

The total electrical energy per unit time supplied to the inner cylinder, Q , is transformed into heat energy flux and of course, is transported via several different modes. In a field free environment, most of the heat flux is transferred from the inner cylinder to the outer cylinder either by conduction through the gas (Q_{cond}), or by convection within the gas (Q_{conv}). The remainder of the heat transferred can be lumped in the form of unspecifiable heat losses, Q_L , which arise from radiative heat losses, conduction through the cell end seals, thermometer and heater lead losses, etc. Thus, an overall heat balance can be written

$$Q = Q_{\text{conv}} + Q_{\text{cond}} + Q_L \quad . \quad [\text{VI-1}]$$

The left hand side of this equation is readily found through determinations of the voltage drops across the cell heater itself and the 10Ω standard resistor, as indicated in Chapter IV. Each member of the right hand side can be expressed in terms of an overall heat transfer coefficient and the temperature gradient driving force, ΔT , or

$$Q_{\text{cond}} = \hat{S}_\Lambda \cdot \Delta T \quad [\text{VI-2}]$$

$$Q_{\text{conv}} = k_c \Delta T \quad \text{[VI-3]}$$

$$Q_L = k_L \Delta T \quad \text{[VI-4]}$$

where in the first expression, \hat{S} is the appropriate shape factor for concentric cylinders and Λ_o is the thermal conductivity. In the last two expressions, it is tacitly assumed that these heat transfer modes are dependent only on ΔT . When in fact most radiative heat losses are proportional to ΔT^4 and free convection to ΔT^2 , for small changes in ΔT , incorporation of the multiple dependence into the now temperature gradient dependent heat transfer coefficient appears to offer only negligible error. With this rationale, the total heat transfer in the absence of a field can now be expressed as the total sum of all the thermal energy fluxes within the cell, or

$$Q = \hat{S}\Lambda_o\Delta T + k_c\Delta T + k_L\Delta T \quad \text{[VI-5]}$$

In the presence of an applied magnetic field, the following events are visualized to occur: i) due to the S-B effect for that gas under those conditions, the normal thermal conductivity, Λ_o , is decreased by an amount $(\Delta\Lambda_o/\Lambda)_{\text{SBE}}$; ii) both the free convective and losses heat transfer coefficients are assumed to remain magnetically unaffected; iii) a new contribution arising solely from magnetoconvective influences is created; iv) the total energy flux into the cell remains fixed at Q ; and v) the overall temperature gradient, ΔT , is changed by an

amount δT_1 . In this light, equation VI-5 in the presence of a magnetic field can now be written as:

$$Q = \hat{S} \left(\Lambda_0 + \left(\frac{\Delta\Lambda}{\Lambda_0} \right)_{\text{SBE}} \Lambda_0 \right) (\Delta T + \delta T_1) + k_c (\Delta T + \delta T_1) + k_L (\Delta T + \delta T_1) + Q_{\text{MC}} \quad [\text{VI-6}]$$

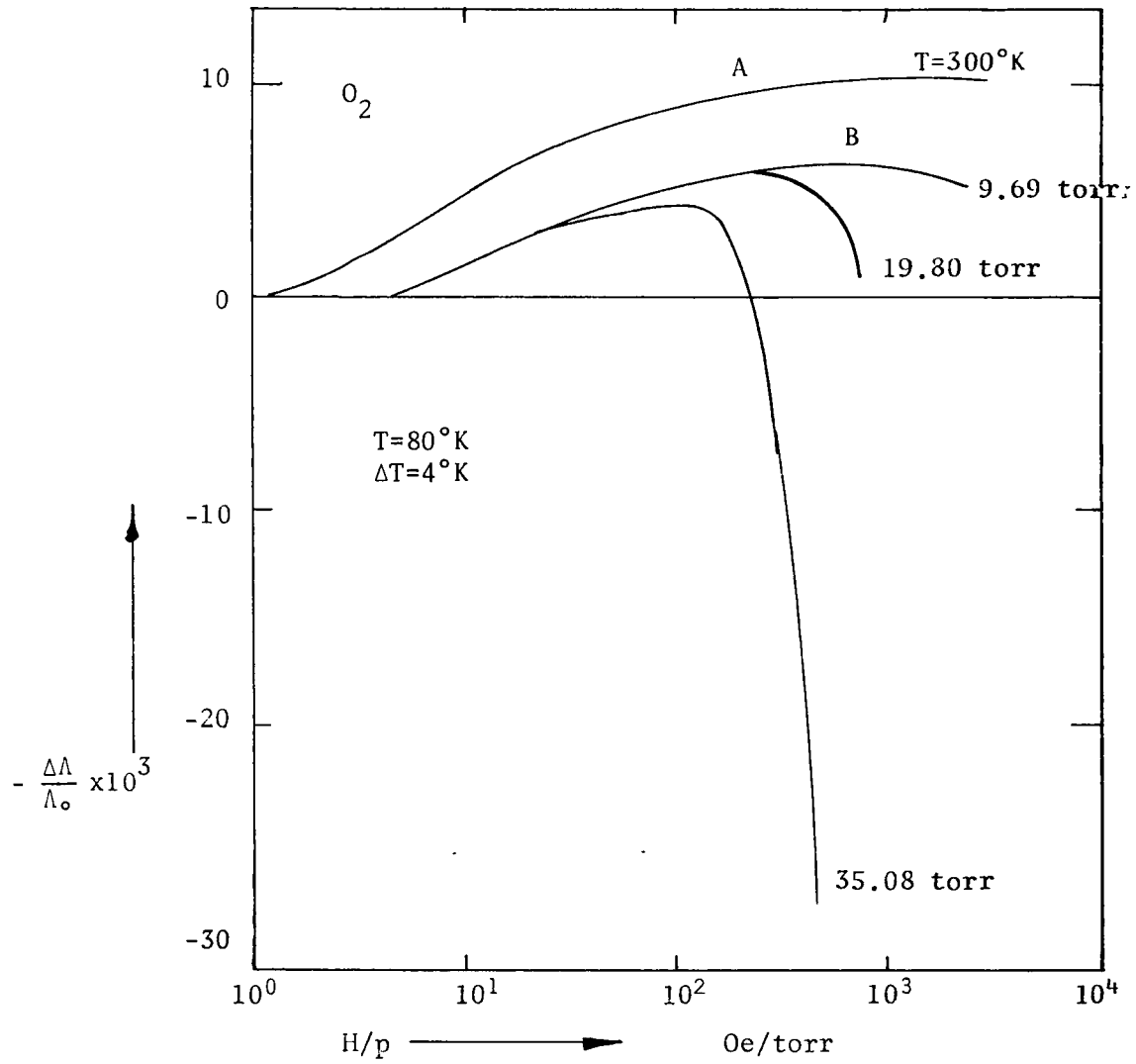
where Q_{MC} represents the concentration of all magnetoconvective phenomena. Solving for Q_{MC} in terms of equation VI-5,

$$Q_{\text{MC}} = Q - (\Delta T + \delta T_1) \left\{ \left(\frac{Q}{\Delta T} \right) + \hat{S} \left(\frac{\Delta\Lambda}{\Lambda_0} \right)_{\text{SBE}} \Lambda_0 \right\} \quad [\text{VI-7}]$$

is obtained. Thus, it was hypothesized that the heat energy flux transferred by the mechanism of magnetoconvection, Q_{MC} , was proportional to the departure of the experimental data from the ordinary SBE behavior at the same conditions of average temperature, cell pressure, temperature gradient, and field strength. Representative examples of such SBE deviations for oxygen at 80°K , $\Delta T=3.8^\circ\text{K}$, at several isobars are shown in Figure XV as functions of H/p with parametric pressure. Readily observable from these deviations is that the observable SBE increases monotonically with increasing field strength to some characteristic value dependent on the pressure, whereupon a noticeable decrease in the SBE occurs (recall a decrease in the SBE results in an increase in heat transfer). Thus, in the higher pressure regions where most magnetoconvective data were obtained, there is no corresponding SBE data with which to compare. This is quite clear in light of the fact that

these high pressure deviations shown in Figure XV are visualized to be the sole result of magnetoconvective processes. Thus, it is clearly evident that zero pressure SBE envelopes are the only source of SBE data with which to treat magnetoconvective data. Isobars such as B (9.67 torr) closely approximate this zero pressure envelope at 80°K and are therefore used to feed SBE data to equation VI-7. Similarly, this estimation procedure was repeated for various values of the average gas temperatures covering the range of temperatures over which the magnetoconvection effect, Q_{MC} , was desired to be measured, one, at 300°K, is given as curve A in Figure XV. The overall errors in the magnetoconvective contribution, Q_{MC} , to the total heat transferred resulting from this procedure is estimated to be insignificant since in general, the magnetoconvection effect is one or two orders of magnitude greater than the SBE; hence, even an error of 10% in determining the zero pressure SBE produces less than 1% error in most of the calculated values for Q_{MC} .

The ranges over which the experimental variables could be changed were controlled by the equipment limitations: H, 7 kOe to 14.1 kOe; p, 5 torr to 36 torr; ΔT , 12°K to 22°K; T_o , 79°K to 112°K. With the exception of ΔT , all experimentally controlled parameters were independently varied to obtain magnitudes as well as parametric dependencies of magnetoconvection as functions of pressure, temperature, and field strength. Since ΔT and T_o could not be independently varied, only parametric dependencies of Q_{MC} on ΔT could be obtained, no absolute magnitudes were available. Thus, to obtain the magnetoconvective



DEVIATIONS IN THE SENFTLEBEN-BEENAKKER EFFECT

FIGURE XV

data, the voltages across the inner cell heater and the 10Ω standard resistor are determined whence comes Q , the temperature of the outer plate and the temperature difference between plates is determined from their PRT resistances and calibration data, δT_1 is determined from the change in ΔT upon magnet energization, and the estimated zero pressure SBE data at that temperature are all incorporated in equation VI-7 (a simple FORTRAN program accomplishes this task) and the results are shown in Tables II, III, and IV. A graphical presentation and discussion of these results are deferred until Chapter VII.

TABLE II

EXPERIMENTAL RESULTS OF MAGNETOCONVECTION IN MILLI-WATTS AS A FUNCTION OF THE ABSOLUTE TEMPERATURE AT 36 TORR AND $\Delta T=22.6^{\circ}\text{K}$ WITH THE FIELD AS PARAMETERS.

T ($^{\circ}\text{K}$)	7.05 k Oe	8.82 k Oe	10.6 k Oe	12.3 k Oe	14.1 k Oe
79.0	0.318	0.697	1.255	1.916	2.762
86.25	0.259	0.611	1.072	1.648	2.351
98.0	0.210	0.390	0.727	1.075	1.572
112.0	0.106	0.192	0.316	0.488	0.732

TABLE III

EXPERIMENTAL RESULTS OF MAGNETOCONVECTION IN MILLI-WATTS AS A FUNCTION OF THE FIELD STRENGTH AT VARIOUS CONDITIONS AS INDICATED.

Field Strength (Oe)	A p=19.2 T _o =89.5 ΔT=22.7	B p=35.4 T _o =112.0 ΔT=22.6	C p=35.6 T _o =81.7 ΔT=12.5	D p=35.6 T _o =98.0 ΔT=22.6	E p=28.0 T _o =86.2 ΔT=22.6	F p=35.8 T _o =86.3 ΔT=22.6
7.05 k	0.116	0.106	0.142	0.210	0.225	0.259
8.82 k	0.229	0.192	0.278	0.390	0.479	0.611
10.6 k	0.398	0.316	0.519	0.727	0.844	1.072
12.3 k	0.628	0.488	0.770	1.080	1.294	1.647
14.1 k	0.951	0.732	1.113	1.572	1.954	2.351

TABLE IV

EXPERIMENTAL RESULTS OF MAGNETOCONVECTION IN MILLI-WATTS AS A FUNCTION OF THE ABSOLUTE PRESSURE AT $T=86.1$ °K AND $\Delta T=22.6$ °K FIXED , PARAMETRIC FIELD.

p (torr)	7.02 kOe	8.82 kOe	10.6 kOe	12.3 kOe	14.1 kOe
15.08	0.048	0.095	0.167	0.259	0.399
19.24	0.094	0.186	0.324	0.511	0.774
28.00	0.225	0.480	0.844	1.294	1.454
35.80	0.259	0.611	1.072	1.648	2.352

Simulation Study of the New Glenda Effect Model Under Analogous
Conditions of J. Vevai (18) at the Measured Gradient

Having these elegant experimentally observed data and results for the magnetoconvective effect over a wide operating range of temperatures, pressures, temperature gradients and field strengths, it only remained to compare these figures with those predicted by the Glenda effect model both in magnitude and parametric dependence under the same conditions found in the experimental work. It is recalled from Chapter III that the Glenda effect model predicted a functional and quantitative dependence as expressed in equation III-52, or separating the constant and fixed parameters from the experimentally controllable variables,

$$Q_{G1} = \frac{C}{v} \frac{C \ell D^3 \omega}{45M} \left(\frac{\partial H}{\partial z} x \right) \left[\frac{\rho_o \Delta T^2 H}{v_o T_o^2 x} \right] \quad \text{[VI-8]}$$

is obtained where all variables are as previously defined.

With the exception of the characteristic length of the cell, D , and its depth, ℓ , which are the only parameters dependent on cell geometry, all other fixed or constant parameters have been previously described and discussed and are re-defined here for convenience of the reader:

$$C_v \equiv 0.15 \text{ cal } ^\circ\text{K}^{-1} \text{ gm}^{-1} \quad \text{[III-65]}$$

$$C \equiv 1.02 \text{ dyne cm } ^\circ\text{K mol}^{-1} \text{ Oe}^{-2} \quad \text{[VI-9]}$$

$$\omega \equiv 4.18 \times 10^3 \text{ mW sec cal}^{-1} \quad [\text{III-53}]$$

$$M \equiv 32.0 \text{ gm mol}^{-1} \quad [\text{VI-10}]$$

$$\frac{\partial H}{\partial z} \equiv 2.0 \text{ Oe cm}^{-1} \quad [\text{VI-11}]$$

Since the applied field and its associated gradient are always juxtaposed in the model as a product, the incorporation of their signs can safely be performed provided neither changes sign over the range of expected values. In the particular case at hand, it has been shown that both the applied field and its associated gradient remain negative for all values; the resulting annihilation of signs is reflected in the gradient shown in equation [VI-11].

In the case of a rectangular cell such as proposed in Chapter IV, the values for the characteristic distance D and its associated depth λ would be quite clear. Unfortunately, the actual experimental investigation utilizing the cylindrical cell as discussed was more difficult to geometrically define. In fact, the entire Glenda model analysis was attempted in a cylindrical coordinate system, but with the applied field being perpendicular to the cell axis (any other orientation would have provided meaningless results), and the undeniably Cartesian nature of this field (H_x only) in the r^{th} direction of the cylindrical geometry, this analysis was soon abandoned. However, the differences in heat transfer between a cylindrical cell and an analogous rectangular cell

should be relatively small (certainly not five orders of magnitude as previously ascribed) in light of the visualization of a cylindrical cell being the near limit of a progressively rounded rectangular cell. Thus, the actual case of cylindrical geometry is approximately fit to the rectangular model.

The characteristic distance of the cell, D , it will be recalled, is independent of the cell thickness, ℓ , and only reflects the half-spacing between plates and therefore will be approximated by the inside diameter of the cell divided by 4. Choosing the log-mean of the two inside diameters to represent the depth ℓ (a common procedure for average coaxial cylinder values), the Glenda effect heat transfer equation [VI-8] becomes,

$$Q_{GI} = (2.66) \left(\frac{\rho_o \Delta T^2 H}{v_o T_o^2 x} \right) \quad . \quad [VI-12]$$

Incorporating the previously defined relations for density, ρ_o , i.e.

$$\rho_o = (5.118 \times 10^4) \left(\frac{P}{T_o} \right) \quad [III-56]$$

and the empirical correlation for kinematic viscosity given by equations III-61 and 62, the heat transfer in milliwatts arising solely from the Glenda effect can thus be calculated for all values of pressure, average temperature, temperature gradient and applied magnetic field strength of interest. In particular, a simulation study was performed on exactly the conditions given in Tables II, III, and IV (a FORTRAN

program to accomplish this task appears in Appendix C), the results appearing in a corresponding fashion in Tables V, VI, and VII. Included in this simulation study was a least squares computation of the rather ambiguous power to which the average temperature is raised in the model owing to the non-linearity of T_0 in the empirical kinematic viscosity, quite unlike the more obvious powers of the pressure, temperature gradient, field and field gradient in the model. This analysis showed this exponent of T_0 to be -5.07 for all values of T_0 investigated. Thus, the parametric dependence predicted by the Glenda effect model can approximately be given by

$$Q_{G1} \propto p^2 \Delta T^2 T_0^{-5} H_x \left(\frac{\partial H}{\partial z} \right) \quad [VI-13]$$

and should follow the observed parametric dependence found in the experimental work. A graphical presentation and comparative discussion of these results with the analogous experimental observations are discussed in the following chapter. Parenthetically, it is added that ideally, provided the Glenda effect model is a valid description of the magnetoconvective processes in oxygen, it is expected that

$$Q_{G1} \Big|_{\text{theo}} \approx Q_{MC} \Big|_{\text{exp}} \quad [VI-14]$$

TABLE V

THEORETICALLY EXPECTED RESULTS OF MAGNETOCONVECTION IN MILLIWATTS AS A FUNCTION OF THE ABSOLUTE TEMPERATURE AT 36 TORR AND $\Delta T=22.6^{\circ}\text{K}$ WITH THE FIELD AS PARAMETERS.

T ($^{\circ}\text{K}$)	7.05 k Oe	8.82 k Oe	10.6 k Oe	12.3 k Oe	14.1 k Oe
81.7	1.172	1.477	1.774	2.059	2.360
86.3	0.886	1.117	1.342	1.557	1.785
89.5	0.736	0.928	1.115	1.294	1.483
98.0	0.464	0.585	0.703	0.816	0.936
112.0	0.237	0.298	0.358	0.416	0.477

TABLE VI

THEORETICALLY EXPECTED RESULTS OF MAGNETOCONVECTION
IN MILLIWATTS AS A FUNCTION OF THE FIELD STRENGTH AT
VARIOUS CONDITIONS AS INDICATED.

Field Strength (Oe)	A p=19.2 T _o =89.5 ΔT=22.7	B p=35.4 T _o =112.0 ΔT=22.6	C p=35.6 T _o =81.7 ΔT=12.5	D p=35.6 T _o =98.0 ΔT=22.6	E p=28.0 T _o =86.2 ΔT=22.6	F p=35.8 T _o =86.3 ΔT=22.6
7.05 k	0.318	0.237	0.361	0.470	0.558	0.906
8.82 k	0.275	0.298	0.455	0.592	0.703	1.142
10.6 k	0.331	0.358	0.546	0.711	0.844	1.372
12.3 k	0.384	0.416	0.634	0.826	0.980	1.952
14.1 k	0.440	0.477	0.727	0.946	1.123	1.826

TABLE VII

THEORETICALLY EXPECTED RESULTS OF MAGNETOCONVECTION
IN MILLIWATTS AS A FUNCTION OF THE ABSOLUTE PRESSURE
AT $T=86.1^{\circ}\text{K}$ and $\Delta T=22.6^{\circ}\text{K}$ FIXED, PARAMETRIC FIELD.

p (torr)	7.05 k Oe	8.82 k Oe	10.6 k Oe	12.3 k Oe	14.1 k Oe
19.2	0.264	0.332	0.399	0.464	0.531
28.0	0.561	0.707	0.850	0.986	1.130
35.4	0.897	1.130	1.358	1.576	1.806
35.6	0.907	1.143	1.373	1.594	1.827
35.8	0.917	1.155	1.389	1.611	1.847

CHAPTER VII

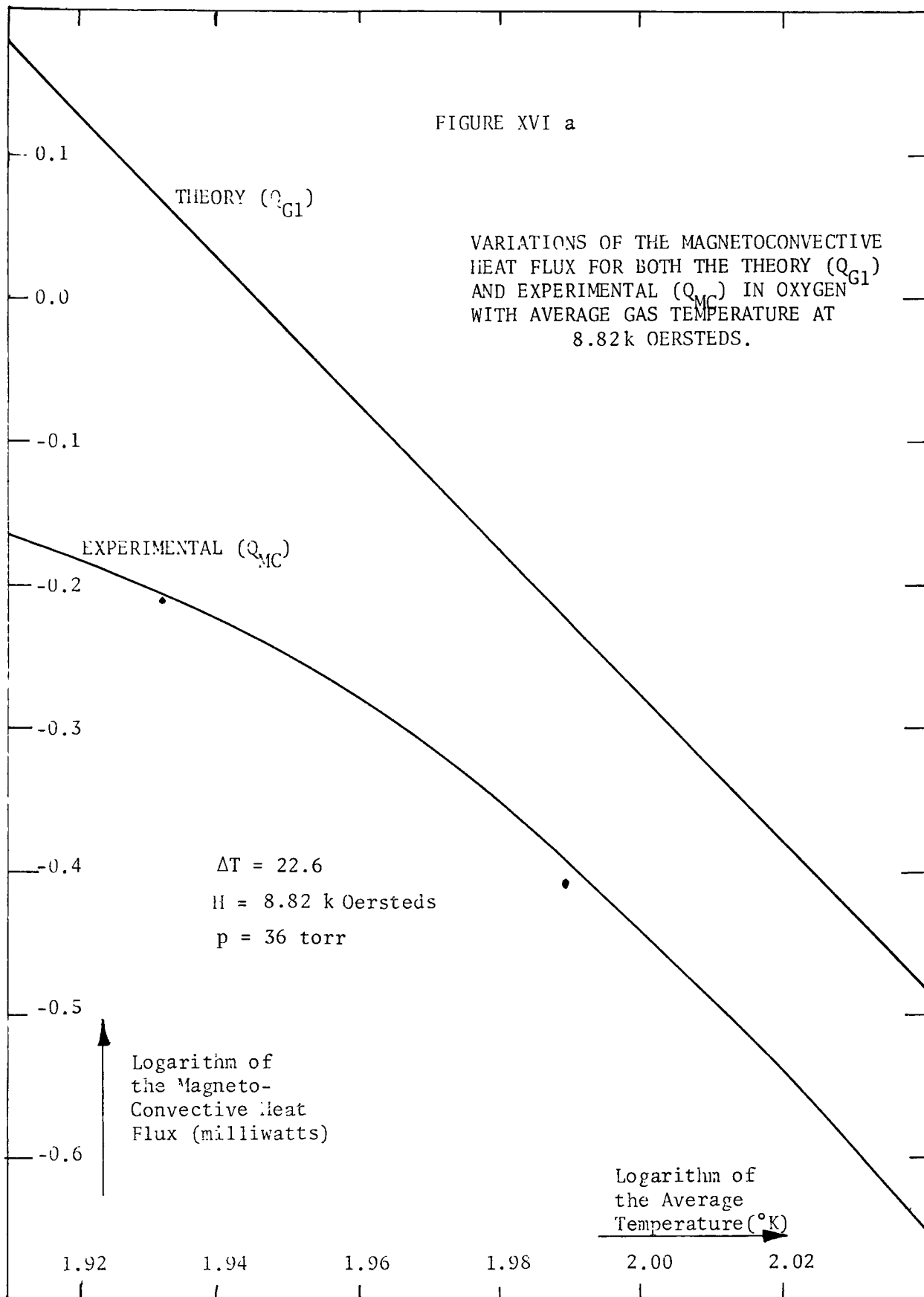
DISCUSSION OF RESULTS, RECOMMENDATIONS FOR FUTURE STUDIES AND CONCLUSIONS

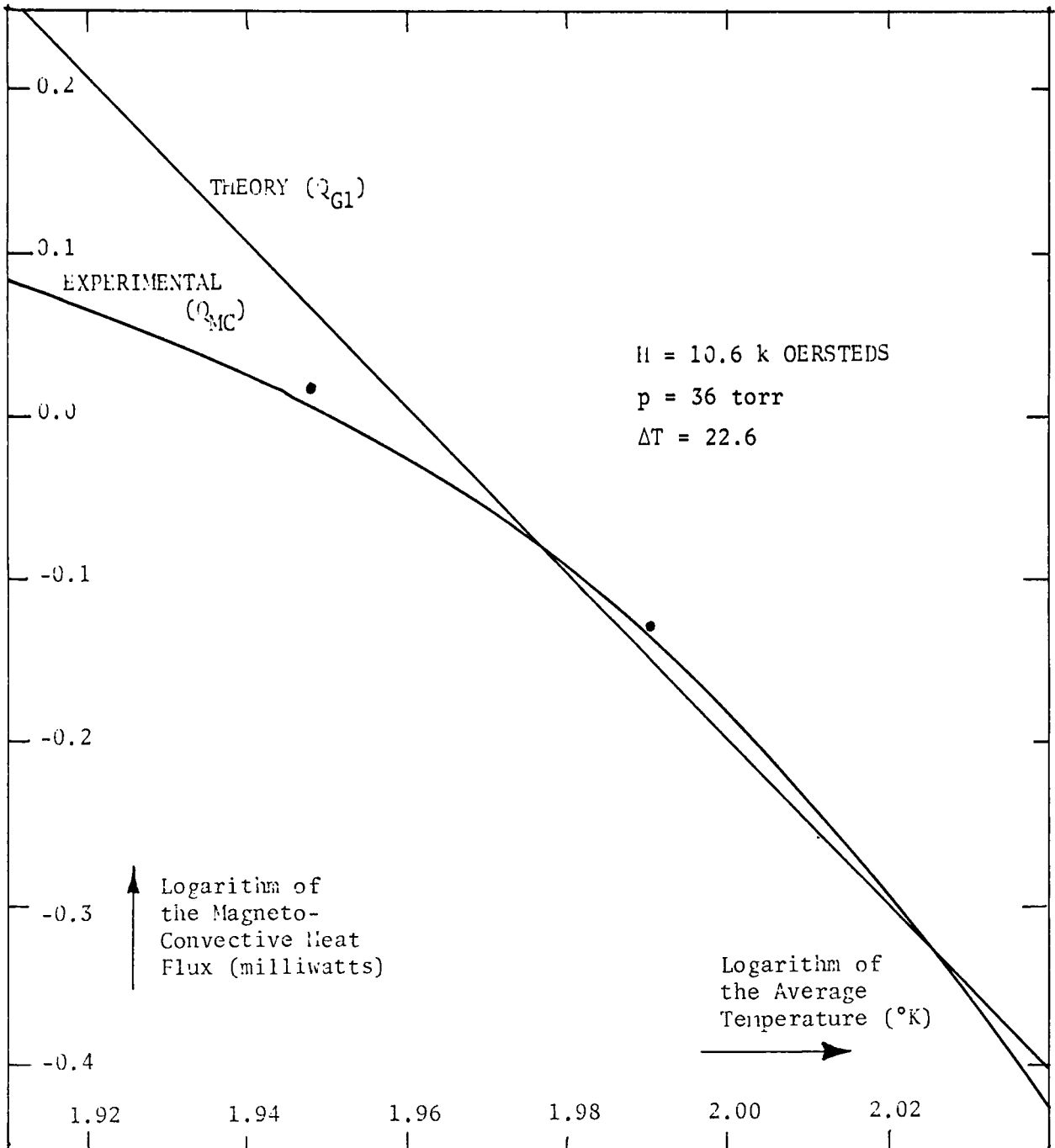
Comparison of Results

Upon inspection of the last six tables, it is quite evident that the values of the magnetoconvective contribution to the overall heat transfer as predicted by the Glenda effect model are in surprisingly close agreement with those same values observed in the laboratory. To improve the visualization of this comparison, and at the same time compare the relative parametric dependencies of the model with the experiment, log-log plots were obtained for each functional dependence of both the theoretical and experimental values of Tables II-VII and plotted together on linear paper, as shown in Figures XVI, XVII, and XVIII for rapid quantitative comparisons. Quite obviously, the slopes of each of these log-log relations gives the relative exponential dependence of the experimental results with the expected theoretical dependencies; their relative positions giving rise to comparative magnitudes of the effect. Upon casual inspection of these Figures, it is readily apparent that the agreement in the magnitudes of both the theory and the experimental is quantitatively quite good, the deviations by in large stemming from a differing field dependence between the theory and experiment as discussed later. In light of the 5 orders of magnitude difference between these experimental results and the

FIGURE XVI a

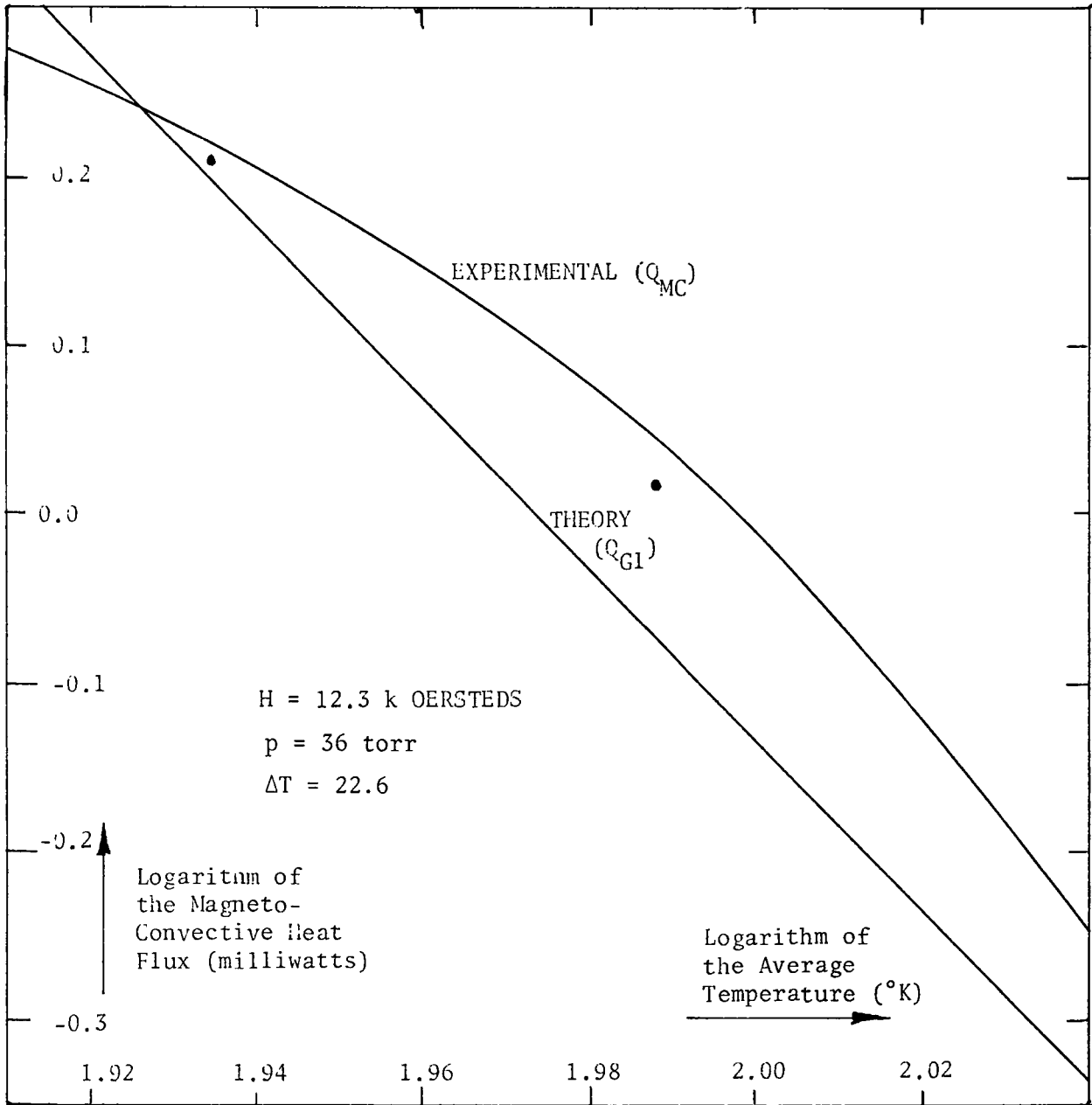
VARIATIONS OF THE MAGNETOCONVECTIVE
HEAT FLUX FOR BOTH THE THEORY (Q_{G1})
AND EXPERIMENTAL (Q_{MC}) IN OXYGEN
WITH AVERAGE GAS TEMPERATURE AT
8.82k OERSTEDS.





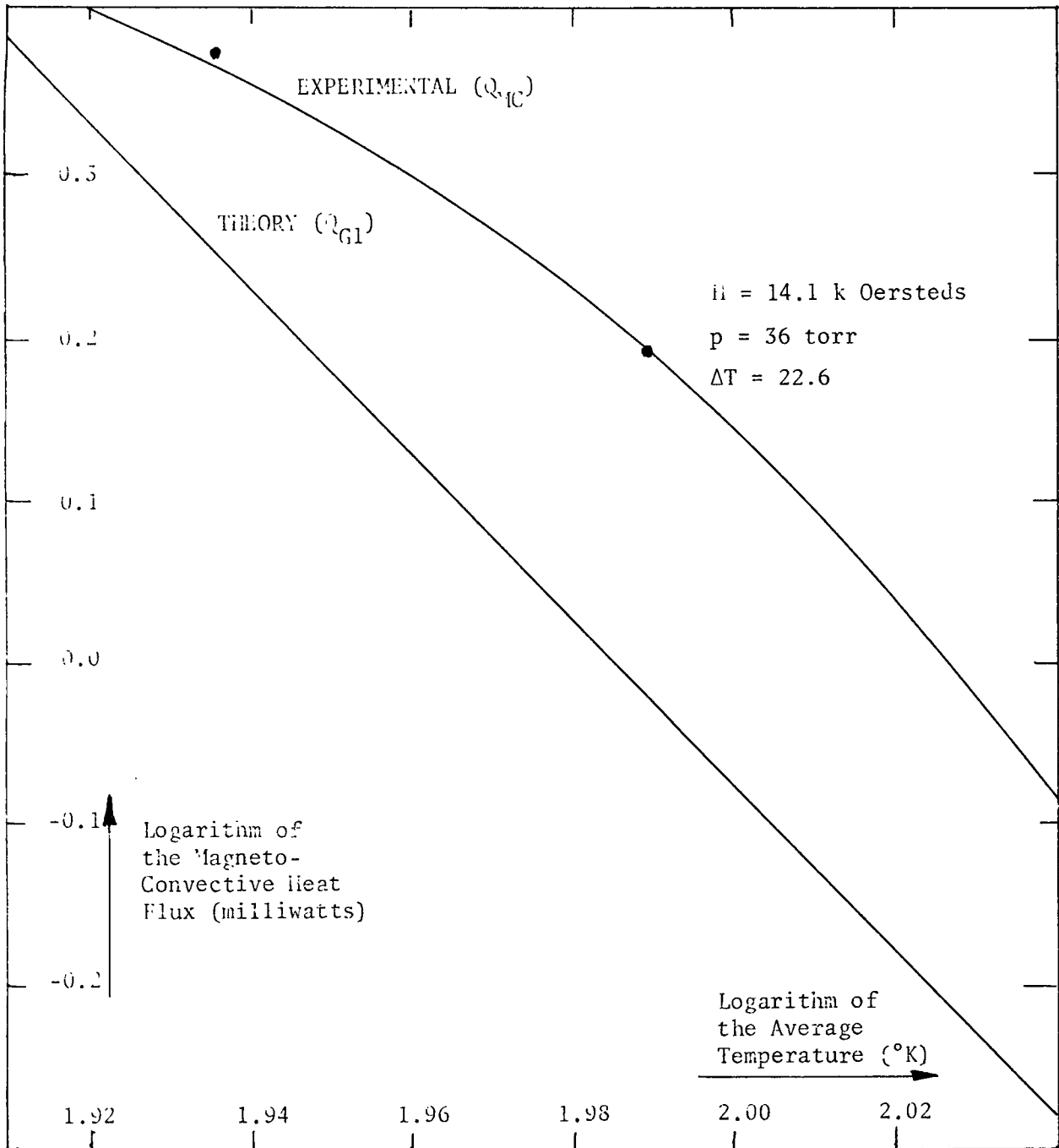
VARIATIONS OF THE MAGNETOCONVECTIVE HEAT FLUX FOR BOTH THE THEORY (Q_{G1}) AND EXPERIMENTAL (Q_{MC}) IN O_2 WITH AVERAGE GAS TEMPERATURE AT 10.6 k OE.

FIGURE XVI b



VARIATIONS OF THE MAGNETOCONVECTIVE HEAT FLUX FOR BOTH THE THEORY (Q_{G1}) AND EXPERIMENTAL (Q_{MC}) IN O_2 WITH AVERAGE GAS TEMPERATURE AT 12.3 k OE.

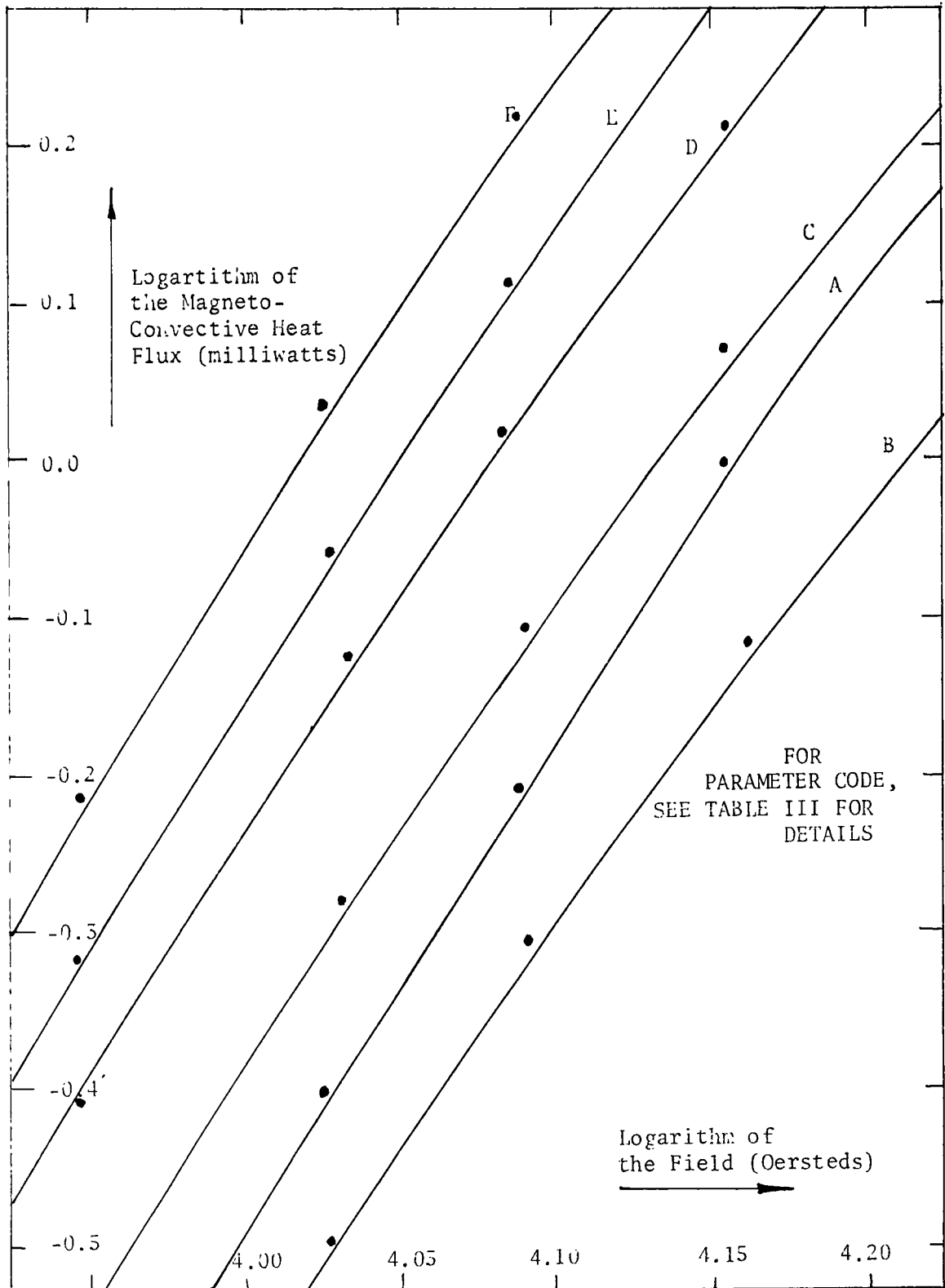
FIGURE XVI c



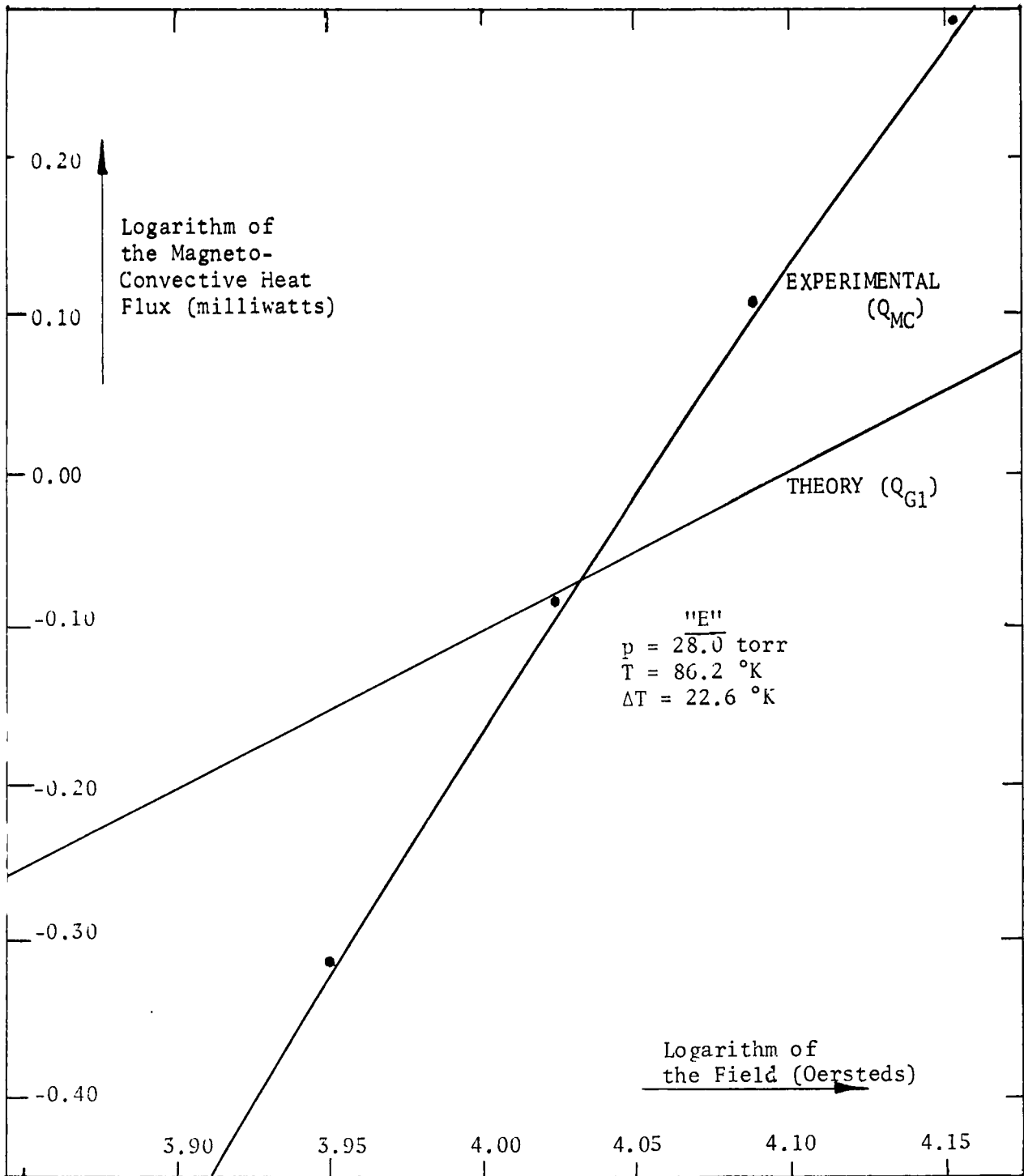
VARIATIONS OF THE MAGNETOCONVECTIVE HEAT FLUX FOR BOTH THE THEORY (Q_{G1}) AND EXPERIMENTAL (Q_{MC}) IN OXYGEN WITH AVERAGE GAS TEMPERATURE AT 14.1 k Oe.

FIGURE XVI d

FIGURE XVII a

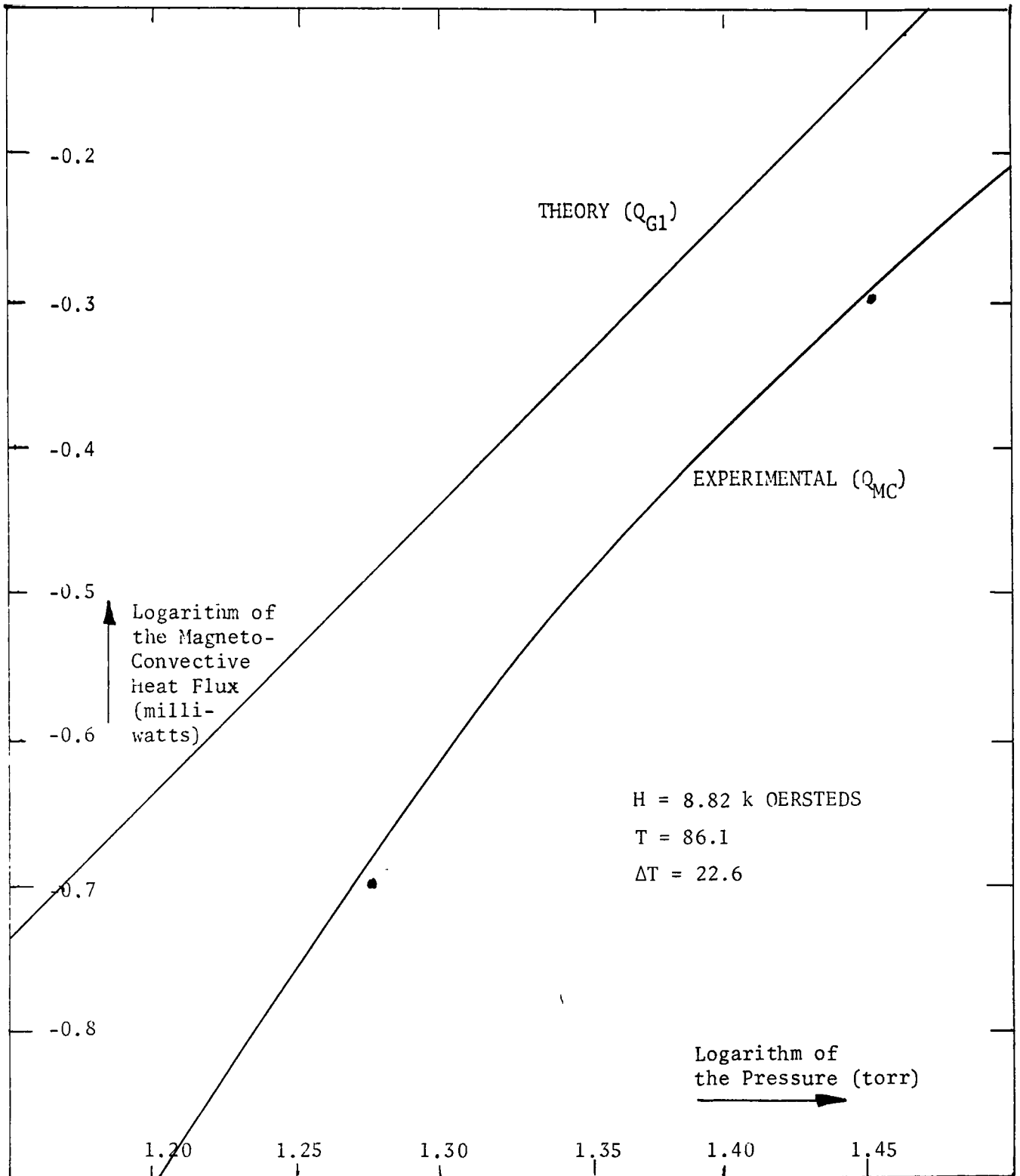


EXPERIMENTAL MAGNETOCONVECTIVE HEAT FLUX (Q_{MC}) IN O_2 WITH THE FIELD.



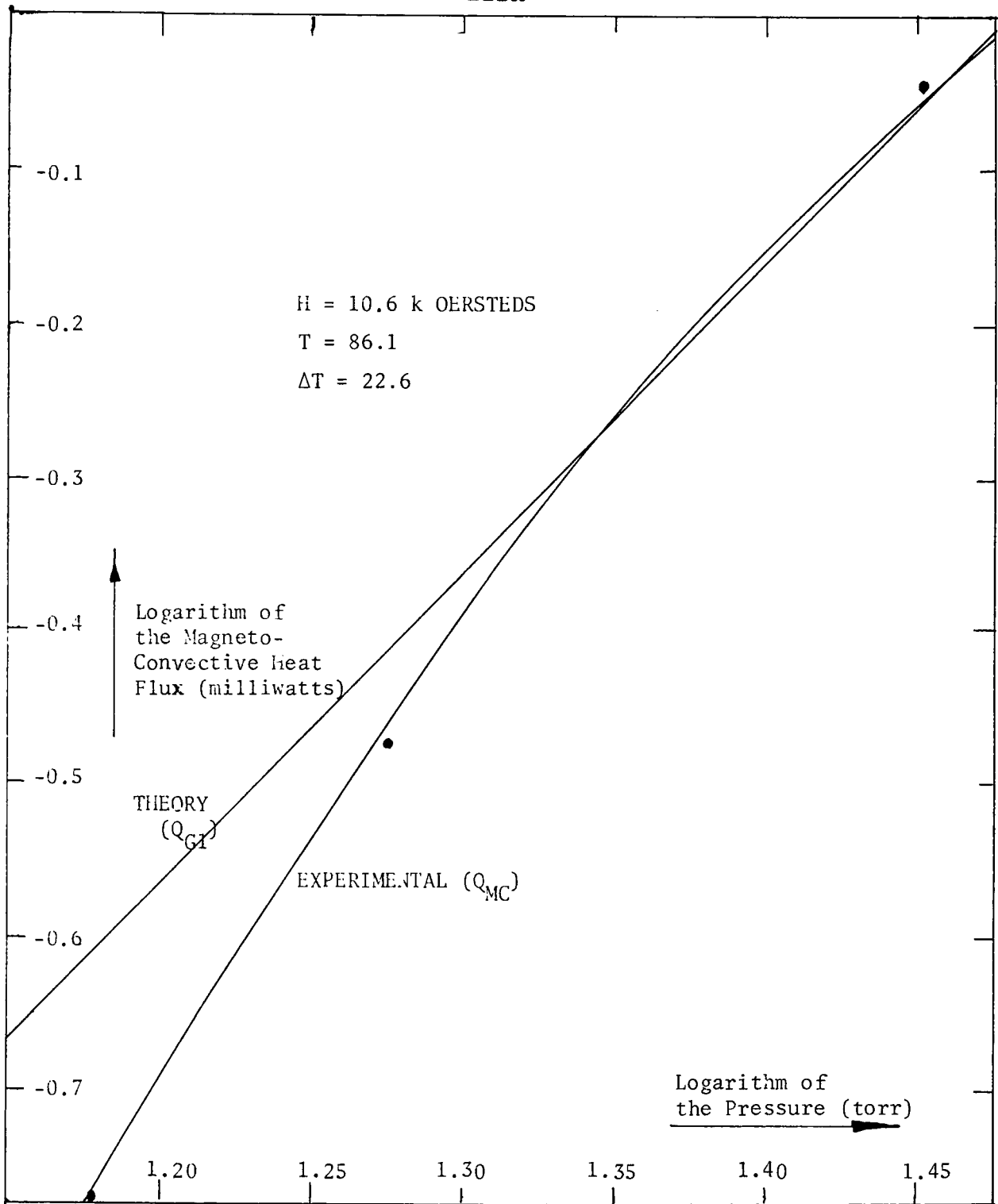
VARIATIONS OF THE MAGNETOCONVECTIVE HEAT FLUX FOR BOTH THE THEORY (Q_{G1}) AND EXPERIMENTAL (Q_{MC}) IN O_2 WITH THE FIELD UNDER GIVEN CONDITIONS.

FIGURE XVII b



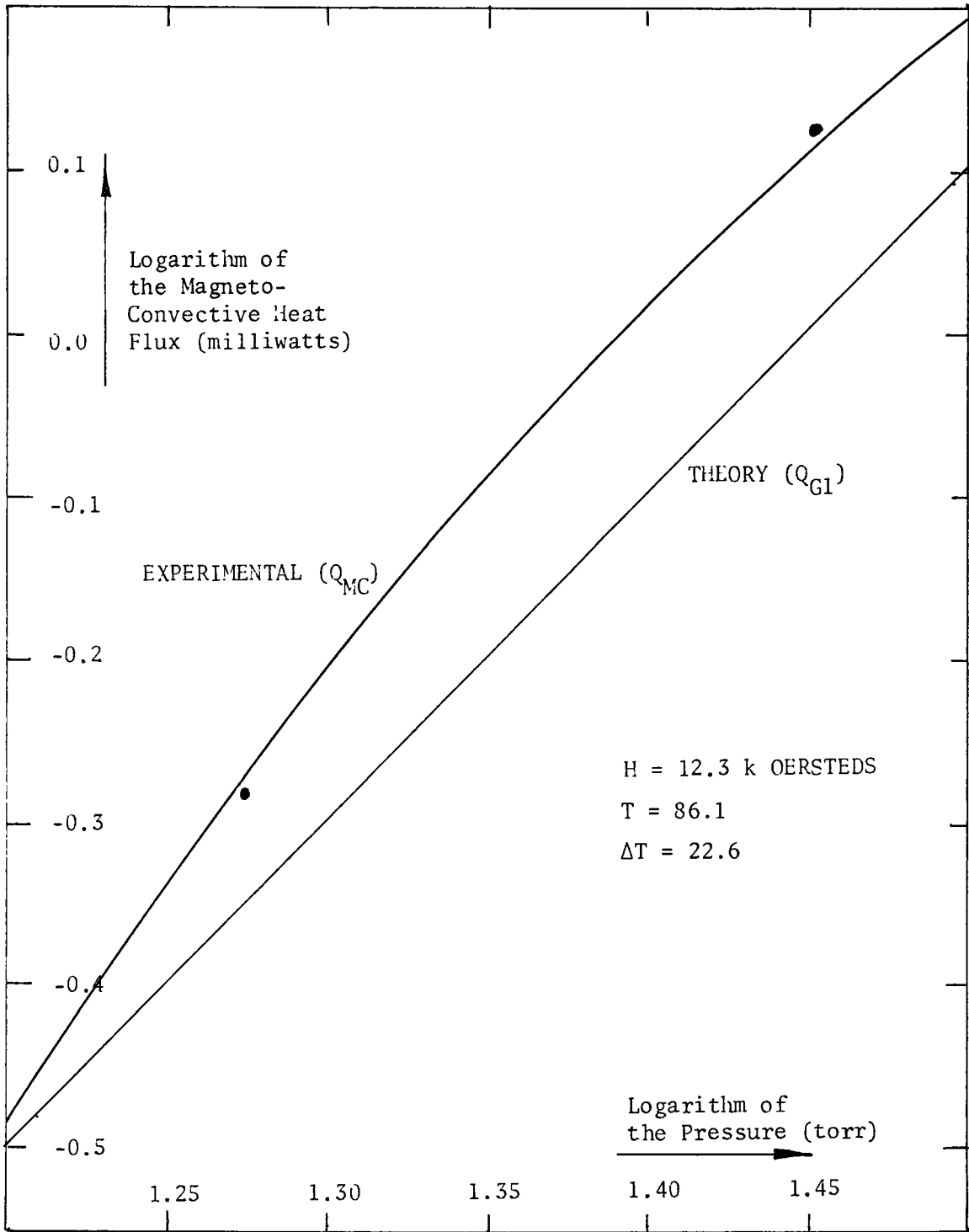
VARIATION OF THE MAGNETOCONVECTIVE HEAT FLUX FOR BOTH THE THEORY (Q_{G1}) AND EXPERIMENTAL (Q_{MC}) IN O_2 WITH PRESSURE AT 8.82 k OERSTEDS.

FIGURE XVIII a



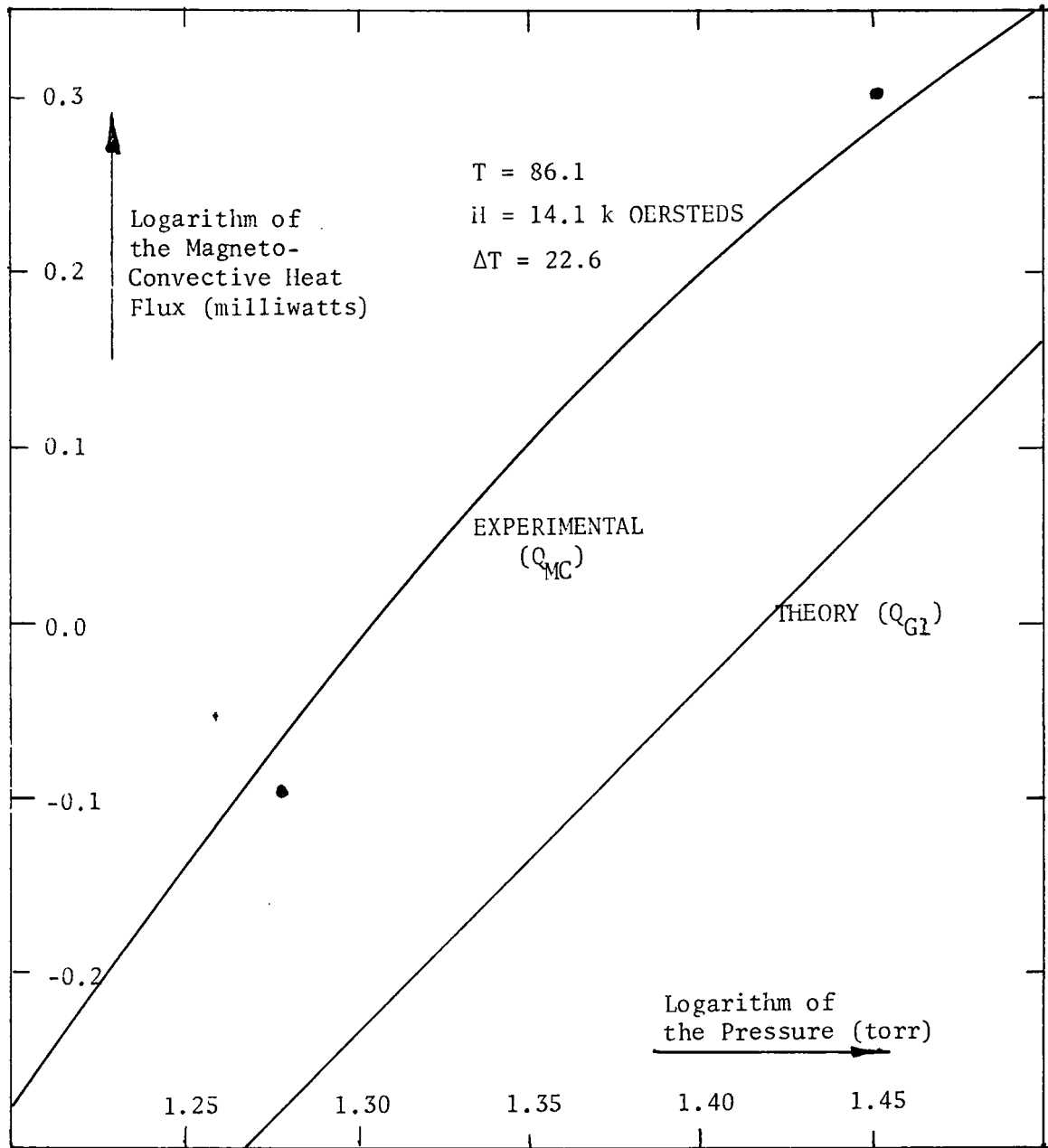
VARIATION OF THE MAGNETOCONVECTIVE HEAT FLUX FOR BOTH THEORY (Q_{G1}) AND EXPERIMENTAL (Q_{MC}) IN O_2 WITH PRESSURE AT 10.6 k OERSTEDS.

FIGURE XVIII b



VARIATIONS OF THE MAGNETOCONVECTIVE HEAT FLUX FOR BOTH THEORY (Q_{G1}) AND EXPERIMENTAL (Q_{MC}) IN O_2 WITH PRESSURE AT 12.3 k OERSTEDS.

FIGURE XVIII c



VARIATIONS OF THE MAGNETOCONVECTIVE HEAT FLUX FOR BOTH THEORY (Q_{G1}) AND EXPERIMENTAL (Q_{MC}) IN O_2 WITH PRESSURE AT 14.1 k OERSTEDS.

FIGURE XVIII d

old (Park) model expectations, this seemingly excellent agreement is indeed quite striking in itself, but the relative agreement in the parametric dependence as well is an extra treat.

The Glenda effect model predicts a -4.5 power dependence of the average temperature based on ideality, but when the empirical viscosity correlation was used, the least squares treatment gave a -5.07 power dependence on T_0 as shown. Experimentally, the parametric dependencies fall somewhere between -4.8 and -5.2 and is therefore in excellent agreement with the model predictions. That the experimental data deviate considerably at the lower temperatures is an expectation in light of the ideal gas approximation used throughout the model and the actual approach of oxygen to the saturation region at those pressures as the temperature decreases. The magnetic field parametric placement is slightly off at this time, since the model anticipates linearity in the field whereas, as will be discussed, the experimental evidence seems to demand a cubic field dependence. However, all values seem to be in the right ball park, the value corresponding to 10.6 kOe matching almost perfectly. It is recalled additionally that the model is most in error at large field settings (owing to the high drift in the field at large values), so that the precise setting of the 14.1 kOe plot is in high error (as high as 100%). Thus, from this analysis, it is concluded that the magnitudes of both the experimental and theoretical are in good agreement as are the parametric dependencies of average temperature at -5.0 .

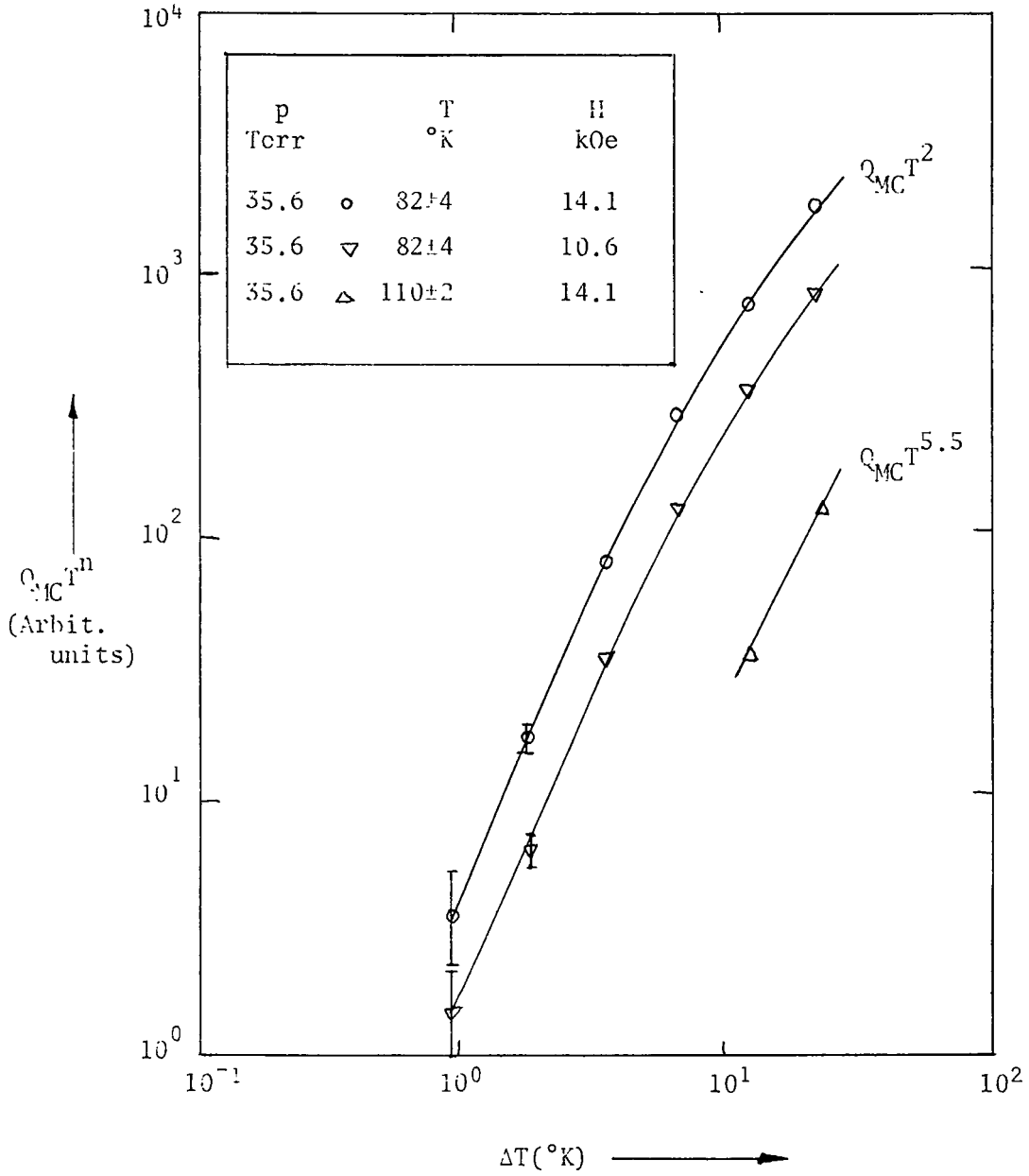
As evident in Figure XVIIb, there is no mistaking the considerable

deviation between the model and the experimental evidence in this case insofar as the parametric dependence on the field strength is concerned. The Glenda effect model predicts, for uniform gradient, a linear dependence on the applied field; of course, as can be seen, the experimental evidence is at variance with this expectation since the observed dependence is very nearly cubic. Despite the fair agreement in magnitude, no explanation can be offered at this time to rationalize this discrepancy in observed and predicted behavior of the heat transfer toward the field. However, it should be added that despite this observed experimental behavior of the magnetoconvective heat transfer with the field, it cannot be concluded ipso facto that it is uniquely the field which must be raised cubically to obtain the indicated change in heat transfer. Indeed, it has been demonstrated that the term of significance in the Glenda effect model is neither the field nor the gradient, but rather it is their completely inseparable product. Thus, a cubic dependence of magnetoconvective heat transfer with field may in actuality be a reflection of the inseparable field-field gradient product which rises cubically with a linear field. Nonetheless, in light of the relatively constant field gradient actually observed for most field values considered, this discrepancy remains unsettled. Nevertheless, the qualitative agreement in magnitude between the experimental and theoretical results is laudable in light of past modelling agreements.

As in the average temperature dependence, it is noted that there is excellent agreement between the theory and experimental in the

pressure dependence both in magnitude and parametric dependence. The model predicts, owing to the presence of density squared, a p^2 dependence with Q_{G1} . The experimental evidence shows a p^3 dependence below 20 torr and a p^2 dependence (actually closer to $p^{1.7}$) at pressures of 25 torr and above; no data were available past 36 torr (fear of cell rupture). The deviations in field parameters behave analogous to the temperature dependence discussed above; again the value at 10.6 kOe almost corresponding perfectly. Again, deviations from ideality (recall here the ideal density is squared) are visualized to rationalize the high pressure deviations. As yet, no conclusions can be drawn regarding the low pressure deviations, although one may wonder about the nature of viscous interactions at such low pressures. Thus, it can be concluded that the magnitude of the pressure dependence is quite good, as is the parametric dependence, at least at pressures beyond 25 torr.

As mentioned earlier, it was not possible to hold the average gas temperature, T_0 , constant in the present apparatus while varying ΔT . Hence, in the experimental study, data were taken for which T_0 was allowed to vary with ΔT . In this arrangement, only a functional dependence of the magnetoconvective heat transfer on the temperature gradient could be obtained; no absolute magnitudes were available. Plotting the magnetoconvection contribution, Q_{MC} , in arbitrary units against the temperature gradient, as shown in Figure XIX, it can readily be seen that the slope is 2 requiring a quadratic temperature gradient dependence.



VARIATION OF THE MAGNETOCONVECTIVE HEAT FLUX WITH THE TEMPERATURE GRADIENT ACROSS THE CELL

FIGURE XIX

In general therefore, for all parametric studies undertaken, there exists a fair agreement in magnitude over the entire region of study between the theoretically predicted values and the experimentally observed results. Parametrically, as shown earlier, the model demands a dependence on the order of

$$Q_{G1} \propto p^2 \Delta T^2 T_0^{-5} H_x \left(\frac{\partial H}{\partial z} x \right) \quad [\text{VI-13}]$$

whereas the experiment requires

$$Q_{MC} \propto p^2 \Delta T^2 T_0^{-5} H_x^3 \quad [\text{VII-1}]$$

for pressures greater than 25 torr. The sole deviation being the field dependence, which again is not prima facie evidence that indeed it is the cube of the field that is being followed, the overall agreement is quite striking. It is parenthetically added that despite the not-so-perfect agreement between theory and practice, the improvement in the agreement in magnitude by five orders over the sole former work in this area is worthy of note (the parametric dependence of this old model disagreed in the field with the experimental also). It must be additionally kept in mind, that all the experimental endeavours, with the exception of the field gradient studies, all taken with the extremely sensitive SBE instrumentation, possesses negligible associated error; at the same time, the new Glenda effect model, in the field gradient studies alone, possesses characteristic errors ranging from 25% at the low field values,

to over 100% at the high values. Thus, it can be concluded that these results indicate at least ballpark agreement, a nonetheless hitherto unprecedented accomplishment in the field of magnetoconvection.

Future Studies

Having what appears to be a viable model to describe the Glenda effect in oxygen, all future work therefore revolves about the collection of more data to extend its range. Primary consideration in this experimental effort should be completion of the rectangular cell construction including thorough testing over the expected operating range. Attention should be focused on the higher pressure and temperature ranges, in the 100 torr and 150°K ranges. Despite the T^{-5} dependence, the effect should still be observable at higher temperatures if the proper pressures and temperature gradients are established.

To clarify the field dependence discrepancies, variations in the field-field gradient product should be the object of advanced studies as well. Other gradients should be established across the cell other than the indigenous field gradient to establish the dependence of the field gradient as well. To accomplish this task, either the addition of thin iron wedges of varying slopes to the pole caps should be made, or commercial caps of small and varying gradient purchased. The greatest consideration here, however, is the assurance of the separation of the field and field gradient: each must be allowed to vary but independently of the other.

In terms of long range planning, the turbulent region Glenda effect should boldly be investigated. This, of course, would require much larger field-field gradient products, thus paving the way to analysis with much smaller magnets having nevertheless large gradients, typical of those used in simple Gouy balance experiments, such as available in the laboratories of Professor Richardson. Concomitant with this extension, however, would be the need for computer modelling of the now highly non-linear magnetic body force over the region of interest, i.e.,

$$H \text{grad } H \Big|_{\text{eff}} = \frac{1}{|z_1 - z_2|} \int_{z_1}^{z_2} H_x(z) \left(\frac{\partial H}{\partial z} \right) dz \quad [\text{VII-1}]$$

where the entire integral would be a strong function of z . The magnitude of this body force is nearly limitless and at these high values, the Grashof contribution could be easily considered negligible. Of immediate interest would be an a posteriori study, into the turbulent region, of the correlation between this magnetic body force, driving force and a modified surface heat transfer coefficient. Later, more elegant studies of the turbulent magnetoconvective effect could be undertaken, e.g. the stability of the transition region, stochastic models, etc. Obviously, as far as applications are concerned, such as heat transfer of oxygen in tanks in space, more interest would be placed on the empirical correlations of the heat transfer far into the turbulent regions. Effectively then, heat transfer processes could be devised to viably compete with the more classical forced methods such as fans

and pumps, highly beneficial in applications where classical forcing methods would be disadvised, such as high pressure or high temperature environments.

Another area that should be actively pursued without hesitation is the modelling of the Glenda effect in magnet systems having z-directed applied fields. In particular, it has been noted in these laboratories (18), that there is an extremely pronounced increase in heat transfer in oxygen at 36 torr at 80°K when subjected to the intense z-directed magnetic fields of the superconducting magnet system, the gradients of which are omnidirected and rather severe. Although the analysis can be simplified somewhat through the now possible use of a cylindrical coordinate system ($\vec{H} = H_z \hat{z}$) and the already extant cylindrical cell and concomitant data, the incorporation of such a field and its associated gradients cannot be considered a priori to be a simple extension of the original Glenda effect model proposed here. Indeed, upon reference to equation II-39 in Chapter II, showing the complete componential makeup of the significant electromagnetic body force, $\vec{j} \times \vec{B}$, it can be seen that such a z-directed field offers no additional magnetic body force in that self-same direction; any increase in convective flow, then, cannot be rationalized by the simple superposition of the vertical Grashof and Glenda velocities as was considered in this current model. Indeed, the body forces responsible for increased convective flow are clearly x and y directed and are very intense owing to the magnitude of the applied field and its associated gradients, i.e. from equation II-39,

$$\vec{j} \times \vec{B} = \left(\left(\frac{\partial H}{\partial z} x - \frac{\partial H}{\partial x} z \right) B_z \right) \vec{i} - \left(\left(\frac{\partial H}{\partial y} z - \frac{\partial H}{\partial z} y \right) B_z \right) \vec{j} \quad . \quad [\text{VII-2}]$$

Despite the magnitudes of these forces, the omni-present flow resulting from the normal Grashof convection cannot be neglected and undoubtedly resolve should be made to implementation of the stream function to render the now non-vanishing inertial terms amenable. The situation is somewhat simplified through the elimination of the H_x and H_y induced terms above, and the neglect of the gradient of the permeability, $\nabla\mu$, now much smaller than the field gradient associated body forces, but the analysis remains as an intriguingly unsolved challenge. To visualize the processes involved under such conditions, it is best to imagine the magnetoconvection occurring in the absence of gravity; the sole motivation for fluxive heat transport from the hotter to cooler wall then becomes the gradient in the permeability and the resulting differences in body force in the x and y direction. The analogous, non-magnetic case of a hot horizontal plate initiating convection in a quiescent fluid cooled by another plate exemplifies this process and should provide the initial modelling strategies by which this analysis is conducted.

As a final consideration for future work, the liquid analogue of this work should be investigated. This analysis will entail considerable difficulty since it is doubtful if the Boussinesq approximation would still be valid for liquids. A way to avoid this problem would be to obtain empirical correlations on the temperature and concentration dependencies of the mass susceptibility. Another possible technique

would be to expand both the paramagnetic permeability and density coefficients of the magnetic body force in a Taylor's series about the average temperature, T_0 .

Conclusions on the Project

Briefly, the events that lead to the development and confirmation of the Glenda effect model are here recounted. The original experimental efforts to construct the rectangular cell (object: verification of the old Park theory with the new cell) were interrupted to become facile in the theoretics of all of magnetogasdynamics to respond to the doubts regarding magnetic pressure validity. In this effort, the question of field gradients arose and work commenced on developing a gradient based model (the Glenda effect). Several attempts were made - each violated some fundamental axiom of engineering - then the present model was developed - only a gradient was needed. Anticipating that the existing inhomogeneity was too small to measure, methods were sought to superpose a linear gradient on the applied field - none were successful. By this time, however, all the associated support systems, e.g. all electronics, vacuum systems, loading racks, etc., had been completely re-worked and ready for new measurements. Using a previously untested method of field strength measurement, it was learned that the inherent gradient was on the order of the theoretically anticipated value of ≈ 1 Oe/cm. After a computer simulation of the theory and comparison of the results with the excellent experimental data, the model fit the data so well that it was deemed pointless to continue further data acquisition.

In a paragraph, that is the gist of this project.

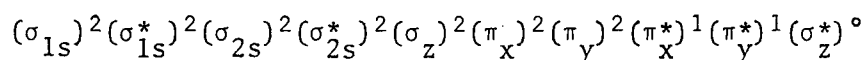
It should be observed in conclusion that the similarity of the results of both the experimental and theoretical is quite remarkable in light of all of the oftentimes seemingly gross assumptions on which the Glenda effect model is based and the errors associated with the measurements. Additionally, as its own name indicates, the Boussinesq approximation is indeed only an approximation, and in light of its frequency in the derivation, deviations should be expected. Moreover, the ideal nature of the equation of state used liberally throughout the derivation to characterize the density casts additional deviations to the model. Furthermore, the mere fact that any real experimental cell by necessity is closed-ended, this alone severely limits the application of the model. Again, the cylindrical nature of the actual cell used to compare the experimental observations and the rectangular theory predictions leads to further expected discrepancies. Nevertheless, in light of all these opposing factors, the evidence shows the model to predict extremely well, for both magnitude and parametric dependence, the behavior of oxygen gas convecting in a magnetic field having a non-vanishing field gradient. The Glenda effect has a model.

APPENDIX

APPENDIX A

THE MOLECULAR ORBITAL STRUCTURE OF OXYGEN

Atomic oxygen has the electronic configuration $1s^2 2s^2 2p^4$ which, upon reacting with itself, gives the following MO sequence:



Thus, by Hund's first rule of maximum multiplicity, oxygen has two unpaired electrons, each occupying different doubly degenerate antibonding π -orbitals. It is parenthetically added that orbital mixing does not occur here as in heteronuclears or homonuclears of lower atomic number since the energy separation between 2s and 2p in oxygen is such to preclude mixing. Thus, the effective bond order is 2, its bond strength is $118 \text{ kcal mol}^{-1}$, and bond length 1.21 \AA . Having 2 degenerate unpaired electrons, oxygen is triplet in the ground state. . .

APPENDIX B

THE DERIVATION OF THE CURIE LAW FROM KINETIC THEORY

Consider one mole of a paramagnetic gaseous species confined in space by a suitable container subjected to a magnetic field in a rectangular coordinate system. Since these particles are paramagnetic, they have an inherent, characteristic, magnetic moment, λ , which is constant and independent of field strength and temperature. Letting N^* be the number of particles at some instant of time t that are aligned with the magnetic field such that their orientation with the applied field is at some angle θ , the net contribution this field makes to the total magnetic flux is $N^*\lambda\cos\theta$, or expressing this in terms of the magnetic susceptibility, $N^*\lambda\cos\theta/H$. In the absence of an applied field, all values of θ are equally possible owing to thermal agitation; thus, integrating over all θ , the susceptibility vanishes (permeability, except for diamagnetic contributions is unity). In the case of a non-zero applied field, preferred orientations are possible, depending on the energy of the system and the Boltzmann distribution. Seeking a statistical distribution of these particles at a particular angle θ with respect to a particular field, H , it is assumed that translational and vibrational changes cause no change in orientation with the field. Thus, with respect to the applied field, the only energy contribution to the particle is rotational; the Hamiltonian operator loses its kinetic energy character and becomes solely dependent on the potential

energy of one particle which can be envisioned as an oscillating dipole:

$$\text{P.E.} = - \lambda H \cos \theta$$

Using the Boltzmann distribution, it is recognized that the number density (i.e. probability) that a given magnetic moment will fall within the angular displacement $d\Omega$, where $d\Omega$ is $\cos\theta d\phi d\theta$ (i.e. planar displacement for all possible orientations), is proportional to the exponential of the ratio of the characteristic molecular energy to its kT energy, or, for all N_0 particles, the total susceptibility can be given by

$$\chi_M = \frac{N_0 \lambda \int_{\Omega} \cos \theta e^{\lambda H \cos \theta / kT} d\theta}{H \int_{\Omega} e^{\lambda H \cos \theta / kT} d\theta} \quad [\text{App B-2}]$$

Expanding the exponentials in a power series,

$$\chi_M = \frac{N_0 \lambda \int_{\Omega} (\cos \theta + \lambda H \cos^2 \theta / kT + \dots) d\theta}{H \int_{\Omega} (1 + \lambda H \cos \theta / kT + \dots) d\theta} \quad [\text{App B -3}]$$

where the first two terms only have been retained in the expansions. Since $\cos \theta$ is an odd function, the integral over all possible θ (a sphere) of $\cos \theta$ is zero, whereas $\cos^2 \theta$ over a sphere is $1/3$. Thus,

$$\chi_M = \frac{N_o \lambda^2}{3kT} \quad [\text{App B-4}]$$

and since

$$\chi_M = \frac{C}{T}, \quad [\text{App B-5}]$$

$$C = \frac{N_o \lambda^2}{3kT} \quad [\text{App B-6}]$$

Q.E.D.

APPENDIX C

•
•
•

DIMENSION T(7),H(5),P(5),DT(3)
PROGRAM TO COMPUTE MAGNETIC-CONVECTIVE HEAT TRANSFER (THE GLENDA
EFFECT) BASED ON AVAILABLE EXPERIMENTAL DATA OF J. VEVAI (1973)
AND A FIELD GRADIENT OF 2 OERSTEDS PER CM. THE CONDITIONS ARE
LISTED IN THE DATA FOLLOWING

DATA T/81.7,86.3,89.5,98.0,112.,86.1,86.2/

T ARE THE AVERAGE ABSOLUTE TEMPERATURES, IN DEGREES KELVIN, FOR THE RUNS.

DATA H/7000.,8820.,10600.,12300.,14100./

H ARE THE MAGNETIC FIELD INTENSITIES IN OERSTEDS FOR THE RUNS.

DATA P/19.2,28.,35.4,35.6,35.8/

P ARE THE ABSOLUTE PRESSURES OF THE CELL IN TORR FOR THE RUNS.

DATA DT/22.6,12.47,22.7/

DT ARE THE TEMPERATURE GRADIENTS ACROSS THE CELL IN DEGREES
KELVIN FOR THE RUNS.

CALL TSPAN (P(3),DT(1),H,T)

TSPAN COMPUTES THE GLENDA-EFFECT HEAT TRANSFER AS A FUNCTION OF
TEMPERATURE WITH THE FIELD AS PARAMETERS, PRESSURE AND DELTA HELD
CONSTANT AT 35.4 TORR AND 22.6 DEGREES K RESPECTIVELY

CALL HSPAN (T,H,P,DT)

HSPAN COMPUTES THE GLENDA-EFFECT HEAT TRANSFER AS A FUNCTION OF
MAGNETIC FIELD WITH THE PRESSURE, DELTA T, AND T AVERAGE AS VARIOUS
PARAMETERS.

CALL PSPAN (T(6),DT(1),H,P)

PSPAN COMPUTES THE GLENDA EFFECT HEAT TRANSFER AS A FUNCTION OF
THE PRESSURE WITH THE FIELD AS PARAMETERS, THE AVERAGE TEMPERATURE
AND DELTA T HELD CONSTANT AT 86.1 AND 22.6 DEGREES K RESPECTIVELY.

EACH SUBROUTINE TABULATES ALL DATA AND RESULTS AS WELL AS PLOTS
EACH FUNCTIONAL DEPENDENCE.

STOP
END

```

SUBROUTINE TSPAN (P,DT,H,T)
DIMENSION F(5),T(5),Q(5,5),Yw(5,5),ICX(6),ICY(6),ICHR(5)
DATA ICX/'ABSC','LUTE','TEM','PERA','TURE','/'
DATA ICY/'HEAT','IN','MIL','LI W','ATTS','/'
DATA ICHR/'A','R','C','D','E'/'
N=1
DO 100 I=1,5
DO 200 J=1,5
Q(J,I)=HEAT(F(I),T(J),P,DT)
200 CONTINUE
100 CONTINUE
CALL PRINT1 (P,DT,H,T,Q)
300 CALL PLOT2 (T,Q,Yw,5,5,5,5,0.0,0.0,0.0,0.0,ICHR,ICX,ICY,C.C,0.C,
20)
IF (N.EQ.0) GO TO 400
CALL XLOG(T,Q,5,5,N)
GO TO 300
400 CALL XLSTQ(T,Q,5,5)
RETURN
END

```

```

SUBROUTINE HSPAN (T,H,P,DT)
DIMENSION F(5),T(7),P(5),DT(3),Q(5,6),Yw(5,6),ICX(6),ICY(6),ICHR(
6),A(7)
DATA ICX/'MAGN','ETIC','FIF','LO I','N CA','USS '/'
DATA A/81.7,86.3,89.5,98.C,112.,86.1,86.2/
DATA ICY/'HEAT','IN','MIL','LI W','ATTS','/'
DATA ICHR/'A','R','C','D','E','F'/'
N=1
DO 199 I=1,7
199 T(I)=A(I)
DO 100 I=1,5
100 Q(I,1)=HEAT(F(I),T(3),P(1),DT(3))
DO 200 I=1,5
200 Q(I,2)=HEAT(F(I),T(5),P(3),DT(1))
DO 300 I=1,5
300 Q(I,3)=HEAT(F(I),T(1),P(4),DT(2))
DO 400 I=1,5
400 Q(I,4)=HEAT(F(I),T(4),P(4),DT(1))
DO 500 I=1,5
500 Q(I,5)=HEAT(F(I),T(7),P(2),DT(1))
DO 600 I=1,5
600 Q(I,6)=HEAT(F(I),T(2),P(5),DT(1))
CALL PRINT2 (P,DT,H,T,Q)
800 CALL PLOT2 (H,Q,Yw,5,6,5,6,0.0,0.0,0.0,0.0,ICHR,ICX,ICY,0.C,0.C,
50)
IF (N.EQ.0) GO TO 700
CALL XLOG(H,Q,5,6,N)
GO TO 800
700 CALL XLSTQ(H,Q,5,6)
RETURN
END

```

```

SUBROUTINE PSPAN (T,DT,H,P)
DIMENSION F(5),P(5),Q(5,5),Yw(5,5),ICX(6),ICY(6),ICHR(5),A(5)
DATA ICX/'ABSC','LUTE','PRE','SSUR','E','/'
DATA A/7000.,8820.,10600.,12300.,14100./
DATA ICY/'HEAT','IN','MIL','LI W','ATTS','/'
DATA ICHR/'A','R','C','D','E'/'
N=1
DO 199 I=1,5
199 F(I)=A(I)
DO 100 I=1,5
DO 200 J=1,5
Q(J,I)=HEAT(F(I),T,P(J),DT)
200 CONTINUE
100 CONTINUE
CALL PRINT3 (P,DT,H,T,Q)
300 CALL PLOT2 (P,Q,Yw,5,5,5,5,C.C,0.C,0.C,0.C,ICHR,ICX,ICY,0.C,0.C,
40)
IF (N.EQ.0) GO TO 400
CALL XLOG(P,Q,5,5,N)
GO TO 300
400 CALL XLSTQ(P,Q,5,5)
RETURN
END

```

```

SUBROUTINE PRINT1(P,DT,H,T,Q)
DIMENSION F(5),T(5),Q(5,5)
WRITE (6,100) P,DT
100 FORMAT (1HC,2C(/),10X,'THE GLENDA-EFFECT CONTRIBUTION TO HEAT TRAN
1SFER IN MILLIWATTS AS A FUNCTION OF THE ABSOLUTE TEMPERATURE',/,
210X,'WITH THE MAGNETIC FIELD AS PARAMETERS AND THE PRESSURE AND DE
3LTA T CONSTANT AT P=',F5.2,' AND DELTA T=',F5.2,2(/))
WRITE (6,200) (H(I),I=1,5)
200 FORMAT (1F0,5X,'ABSOLUTE TEMPERATURE',5X,5('F=',F7.1,5X),2(/))
DO 300 J=1,5
WRITE (6,400) T(J),(Q(J,I),I=1,5)
400 FORMAT (1F,13X,F5.1,12X,F7.4,4(7X,F7.4))
300 CONTINUE
WRITE (6,500)
500 FORMAT (1HC,5(/),25X,'A PLOT OF THE GLENDA-EFFECT HEAT TRANSFER VE
2RSUS ABSOLUTE TEMPERATURE',/,25X,
3'A THROUGH E ARE THE FIELD PARAMETER VALUES, 7.0 TO 14.1 KILOGAUSS
4',//)
RETURN
END

```

```

FUNCTION HEAT(H,T,P,DT)
REAL NU
RHC=(P/T)*5.118E-4

```

```

RHC IS THE GAS DENSITY BASED ON THE IDEAL GAS LAW

```

```

NU=203.9E-6*((423./(T+127.))*(T/296.)**1.5)/RHC

```

```

NU IS THE KINEMATIC VISCOSITY BASED ON AN EMPIRICAL EQUATION FOR
OXYGEN FROM THE INTERNATIONAL CRITICAL TABLES.

```

```

HEAT=2.6661*RHC*(DT)**2*H/(NU*(T)**2)

```

```

HEAT IS THE HEAT TRANSFERED IN MILLI WATTS, OF JUST THE GLENDA
EFFECT CONTRIBUTION TO THE OVERALL HEAT TRANSFER.

```

```

RETURN
END

```

```

SUBROUTINE PRINT2 (P,DT,H,T,G)
DIMENSION P(5),T(7),DT(3),H(5),Q(5,6)
WRITE (6,100)
100 FORMAT (1HC,13(/),10X,'THE GLENDA-EFFECT CONTRIBUTION TO HEAT TRAN
2SFER IN MILLIWATTS AS A FUNCTION OF THE MAGNETIC FIELD',/,
310X,'WITH VARIOUS PARAMETRIC VALUES OF THE PRESSURE, DELTA T, AND
4AVERAGE TEMPERATURE',//)
WRITE (6,200) P(1),P(3),P(4),P(4),P(2),P(5)
200 FORMAT (1F0,25X,6('P=',F4.1,6X))
WRITE (6,300) T(3),T(5),T(1),T(4),T(7),T(2)
300 FORMAT (1H,5X,'FIELD STRENGTH',6X,6('T=',F5.1,5X))
WRITE (6,400) DT(3),DT(1),DT(2),DT(1),DT(1),DT(1)
400 FORMAT (1H,25X,6('DT=',F4.1,5X),//)
DO 600 J=1,5
WRITE (6,500) F(J),(Q(J,I),I=1,6)
500 FORMAT (1H,10X,F7.1,8X,6(F7.4,5X))
600 CONTINUE
WRITE (6,700)
700 FORMAT (1F0,5(/),25X,'A PLOT OF THE GLENDA-EFFECT HEAT TRANSFER VE
2RSUS MAGNETIC FIELD STRENGTH',/,25X,
3'A THROUGH F ARE THE VARIOUS PARAMETRIC VALUES, AS SHOWN ABOVE',//
4/)
RETURN
END

```

```

SUBROUTINE PRINT3 (P,DT,H,T,C)
DIMENSION P(5),Q(5,5)
WRITE (6,100) T,DT
100 FORMAT (1H0,10(//),10X,'THE GLENDA-EFFECT CONTRIBUTION TO HEAT TRAN
2SFER IN MILLIWATTS AS A FUNCTION OF THE PRESSURE',/,
310X,'WITH THE MAGNETIC FIELD AS PARAMETERS AND THE AVERAGE TEMPERA
4TURE',/,10X,'AND DELTA T CONSTANT AT T=',F5.1,' AND DELTA T=',F5.2
5,//)
WRITE (6,200) (H(I),I=1,5)
200 FORMAT (1H0,5X,'PRESSURE, IN TCRR',7X,5('H=',F7.1,5X),//)
DO 300 J=1,5
WRITE (6,400) P(J),(Q(J,I),I=1,5)
400 FORMAT (1H ,11X,F5.1,13X,F7.4,4(7X,F7.4))
300 CONTINUE
WRITE (6,500)
500 FORMAT (1H0,5(//),25X,'A PLOT OF THE GLENDA-EFFECT HEAT TRANSFER VE
2RSL5 ABSOLUTE PRESSURE',/,25X,
3'A THROUGH E ARE THE FIELD PARAMETER VALUES, 7.0 TO 14.1 KILOGAUSS
4',//)
RETURN
END

```

```

C SUBROUTINE XLQCG(T,Q,L,M,N)
C THIS SUBROUTINE CONVERTS ANY VECTOR (T) AND ANY L BY M MATRIX (Q)
C TO THEIR COMMON LOGARITHMS AND RETURNS THE ARRAY TO THE MAIN FOR
C PLOTTING AND LEAST SQUARES ANALYSIS.
DIMENSION T(6),Q(L,M)
N=0
DO 100 I=1,L
T(I)=ALOG10(T(I))
100 CONTINUE
DO 200 I=1,M
DO 300 J=1,L
Q(J,I)=ALOG10(Q(J,I))
300 CONTINUE
200 CONTINUE
CALL PRINT4(T,Q,L,M)
RETURN
END

```

```

SUBROUTINE PRINT4(X,Q,N,M)
DIMENSION X(N),Q(N,M)
WRITE (6,100)
100 FORMAT (1H0,5(//),25X,'TAKING THE COMMON LOGARITHMS OF ALL OF THE A
2BOVE VALUES',/,25X,'WE OBTAIN THE FOLLOWING CORRESPONDING VALUES..
3...',//)
DO 200 J=1,N
WRITE (6,300) X(J),(Q(J,I),I=1,M)
300 FORMAT (1H ,15X,F8.5,9X,6(F8.5,5X))
200 CONTINUE
WRITE (6,400)
400 FORMAT (1H0,5(//),45X,'AND A LOG-LOG PLOT.....',5(//))
RETURN
END

```

```

C SUBROUTINE XLSTQ(X,Y,N,M)
C THIS SUBROUTINE SEPARATES THE Q ARRAY INTO VECTORS FOR LEAST
C SQUARES TREATMENT AND PRINTS LEAST SQUARES HEADING.
DIMENSION X(N),Y(N,M),Y1(5)
WRITE (6,300)
300 FORMAT (1H0,5(//),25X,'A LINEAR LEAST SQUARES ANALYSIS OF THE DATA
2FOR THE ABOVE LOG-LOG PLOT SHOWS.....',3(//),32X,'SLOPE',23X,'CORRE
3LATION COEFFICIENT',3(//))
DO 200 J=1,M
DO 100 I=1,N
Y1(I)=Y(I,J)
CALL XLSTQ1(X,Y1,S,C,N)
WRITE (6,400) S,C
400 FORMAT (1H ,30X,F6.2,30X,F7.6)
200 CONTINUE
RETURN
END

```

```

SUBROUTINE XLSTQ1(X,Y,SLOPE,CORCOF,N)
DIMENSION X(N),Y(N)
GENERALIZED LLAST SQUARES SUBPROGRAM FOR POLYNOMIALS OF DEGREE ONE
REAL INTER
SUMX=0.0
SUMY=0.0
SUMXY=0.0
SUMX2=0.0
SUMY2=0.0
DO 500 I=1,N
SUMX=SUMX+X(I)
SUMY=SUMY+Y(I)
SUMXY=SUMXY+X(I)*Y(I)
SUMX2=SUMX2+X(I)**2
SUMY2=SUMY2+Y(I)**2
500 CONTINUE
DET=FLOAT(N)*SUMX2-SUMX**2
SLOPE=(FLOAT(N)*SUMXY-SUMX*SUMY)/DET
INTER=(SUMY*SUMX2-SUMXY*SUMX)/DET
XINTER=-INTER/SLOPE
TFA=(FLOAT(N)*SUMX2-SUMX**2)**.5
PGX=(FLOAT(N)*SUMY2-SUMY**2)**.5
CORCOF=ABS((FLOAT(N)*SUMXY-SUMX*SUMY)/(TFA*PGX))
RETURN
END

```

REFERENCES

1. Senftleben, H., Phys.Z., 31, 961, (1930).
2. Beenakker, J.J.M., Scoles, G., Knapp, H.F.P., and Jonkman, R.M., Phys. Let., 2, 5, (1962).
3. Beenakker, J.J.M., et al., Phys. Rev., 4A, 788, (1971).
4. Vevai, J.E., Honeywell, W.I., and Eliot, D.G., Phys. Let., 38A, 265, (1972).
5. Park, W-H, and Honeywell, W.I., Chem Eng. Comm., 1, 167, (1973).
6. Gershuni, G.Z., and Zhukhovitskii, E.M., Sov. Phys. JETP, 34, 670 (1958).
7. Lehrer, V.E., and Ebbinghaus, E., Z. Ang. Phys., 2, 2-20, (1950).
8. Kibler, K.G. and Wiley, R., Ind. Res., April, 1972, p. 50.
9. Lykoudis, P.S., and Yu, C.P., Int'l J. Heat & Mass Transf., 6, 853, (1963).
10. Carruthers, J.R. and Wolfe, R., J.App. Phys., 39, 5718, (1968).
11. Chu, B-T, Phys Fluids, 2, 473 (1959).
12. From ChE. 633, the University of Houston, under A.E. Dukler.
13. Ede, A.J., Advances in Heat Transf., Vol 14, T.R. Irvine, ed., Academic Press, N.Y., 1967.
14. Klauer, F., et al., Z. Tech. Phys., 22, 223 (1941).
15. Barrow, G.M., Physical Chemistry, McGraw-Hill, New York, 1966.
16. Int'l Crit. Tables, Washburn, E.W., ed., Vol. 5, 1st ed., p. 2, McGraw-Hill, New York, 1929.
18. Vevai, J.E., Ph.D. Dissertation, University of Houston, Dept. of Chemical Engineering, Houston, Texas, 1973.

19. Elliot, D.G., Ph.D. Dissertation, University of Houston, Dept. of Chemical Engineering, Houston, Texas, 1969.
20. Van Vleck, J.H.; The Theory of Electric and Magnetic Susceptibilities, Oxford University Press, London, 1932.

GENERAL READING BIBLIOGRAPHY

1. Roberts, P.H., An Introduction to Magnetogasdynamics, American Elsevier Publishing Company, Inc., 1967, New York.
2. Kalkiman, Elements of Magnetogasdynamics, W.S. Saunders Co., Philadelphia, 1967, trans. Scripta Technica, Inc.
3. Gundersen, R.M., Linearized Analysis of One-Dimension Magnetohydrodynamic Flows, Springer-Verlag, New York, 1964.
4. Ferrar, V.C.A. and Plumpton, C., An Introduction to Magneto-Fluid Mechanics, 2nd Ed., Clarendon Press, Oxford, 1966.
5. Jeffery, Alan, Magnetohydrodynamics, Oliver and Boyd, Interscience (John Wiley), New York, 1966.
6. Nussbaum, Allen, Electronic and Magnetic Behavior of Materials, Prentice-Hall, Englewood Cliffs, New Jersey, 1967.
7. Holt, E.H., and Haskell, R.E., Foundations of Plasma Dynamics, The MacMillan Co., New York, 1965.
8. Pai, Shih-I, Magnetogasdynamics and Plasma Dynamics, Springer-Verlag, Englewood Cliffs, New Jersey, 1962.
9. Hughes, W.F., and Brighton, J.A., Theory and Problems of Fluid Dynamics, McGraw-Hill Book Co., New York, 1963.
10. Cotton, F.A., Wilkinson, G., Advanced Inorganic Chemistry, Wiley Interscience, New York, 1972.

NOMENCLATURE

NOMENCLATUREEnglish -

A	Helholtz Free Energy.
\vec{B}	Magnetic-flux vector within matter.
C	Curie constant for paramagnetically susceptible matter, $\text{erg } ^\circ\text{K Oe}^{-2} \text{ mol}^{-1}$.
c	Speed of light in a vacuum, 3.0×10^{10} cm/sec.
C_v	Heat capacity at constant volume, $\text{cal } ^\circ\text{K}^{-1} \text{ gm}^{-1}$.
\bar{c}	Average molecular speed, cm sec^{-1} .
D	Characteristic distance, cm.
\vec{D}_e	Electric excitation vector.
e	Electronic charge, 4.8030×10^{-10} esu.
\vec{E}	Externally applied electric field vector.
\vec{H}	Externally applied magnetic field, Oe.
\vec{F}	External body force per unit volume vector.
\vec{f}	Pondermotive force vector per unit volume.
g	Acceration due to gravity at the surface of the earth, -980 cmsec^{-2} .
\vec{G}	Electromagnetic momentum.
g_l	Lande-g factor.
Gl	Dimensionless Glenda number, $\frac{2D^3 \Delta T C H}{M v_0^2 T_0^2 x} \left(\frac{\partial H}{\partial z} x \right)$.
Gr	Dimensionless Grashof Number, $\frac{\beta D^3 g \Delta T}{v_0^2}$.
h	Magnetic body force, $H_x \frac{\partial H}{\partial z} x$, $\text{Oe}^2 \text{ cm}^{-1}$.
\hat{h}	Planck's constant, 6.6256×10^{-27} erg sec.
Ha	Dimensionless Hartmann number.

H_0	Externally applied constant magnetic field in the x-direction, Oersted.
\vec{I}	Intensity of magnetization vecto.
\vec{j}	Electrical current.
k	Boltzmann constant, 1.36×10^{-16} ergs $^{\circ}\text{K}^{-1}$.
k_c	Pseudo natural convection heat transfer coefficient, $\text{mW } ^{\circ}\text{K}^{-1}$.
k_l	Pseudo radiative heat transfer coefficient, $\text{mW } ^{\circ}\text{K}^{-1}$.
l	Actual cell depth, in y direction, cm.
L	Overall cell length.
m	Mass.
M	Molecular weight, gm mol^{-1} ; for oxygen, $M=32 \text{ gm mol}^{-1}$.
m_e	Electronic rest mass, 0.9109×10^{-27} gm.
m_a	Mass of a single atom, gm atom^{-1} .
Mc	Dimensionless magnetoconvection number after Park.
N_0	Avagadro's number, $6.023 \times 10^{23} \text{ mol}^{-1}$.
p	Pressure, torr.
Pr	Dimensionless Prandtl number, $\frac{\nu}{\alpha}$.
q	Arbitrary heat transfer quantity.
Q	Total heat transfer, energy sec^{-1} .
Q_{GI}	Magnetothermal contribution, arising from the Glenda effect, to the total heat transferred based on the model only.
Q_{cond}	Heat transfer due to conduction only, energy time^{-1} .
Q_{conv}	Heat transfer due to free convection processes only, energy/time .
Q_{loss}	All lumped heat transfer losses, energy time^{-1} .
Q_{MC}	Experimentally based heat transferred due to magnetic contributions to convection only, energy/sec . If Glenda effect model is correct, $Q_{GI} = Q_{MC}$.

R	Universal gas constant, 8.314×10^7 ergs $^{\circ}\text{K}^{-1}$ mol $^{-1}$.
Re_m	Magnetic Reynolds number, characterizing the relative influence of fluid velocity and applied fields.
s	Electron spin quantum number.
S	Entropy.
\tilde{S}	Total spin quantum number.
\hat{S}	Appropriate shape factor for the geometry involved in conductive heat transfer.
t	Time.
T	Instantaneous, dimensionalized temperature, $^{\circ}\text{K}$.
T_0	Average T over ΔT , $^{\circ}\text{K}$.
T^*	Dimensionless temperature, $T\Delta T^{-1}$.
\vec{u}	Fluid velocity vector, cm sec $^{-1}$.
\vec{u}^*	Dimensionless velocity vector, $\vec{u}D\nu_0^{-1}$.
\hat{U}	Internal energy.
w	Thermodynamic work function.
x^*	Dimensionless coordinate, xD^{-1} .

Greek

α	Thermal diffusivity, $\Lambda_0 \rho^{-1} C_v^{-1}$.
β	Coefficient of thermal expansion, $= -\frac{1}{\rho} \left(\frac{\partial \rho}{\partial T} \right)_p \bigg _{T_0}$ for an ideal gas, $= 1/T$.
$\hat{\gamma}$	Ratio of the heat capacities.
ΔT	Dimensionalized temperature gradient, $^{\circ}\text{K}$.
δ_{ij}	Kronecker delta

δT_1	Experimental change in temperature of the inner plate of a magnetoconvection cell.
ϵ	Dielectric constant of a substance.
$\tilde{\epsilon}$	Vibrational energy level spacing, ergs.
η	Instantaneous absolute viscosity, $\text{gm cm}^{-1} \text{sec}^{-1}$.
η_0	Average η over ΔT , $\text{gm cm}^{-1} \text{sec}^{-1}$.
λ	Characteristic, permanent magnetic moment of a substance; a property of that substance.
λ_0	One Bohr magneton, $0.927 \times 10^{-20} \text{ ergs Oe}^{-1}$.
Λ_0	Standard thermal conductivity.
μ	Magnetic permeability of matter; not a property of matter.
μ_0	Average μ over ΔT .
ν_0	Average kinematic viscosity over ΔT , $\text{cm}^2 \text{sec}^{-1}$.
ρ	Instantaneous density, gm cm^{-3} .
ρ_0	Average ρ over ΔT , gm cm^{-3} .
ρ^e	Current density.
σ	Electrical conductivity of matter.
σ_c	Molecular collision cross section, \AA .
$\underline{\underline{T}}_{ij}$	Stress tensor.
Ψ	Element of the surface of a control volume.
ω	Conversion constant, $4.18 \times 10^3 \text{ mW sec cal}^{-1}$.
$\vec{\nabla}$	Del operator.
$\left(\frac{\Delta\Lambda}{\Lambda_0}\right)_{\text{SB}}$	The change in thermal conductivity arising from the Senftleben-Beenakker effect only.
χ_w	Mass susceptibility, per unit mass.
χ_M	Molar susceptibility, per unit mole.
χ_v	Volumetric susceptibility, per unit volume.

γ

$$\text{Thermomagnetic permeability, } = - \frac{1}{\mu_0} \left(\frac{\partial \mu}{\partial T} \right) P \Big|_{T_0}$$

$$\text{For this work, } = - 2 \frac{C_p}{RT_0} \chi_3 \quad .$$